UNIVERSIDADE DE LISBOA
FACULDADE DE CIÊNCIAS
DEPARTAMENTO DE BIOLOGIA ANIMAL

CRISPR-Cas9 mutagenesis of the zebrafish *foxm1*

Ana Leonor Azevedo dos Santos Carvalho

Mestrado em Biologia Evolutiva e do Desenvolvimento

Dissertação orientada por:

José Bessa

Gabriela Rodrigues

2018

Acknowledgments

I would like to dedicate this dissertation to my family that supported me during this journey. Thank you for encouraging me to explore my options and pursue my dreams. You are the reason for everything, I love you all.

I am also grateful for my friends who always supported me, my long hours at the lab and lack of time to meet them. Thank you for understanding and being there for me.

For all the guidance, help and patience I would like to acknowledge Fábio Ferreira which had a great impact in the present work.

For all the orientation given during the project I want to recognize my supervisor José Bessa. I am thankful for the opportunity to work in such an interesting project and his orientation throughout this dissertation.

Finally, I would like to acknowledge Elsa Logarinho and the Ageing and Aneuploidy group for all the knowledge shared regarding the cell cycle, *foxm1*, senescence and the overall aging process. Their contribute through meetings and recent studies was preponderant for the development of this master thesis.

Last but not least, the Vertebrate Development and Regeneration group from i3S should be acknowledged. All the group members were essential in moments of stimulating scientific discussion and the reason behind such an amazing work environment. Thank you for being part of my journey.

Abstract

Aging is a complex process that has been associated with multiple biological phenotypes linked to chronic diseases, such as decay of cell renewal and accumulation of senescent cells. FoxM1, the transcription factor that primarily drives late cell cycle gene expression, has been recently assigned as a major regulator of cellular aging.

To study the role of FoxM1 in organismal aging, we used the zebrafish model and the CRISPR/Cas9 gene editing system to generate loss-of-function foxm1 mutations. Strikingly, all the different isolated mutations corresponded to small in-frame deletions, suggesting that foxm1 loss-of-function is deleterious.

In a complementary approach, we applied the same molecular tools to generate mosaics of differentiated muscle cells mutated for foxm1. We observed that the number of putative mutant cells tend to slowly decrease throughout time, whereas the number of labelled surrounding wild type cells tend to increase, when comparing with a control. In this context, preliminary results showed that the expression of genes involved in muscle regeneration and repair, as well as in senescence phenotype, reflected a tendency to increase. These results suggest that *foxm1* expression potentially acts non-autonomously in muscle tissue homeostasis, which could be compatible with a senescent cell identity.

Finally, during the course of our experiments, we also found that the continuous expression of Cas9 in transgenic cells induces toxicity. This result shows that the current techniques used for loss-of-function based CRISPR-Cas9 expression vectors must be improved.

Keywords: *foxm1*, zebrafish, senescence, muscle

Resumo

O ciclo celular é um processo vital aos eucariotas e o seu controlo é essencial para manutenção da homeostase dos organismos. Vários genes têm sido descritos como reguladores das diferentes fases deste processo, contribuindo para o desenvolvimento dos indivíduos.

O *FoxM1* é considerado o principal regulador deste ciclo em mamíferos. Este gene codifica um fator de transcrição que regula outros genes com papel relevante nas diferentes fases do ciclo celular, na regulação do metabolismo celular, na remodelação da matriz extracelular sinalização celular e na regulação transcricional. De acordo com as suas funções reguladoras, este gene está associado a proliferação celular. Esta associação atua ao nível de desenvolvimento embrionário, regeneração e reparação de tecidos, progressão e iniciação de processos tumorais e senescência celular. Em murganho, a perda deste gene é letal dando origem a alterações severas em órgãos vitais como coração, fígado e pulmões.

Em linhas celulares a perda de *FoxM1* resulta em fenótipos mitóticos associados ao envelhecimento e poliploidia. Recentemente, foi demonstrado que a expressão de *FoxM1* em células senescentes é reduzida e, recuperando a expressão deste gene em fibroblastos humanos de dadores idosos o fenótipo é recuperado, assemelhando-se a amostras de fibroblastos jovens. Também genes-alvo de *FoxM1* revelaram ter um papel importante no processo de envelhecimento sugerindo um envolvimento de *FoxM1* no mesmo. O envelhecimento é um processo multifatorial complexo caracterizado pela perda gradual de integridade e funcionalidades dos tecidos e células. Este processo está associado a muitos fenótipos biológicos envolvidos em doenças crónicas. Entre estes fenótipos encontram-se descritos o decaimento da renovação celular, acumulação de células senescentes e disfunção mitótica do ciclo celular. A senescência celular consiste numa interrupção do ciclo celular com características fenotípicas e fisiológicas particulares incluindo a existência de um secretoma pro-inflamatório (SASP). Desta forma, as células senescentes podem influenciar as células adjacentes ao induzirem um efeito parácrino. Contudo, a avaliação *in vivo* do papel de *FoxM1* no envelhecimento, usando animais modelo vertebrados, não foi ainda devidamente explorada.

Neste projeto aplicou-se o sistema CRISPR-Cas9 para criar mutações no gene *foxm1* do peixe-zebra (*Danio rerio*). Este modelo animal apresenta um padrão de envelhecimento gradual, semelhante ao que acontece em humanos. O peixe-zebra tem também o seu genoma totalmente sequenciado e possui pelo menos um ortólogo para a grande maioria de genes codificantes humanos. Também o seu desenvolvimento externo, transparência embrionária, custo, facilidade de manipulação e apresentação dos marcadores e fenótipos de senescência humanos tornam este modelo relevante no estudo de envelhecimento. Este vertebrado é facilmente manipulado geneticamente, permitindo a geração de diferentes mutantes através de técnicas de biologia molecular. O sistema CRISPR-Cas9 permite uma manipulação genética especifica através da criação de um complexo Cas9-sgRNA que se une a uma sequência especifica de interesse do DNA genómico e induz um corte da dupla cadeia de DNA. Os mecanismos celulares de reparação genómica são iniciados através da junção de extremidades não homólogas (NHEJ). Este processo é propenso a erros com inserção ou remoção de nucleotídeos resultando em mutações passíveis da inativação da proteína e silenciamento do gene. Neste projeto, as regiões-alvo de CRISPR-Cas9 correspondem ao segundo e oitavo exões do *foxm1*, sendo que apenas para o último foi possível obter mutações. O oitavo exão do *foxm1* do peixe-zebra, corresponde à região inicial do domínio funcional da proteína. Na região equivalente do gene ortólogo em células humanas, foi demonstrado anteriormente que mutações neste local origina uma proteína com uma função dominante negativa. Inicialmente testou-se a funcionalidade do sistema CRISPR-Cas9 através de um sgRNA tendo como alvo E-GFP de uma linha estável com fluorescência no sistema nervoso

central. Após verificação da operacionalidade da tecnologia testaram-se nove sgRNAs, seis para o segundo e três para o oitavo exão do *foxm1*. Para tal, extraiu-se DNA de embriões co-injetados com sgRNA e Cas9, amplificando-se o *locus* alvo por reação em cadeia da polimerase (PCR), correndo o produto amplificado num gel de policrilamida, tendo-se verificado a presença de homo e heteroduplexes. Heteroduplexes correspondem a cadeias que são apenas parcialmente complementares pela existência de mutações.

Para o oitavo exão encontrou-se um sgRNA capaz de provocar mutações através de CRISPR-Cas9. Cresceram-se animais co-injetados com este sgRNA (sgRNA 8.3). No entanto, todas as mutações obtidas na progenia correspondem a pequenas deleções *in-frame*, sugerindo que a perda de *foxm1* pode ser letal. Apesar disso, verificou-se a presença de uma mutação na lisina K315 em dois dos peixes injetados cuja descendência foi genotipada. Esta lisina é homologa à lisina K368 humana, a qual foi previamente identificada como um local de sumolação com impacto na atividade transcricional de FoxM1.

Durante o envelhecimento ocorrem mecanismos celulares no músculo que opõe os processos de regeneração e reparação, verificando-se uma perda de massa muscular. Em mamíferos a miogénese está dependente de percursores musculares com expressão de *Pax3* e *Pax7*. Em peixe-zebra *pax7a* contribui para o crescimento muscular ao longo da vida. Vários autores demonstraram o papel de *Pax7* em reparação e regeneração muscular. Outros revelaram ainda a existência de uma de-diferenciação de células maturas sem recrutamento de progenitores em musculo de peixe-zebra.

Assim, e numa abordagem complementar verificou-se a presença de expressão de *foxm1* em células musculares diferenciadas de peixe-zebra. Para esta abordagem recorreu-se à criação de vetores específicos com o sistema CRISPR-Cas9 inativo (ausência de sgRNA) de modo a marcar as células do musculares com fluorescência (E-GFP), procedendo-se depois ao seu isolamento.

Posteriormente, criou-se um vetor CRISPR-Cas9 ativo (com sgRNA) em células musculares diferenciadas marcadas por fluorescência (E-GFP) e, um vetor com fluorescência (mCherry) para marcação do mesmo tipo de células inalteradas (*wild type*). Ao inibir-se *foxm1* em células musculares diferenciadas, observou-se que o seu número tende a diminuir lentamente ao longo do tempo. Adicionalmente, em embriões mosaicos com células mutadas, o número de células musculares inalteradas (*wild type*) tende a aumentar comparativamente com o controlo.

Em defeitos musculares derivados do envelhecimento, a resposta regenerativa pode estar alterada devido a inflamação crónica, pois as células senescentes secretam moléculas, como interleucinas, que alteram o microambiente. A via de sinalização JAK-STAT tem um papel essencial na regeneração muscular, respondendo a IL-6 extracelular, proveniente de SASP e/ou processos inflamatórios, de reparação e regeneração. Neste contexto, embora as diferenças não sejam estatisticamente significativas, genes envolvidos em reparação e regeneração muscular tendem para o aumento em resposta a mutação de *foxm1*. Estes resultados sugerem que as células mutantes para *foxm1* têm um papel não autónomo na homeostase do tecido muscular, compatível com a identidade das células senescentes.

Por último, ao longo das experiências, descobriu-se que a expressão contínua de Cas9 em células transgénicas induz toxicidade. Este resultado mostra que as técnicas atuais de perda de função baseadas em vetores de expressão CRISPR-Cas9 devem ser melhoradas no futuro.

Palavras-chave: *foxm1*, peixe-zebra, senescência, músculo

Index

List of figures

List of Tables

Abbreviations list

APC/C	chromosomal passenger complex
Ccnb1	Cyclin B1
Cdk	cyclin-dependent kinases
CENP-F	Centromere-associated protein F
ChIP	Chromatin Immunoprecipitation assays
CKI	cyclin-dependent kinases inhibitors
CRISPR	clustered regularly-interspaced short palindromic repeat
DBD	DNA binding domain
DNA	Deoxyribonucleic acid
DSB	double stranded breaks
dsDNA	Double stranded DNA
ECL	external cell layer
E-GFP	Green Fluorescent Protein E
E3	embryonic medium
HDR	homology directed repair
Hfg	hepatocyte growth factor
Hpf	hours post-fertilization
IL	Interleukin
JAK	Janus kinase
KD	knockdown
KO	knockout
MAPK	mitogen-activated protein kinase
MO	morpholino
Myf5	myogenic factor 5
NF-κB	nuclear transcription factor kappa B
NHEJ	non-homologous end joining
NRD	N-terminal auto-repressor domain
PAGE	Polycrilamic Gel Eletroforesis
PAM	protospacer adjacent motif
Plk1	Polo-kinase 1
PTU	1-phenyl-2-thiourea
Rb	retinoblastoma protein
RNA	Ribonucleic acid
RVD	repeat variable di-residues
ROS	reactive oxygen species
SAC	Spindle Assembly Checkpoint
SC	satellite cell
SASP	senescence-associated secretory phenotype
SA-β gal	Senescence Associated-β galactosidase
sgRNA	single-guide RNA
STAT	signal transducers and activators of transcription
TALEN	transcription activator-like effector nucleases
TAD	C-terminal transactive domain
TNF	tumor necrosis factor
TS	tissue-specific
ZFN	zinc finger nucleases

Chapter 1. Introduction

1.1 Cell cycle and cell cycle regulatory genes

The cell cycle is an essential process to all eukaryotic organisms[1] and the control of cellular division affects many developmental aspects[2]. The regulation of this process is key to maintain homeostasis[3] and a balance between cell death and proliferation. When cell cycle control is disrupted, several diseases may occur, such as atherosclerosis, neurodegenerative disorders and even neoplasia[3]–[5].

Cell cycle consists of two stages, interphase and mitosis. Interphase comprehends G1, S and G2 (Figure 1.1), growth and replication phases, which are required for the process of DNA duplication and cell division. The mitosis includes the mitotic cell division that generates two daughter cells[4], [6],[7]. The progression through each phase of the cell cycle involves a complex interplay between cyclins, cyclin-dependent kinases (CDK) and other cell cycle regulators[3]. Cell cycle regulators play a crucial role in developmental, growth, repair and homeostatic processes[8], [9]. Hence, the characterization of transcriptional networks involved in cell cycle progression may contribute to the treatment of some diseases[8].

Several cell cycle genes have been described as essential for development due to their functions and relevance in cell division. A few examples of important regulators will be briefly described.

Cyclin B1 is a regulator of the cell cycle, essential for development[10]. This gene encodes a protein that forms a complex with CDC2 which bind to microtubules in interphase and move to the nucleus during G2, to mitosis transition. In the nucleus it allows phosphorylation of nuclear substrates for mitosis[11]. In mice embryos lacking this cyclin, cells arrest at G2 phase, when maternal contribution depletes[10]. In 1998, Brandeis and colleagues generated transgenic mice lacking *Cyclin B1*, leading to embryonic lethality[12].

Polo-kinase 1 (*plk1*) is another cell cycle gene, critical for mitosis during embryonic development[8], [13]. *plk1* encodes a serine/threonine kinase that regulates cell cycle events such as centrosome maturation, DNA checkpoint activation, mitotic entry, spindle assembly, and cytokinesis by identifying and binding to optimal recognition protein motifs[14], [15]. In 2010, Jeong and coworkers showed that *plk1* was necessary for mitotic progression and proliferation during zebrafish embryogenesis. When depleted, there is altered chromosome condensation, impaired chromosome arm separation, irregular spindle organization, and multi or monopolar centrosomes. In this study, cells from embryos lacking *plk1* presented a mitotic delay leading to embryonic growth defects[13].

Centromere-associated protein F (CENP-F) is implicated in the recruitment of spindle assembly checkpoint proteins BubR1 and Mad1 to the chromosomes during mitosis[16]. In 2005, Laoukili and colleagues depleted CENP-F from human osteosarcoma cells (U2OS cells), resulting in chromosome alignment defects. The same study reported that embryonic fibroblasts from *Forkhead box M1* (*FoxM1)* deficient mouse revealed atypical chromosome segregation and polyploid cells accumulation. Those fibroblasts continued mitosis and had a defect on mitotic spindle assembly checkpoint (SAC), along low levels of CENP-F. By depleting CENP-F alone they reached the same result as in *FoxM1* deficient cells[17].

Through Chromatin Immunoprecipitation assays (ChIP), it has been shown that FoxM1 overlaps with the *Cyclin B1* promoter, which supports *FoxM1* role as a transcriptional regulator of this gene[16], [17]. In 2013, Grant and coworkers used HeLa and U2OS cells to show that *FoxM1* is required for the activation of several genes implicated during the cell cycle[18]. *FoxM1* is was also shown to be essential for *Aurora kinase B, Plk*1 and *CENP-F* expression and it activates transcription of *Cdc25B*

required for the Cdk1-Cyclin B complex during G2-M transition of the cell cycle[16], [17], [19]–[22]. As described in several studies abovementioned, *FoxM1* has a key role in cell cycle control (Figure 1.1).

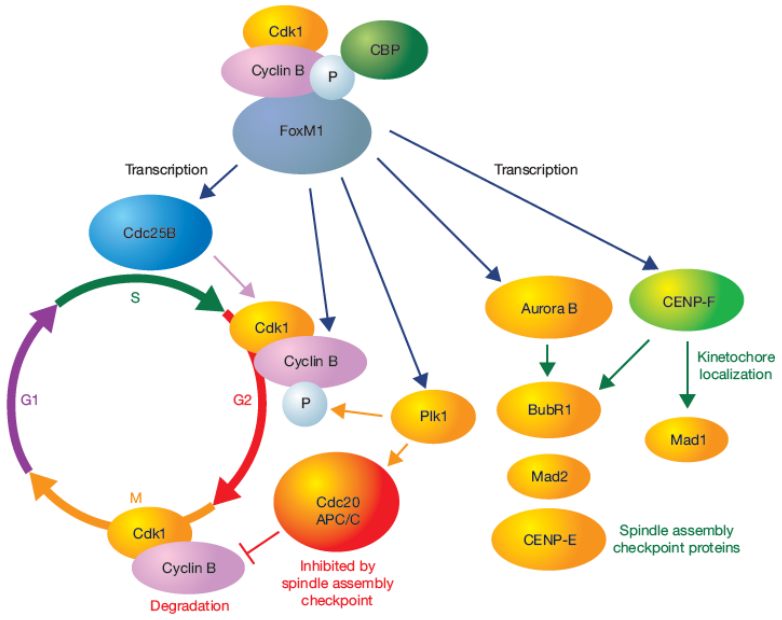

Figure 1.1 FoxM1 regulation of cell cycle genes in a schematic view. On the right there is an image of the cell cycle divided into its phases. On the side, regulating this cycle there is a network of genes and proteins responsible for the regulation of this process which are all controlled by FoxM1 (source: Costa 2005)

1.1.1 *FoxM1*

FoxM1 is considered as a master regulator of the cell cycle in vertebrates[21], [23], [24]. It encodes a transcription factor that regulates the expression of genes controlling G1 to S-phase transition, S-phase progression, G2 to M transition, and mitosis progression[21], [23], [25]–[28]. FoxM1 also enhances the activity of cell cycle kinases (CDKs) and represses cyclin-dependent kinases inhibitors (CKIs)[27], [28]. It has been shown that *FoxM1* depletion lead to a decrease in S-phase cell number[29] and entry into S-phase[24] while its overexpression resulted in an increased number of cells in the S-phase[30]. *FoxM1* is also a relevant gene for mitosis execution. Its loss leads to major defects such as aneuploidy and polyploidy, mitosis delay, mitotic spindle abnormalities, cytokinesis defects, chromosome mis-segregation, faulty SAC and cell death[8], [28], [31], [32]. Thus, FOXM1 promotes correct cell cycle progression and proliferation[16], [19], [31]. Moreover, *FoxM1* controls several genes implicated in cell metabolism, extracellular matrix remodeling, transcriptional regulation and cell signaling, which translates the variety of functions of *FoxM1* cell cycle regulation[31].

FoxM1 exhibits a proliferation-specific expression pattern since it is expressed at high levels in proliferative cells[19], [31], [33]–[36]. *FoxM1* depleted mouse fibroblasts and U2OS cells displayed reduced DNA replication and were blocked during mitosis, failing to proliferate in culture[28]. This proliferation-associated transcription factor functions in several processes such as embryonic development, contact inhibition, cellular senescence, maintenance of the proliferative capacity of cells and adult tissue repair after injury[27], [37]. *FoxM1* was also described to have a role in DNA damage repair and cell renewal, differentiation, migration and survival[33], [35], [37], [38].

The proliferative function of *FoxM1* also contributes for cancer initiation and progression[19], [21], [37]–[40]. Several studies have reported a *FoxM1* upregulation in numerous cancers and transactivation of multiple oncogenes[19], [30], [37], [41]–[43]. In 2016 Smirnov and collaborators

hypothesized that the oncogenic function of *FoxM1* in tumors could be explained by this gene anti-oxidant activity, as a tool to escape premature senescence and apoptosis[44].

FoxM1 is a member of the Forkhead box family of transcription factors[35], [36], [40], [45]. This family has a highly evolutionary conserved DNA binding Forkhead box domain responsible for chromatin remodeling and protein targeting to genomic promoter regions[35], [36], [40]. FoxM1 can be divided in three major domains: 1) A N-terminal auto-repressor domain (NRD), 2) a DNA binding domain (DBD) and 3) a C-terminal transactive domain (TAD)[36], [37] (Figure 1.2). The DNA binding domain is responsible for recognizing and binding to specific FoxM1 binding sites in the DNA. In the FoxM1 inactive state, the N-terminal auto-repressor domain binds to the transactive domain inhibiting FOXM1 ability to induce transcription. However, some CDK proteins can phosphorylate FOXM1 TAD domain releasing it from the influence of the repressor domain, generating an active form of the protein. This active form modulates transcription of the target genes[22], [31], [43], [46].

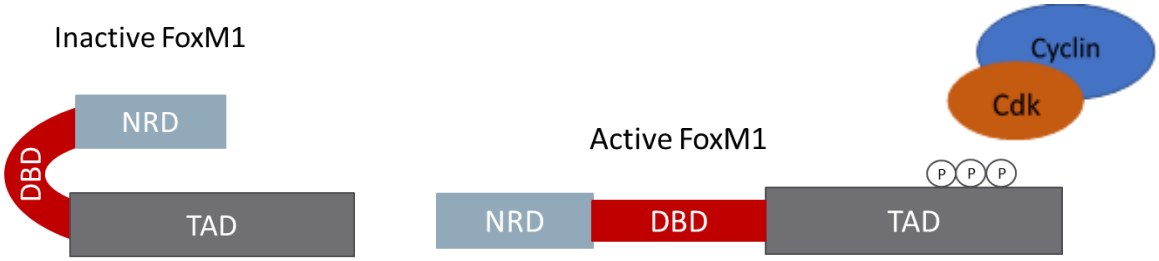

Figure 1.2 Schematic view of FoxM1 domains in Inactive (left) and Active (right) forms of the protein with respective domains: N-repressor domain (NRD), DNA binding domain (DBD) and Transactive domain (TAD)

Several studies have shown that *FoxM1* depletion in mice is lethal, resulting in major defects in vital organs such as heart, lung and liver [25], [26], [32], [47], [48]. In 1998, Korver and colleagues created the first *FoxM1* knockout mouse by inactivating the trident locus of the gene. They revealed a consistent polyploid phenotype in both heart and liver cells demonstrating the role of this locus during the cell cycle[31], [49]. In 2000, Ly and coworkers also associate *FoxM1* downregulation, as well as its target genes involved in the cell cycle regulation, with the increase in the proportion of polyploid cells[50]. Studies using *FoxM1* deficient cells also revealed polyploidy phenotype, reinforcing the relevance of this gene in DNA replication and maintenance of genomic stability[17], [25], [28], [40].

Some studies were developed to understand *FoxM1* role during development in mice by generating *FoxM1* null mutant mice. In these studies, embryos lacking *FoxM1* died *in utero*[25], [32], [51]. The hearts of the embryos shown a reduced size, fewer and disorganized cardiomyocytes, which had large polyploid nuclei, thin myocardium, ventricular dilatation and hypoplasia[26], [32], [49]. This data lead Bolte et al. 2011 to conclude that *FoxM1* shows a cell-autonomous function during cardiac development[26]. *FoxM1* depleted embryos also revealed multiple hepatic alterations[25]. Kim et al. 2005 also described pulmonary lesions[51] and, in 2009, Ustiyan and colleagues proved that conditional deletion of *FoxM1* in mice smooth muscle cells induced mortality in most of the embryos. Mutated pups had severe pulmonary hemorrhage and defects revealing the importance of *FoxM1* in this animal model for embryonic development of smooth muscle structures[48]. In 2012, Ustiyan and collaborators also demonstrated, using a mice model, that *FoxM*1 is essential for proliferation and differentiation in airway formation, through a conditional deletion of *FoxM1* in Clara cells[47]. In mice lacking *FoxM1* along pancreatic development, β-cell proliferation suffered a significant reduction, the animal's β-cell size and mass displayed a gradual decrease with age and presented impaired glucose intolerance, diabetes and premature senescence[52]. Accordingly, alterations in Fox genes such as *FoxM1* can induce human genetic diseases including cancer and play an important role in aging[17], [45].

1.2 Senescence and aging

Aging is a natural and gradual process characterized by the accumulation of molecular and cellular impairment resulting in the loss of fitness with a cost in homeostasis, functionality and reproductive activity[53]–[57]. This natural course of events can be a risk factor to many diseases[55]–[58].

The understanding of the molecular origin of aging, and how this process could be eventually reverted or delayed, is a major challenge in biomedical science. López-Otín *et al.* 2013 defined cellular senescence as a hallmark of aging, since the number of senescent cells increases with age[56]. The contribution of senescent cells to aging can be perceived by their accumulation and contribution to compromise the homeostasis of a tissue; the decline in the regenerative capacity in damaged and atrophic tissues; and the secretion of senescence-associated secretory phenotype (SASP), composed by cytokines and chemokines, matrix-remodeling proteases, and growth factors that propagate the deterioration of the tissue[54].

In 1961, Hayflick and Moorhead first demonstrated that primary human diploid fibroblasts cultured had limited growth capacity. At a certain point cells suffered an irreversible cell cycle arrest called cellular senescence[54], [59], [60].

In 2011, Baker and coworkers, selectively depleted p16 positive senescent cells from a mutant BubR1 progeroid mouse and they reported to delay age-related diseases in tissues such as adipocytes, skeletal muscle and eye[61].

Cellular senescence includes growth arrest in response to several stress factors[59]. This process can be associated with telomere shortening, DNA damage, reactive oxygen species (ROS), exposure to toxins and other mitogenic and metabolic stressors[54], [58], [59], [62]. Overall, cell senescence can be defined as a cell cycle arrest including specific and characteristic phenotype and physiology, functional decay, and secretion of a complex proinflammatory secretome, SASP[53], [58], [63], [64].

However, studying senescence *in vivo* remains a challenge, since there is a lack of strong and consistent markers for this process[58]. Van Deursen stated that there is still a lack of information regarding the variance in SASP composition, spatial and temporal patterns of normal and aged tissues, and the consequences of eliminating senescent cells, considering that they also play a role in tissue development and repair[65].

When there is accumulation of damage in the tissues, the number of senescent cells and SASP also increases[58]. Senescence is achieved by the activation of several networks including p16/retinoblastoma protein (Rb) and p53/p21[54], [58]. These elements of tumor suppressor pathways can then be considered biomarkers of senescence[54].

In response to cellular stress there is induction of apoptosis, a transient cell cycle arrest or senescence[59]. In the case of apoptosis, Cooper 2012 reviews the alterations in caspase activity in models of aging, including an increase in Caspase-3 activity. This caspase activity was shown to be increased in the hippocampus of aged rats[66]. Baar et al. 2017 also used Caspase-3 cleavage as a marker for apoptosis in senescent cells[67].

However, cells can also senesce in response to stress. Following DNA damage, which is one significant stress signal, there is accumulation of H2Ax, a histone variant phosphorylated in serine 139 by phosphoinositide in the presence of DNA double stranded breaks[68], and p53 binding protein to recruit DNA repair proteins to the damaged site[37], [58] and an activation of p53. p53 induces persistently p21 that blocks Cdk4/6 leading to hypophosphorilation of Rb and cell cycle arrest[53], [59], [69]. In addition, p21 can act in an anti-apoptotic manner during stress being responsible for SASP components[53].

Senescent cells are thought to be linked to abnormal intercellular communication due to their inflammatory response[54], [58]. In aging, SASP is responsible for persistent chronic inflammation (called *inflammaging*) and age-related phenotypes. These secretome elements depend on the cell type affected and senescence inducer[58], and include interleukins (IL) IL-6, considered as a pathogenic

factor[54], Il-7 and IL-8. Therefore, while senescent cells can influence adjacent cells by direct communication, SASP allow them to have an autocrine and paracrine effect[53], [58], [63].

The elimination of senescent cells in several tissues lead to reduced levels of IL-6 and IL-1β (markers of chronic inflammation)[67], [70]. Pro-inflammatory factors such as IL-1α, IL-6, tumor necrosis factor (TNF), and nuclear transcription factor kappa B (NF-κB) were found to increase in tissues through aging[58]. Authors have stated that senescence associated IL-6 is the major activator of JAK/STAT3 signaling pathway[71]–[73].

In 2012, Jurk and colleagues described the presence of senescence biomarkers such as H2Ax, activated p38MAPK, IL-6 secretion and Senescence Associated-β-Gal activity in Purkinje cells and cortical neurons of elderly mice, through induction by p21[74].

1.2.1 *FoxM1* and aging

FoxM1 has been described as downregulated in human fibroblasts from elderly and Hutchinson–Gilford progeria patients[50]. *FoxM1* downregulation in hepatic tissue contributes to the development of early-aging phenotypes in adult mice. Those phenotypes can be rescued by overexpressing *FoxM1*[75]. After partial hepatectomy in old mice, hepatocyte proliferation for liver regeneration is low. However, when *FoxM1* levels are increased, liver regeneration is restored[76], [77]. Similarly, Kalinichenko and collaborators also concluded that boosting FoxM1 levels has a major impact in the increment of cell proliferation in aging and lung diseases[78]. In 2008, Stress-induced senescence was also avoided in mouse fibroblasts through overexpression of *FoxM1*[79].

BubR1 is a spindle assembly checkpoint protein encoded by *Bub1b,* a downstream target of *FoxM1*, and an essential gene for mitosis[80], [81]. Total loss of BubR1 causes embryonic lethality in mice. Hypomorphic animals in both alleles develop cachexia, lordokyphosis, bilateral cataracts, muscle atrophy, shorten life-span among other aging-related phenotypes. Mice with this genetic background also exhibit an early accumulation of senescence markers as p16, p21, p53, SA-β-gal, chromosome instability and aneuploidy[80]. This study suggests that BubR1 has a role in aging and, therefore, *FoxM1* as an upstream effector may have a part in this process.

In senescent keratinocytes, the expression of *FoxM1* is decreased, *in vitro* and *in vivo*. When *FoxM1* is depleted, it induces cellular senescence in proliferating epithelial cells. Skin biopsies from younger subjects also reveal a higher expression of *FoxM1* comparing with samples from older patients[44].

Recently, Macedo *et al.* 2018 have linked *FoxM1* decrease with aging progression in human and mouse mitotic cell samples. In this study, the authors depleted *FoxM1* in young human fibroblasts and found that cells recapitulate aging-associated mitotic defects, aneuploidy, SASP and senescence-associated gene expression levels. Interestingly, when Macedo and colleagues restored *FoxM1* levels in old cells, they were able to rescue the cellular aging phenotypes previously encountered, improving cell autonomous and non-autonomous effects between mitotic fidelity and senescence. This work proved that *FoxM1* is essential for modulation of mitosis and senescence pro-inflammatory phenotypes and to promote proliferation in older cells[82].

1.3 Zebrafish model to study cellular senescence

Zebrafish (*Danio rerio*) experience senescence and display a similar gradual aging pattern as humans, making it a promising model, not only to study aging pathways, but to parallel it to human. This vertebrate has a slightly larger life span than other models such as rodents[83]–[85], is inexpensive and easy to maintain for high throughput mutational analysis[83], [85]–[87]. Zebrafish has high fecundity and produces transparent eggs that grant accessibility to organogenesis and phenotypic changes through time[83], [86], [88]–[90]. Embryonic development occurs rapid and externally and genetic

manipulation is easily achieved[86], [87], [91]. Moreover, the zebrafish genome is fully sequenced and this species have at least one orthologue for 71% of human protein-coding genes[85], [87], [92].

This model allows the generation of mutant genetic backgrounds using numerous molecular genetic techniques[86], [88]. Zebrafish exhibits the same senescence associated markers and phenotypes as humans[83], [85], such as: DNA damage visualized through the presence of phosphorylated H2Ax at serine 139, increased p21 expression levels[93], increased β-gal levels[94], lipofuscin accumulation[87], [94], and telomere shortening[93], [95]. These senescence markers were found in diverse tissues, including muscle, in both species. In addition, skeletal muscle degeneration and other muscle abnormalities[90], [93], [94], spinal curvature, age-dependent decline in reproductive and regenerative capacity[86], [87], [94] occur in both human and zebrafish. These characteristics make the zebrafish a suitable model to study senescence.

1.4 Skeletal Muscle

Skeletal muscle is a major anatomical component in the human body. The proportion of this tissue is even higher in zebrafish, where skeletal muscle can take up to 80% of the body mass[96]. This tissue is responsible for locomotion and metabolic homeostasis[96], therefore, a disturbance on this tissue's functions has a significant impact on the organism fitness.

During aging there is loss of muscle mass over time resulting in sarcopenia, normally associated with decreased mobility and augmented morbidity[85], [93], [97], [98]. This decrease in muscle mass is considered a hallmark of aging[99]–[101]. Due to the effect of aging processes the skeletal muscle has been used to study cellular senescence, aging and age-related diseases. Mechanisms involved in modified gene expression, proteostasis, metabolism and stem cell exhaustion occurring in natural aging process, oppose regenerative and muscle repair processes[97].

1.4.1 Muscle regeneration and repair

In mammals, skeletal muscle myogenesis depends on muscle progenitor cells expressing *Pax3* and *Pax7* responsible for myogenic specification[102]. After embryonic development, progenitor cells become quiescent and adopt a characteristic anatomical position between the sarcolemma and basement membrane of myofibers – therefore their designation by satellite cells (SC)[103]. These cells can be easily identified by expression of markers such as *Pax7*, *hepatocyte growth factor (Hfg)*, *cmet* and *myogenic factor 5* (*Myf5*) (reviewed in [104]**)**. SC become activated and undergo asymmetric division in response to stress through activation of several muscle regulatory factors (e.g. *Myf5*, *MyoD*, *myogenin* and *MRF4*), cytokines (e.g. IL-6) and their downstream effectors[97], [102]. New myoblasts proliferate, migrate, undergo differentiation and ultimately fuse to myofibers repairing the tissue and assuring tissue homeostasis (reviewed in [102], [103]). In several studies, depletion of *Pax7* in SC resulted in loss of regenerative capacities after injury and transplantation[105]–[107].

Gurevich et al. 2016 identified zebrafish SC population and visualized regeneration *in vivo*[108]. In Zebrafish, *pax7a* is also expressed in the external cell layer (ECL) where cells contribute to muscle growth throughout life[109], [110].

Some groups explored and visualized *pax7* positive cells in adult zebrafish skeletal muscle and isolated myofibers from adult fishes[109], [111], [112]. Zebrafish has two *pax7* paralogue genes, *pax7a* and *pax7b*[113], [114] expressed in the ECL and quiescent muscle stem cells and progenitors (reviewed in [104]). *cmet* and *pax7a* are expressed in deep myotomal cells and the latter can be used to investigate cell dynamics in the regenerative environment[108]. Regarding *Pax7a* and *Pax7b*, Pipalia and colleagues 2016 revealed that *Pax7a* positive cells initiate myofiber formation and *Pax7b* positive cells contribute to fiber growth after injury[115]. Berberoglu and coworkers also demonstrate that *Pax7*

is implicated in muscle regeneration in zebrafish since *Pax7a* and *Pax7b* double mutants revealed defective muscle repair[116].

The extension of the stressful event may influence the cellular response. For instance, *Pax7a* positive cells were shown to respond to a large injury implying that a different population may be responsible for small damages[117]. Similarly, the developmental stage affects muscle regeneration[104]. The activity of SC becomes impaired with aging namely due to DNA damage repair defects and abnormal SC niche signaling, decreasing skeletal muscle regenerative capacity[97], [118], [119]. Knappe and collaborators 2015, used a zebrafish transgenic line expressing E-GFP under the control of *Pax7a* promoter and verified that cell regeneration is slower in older individuals[117].

Gurevich et al. 2016 used another zebrafish transgenic line with differentiated muscle fibers marked with mCherry (red fluorescence protein) and *myf5* positive cells labelled with E-GFP. This study's results validate that the stem cell niche environment impacts their function. After injury, healthy fibers guide progenitors to the injury site, where they differentiate into myofibers. The importance of uninjured myofibers is of most relevance since they seem to direct regenerative processes in injured skeletal muscle[108].

Regeneration is a broad mechanism, dependent of multiple factors and involves numerous components, thus muscle formation can include SC independent mechanisms[120], [121]. In particular, previous regeneration studies in different tissues revealed the existence of a "de-differentiation process" from mature cells without progenitor cell recruitment[120]–[124]. Kahana group observed this process in adult zebrafish extraocular skeletal muscle, which is of relevance since it indicates that some skeletal muscle cells are repaired through this progenitor independent manner[120], [121].

1.4.1.1 Signaling pathways in muscle regeneration and repair

In aging-related muscular defects the regenerative response may be impaired due to chronic inflammation. In aging, senescent myofibers secrete several molecules, altering the tissues' environment and affecting SC functions[97], [100], [125]. One of the most important pro-inflammatory cytokines involved in senescence is IL-6, released in the SASP. This interleukin plays a role during initial muscle repair and regeneration[100], [102], [126], [127]. IL-6 has been associated to muscle atrophy[73], [128], even though it also regulates satellite cell-mediated hypertrophy[72].

In 2014, studies from Sacco's and Rudnicki's teams have complementarily shown that Janus kinase/signal transducers and activators of transcription (JAK-STAT) signaling has an essential role during muscle regeneration[100], [126]. This pathway responds to extracellular IL-6 through membrane receptors[97], [103], [119]. JAKs then phosphorylate STAT proteins that move to the nucleus and activate transcription of target genes[129] (Figure 1.3).

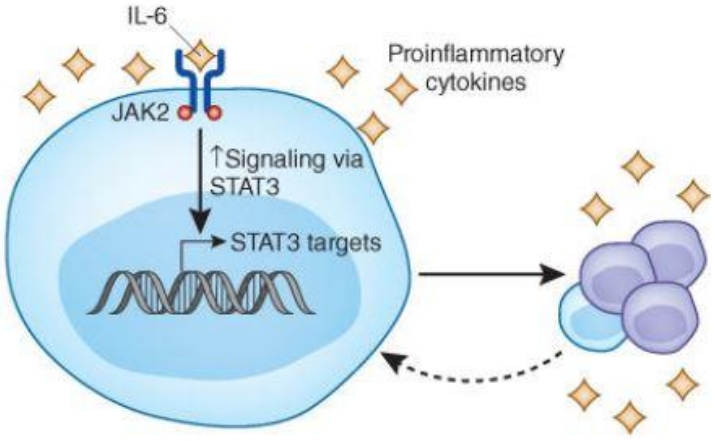

Figure 1.3 IL-6 activation of JAK-STAT pathway. This interleukin binds to the membrane receptor activating JAK which increases STAT3 signaling and activates transcription of target genes. Vicinity cells also respond to this pathway activation. (source: Doles and Olwin 2015)

This pathway is involved in the transduction of extracellular signals in proliferation, migration, survival, apoptosis and even oncogenesis[130]. JAK-STAT is responsible for skeletal muscle differentiation, thus its activation by interleukins affects *MyoD* and stimulates myoblast proliferation and differentiation[126, 131]. JAK-STAT appears to be activated in SC from human aged skeletal muscle[98, 132].

Price and colleagues isolated SC from juvenile, young and old mice and reported increased JAK-STAT signaling transduction with age in muscle. During aging, JAK-STAT activation and expression of its target genes seems to be increased in myogenic *Pax7* positive cells. In this aging study, inhibition of this STAT3 rescued muscle regeneration alterations of old mice and prompted SC increase[100].

Tierney and collaborators also propose that IL-6, as an aging-associated stress molecule, contributes for JAK-STAT pathway reducing muscle regenerative function. The authors depleted STAT3 in SC and demonstrated that this pathway regulates *MyoD* expression and, concordantly to the previous study, JAK-STAT inhibition lead to an improvement in muscle regeneration, inhibiting differentiation and enhancing *Pax7* positive cells self-renewal[126].

The studies from both Sacco's and Rudnicki's groups shown a beneficial effect for proliferation in the deletion of STAT3. However, they used transient STAT3 inhibition through chemical inhibitors or siRNAs which may impact STAT3 activity in other cell types, as inflammatory macrophages in the stem cell niche[133].

In 2010, Zhang and coworkers demonstrated that STAT3 is essential for granulocyte production in granulopoiesis. STAT3 also enhances hemopoietic stem cell expansion under regenerative conditions[134]. Furthermore, IL-6 mediated activation of STAT3 signaling promotes airway epithelium regeneration after damage[135], suggesting that under stressful conditions, STAT3 is an important mediator of cell regeneration. Additionally, other signaling pathways, as mitogen-activated protein kinase (MAPK)-p38, seem to change during aging in SC and impair regeneration[136, 137]. In 2011, Parise group also demonstrated an increase in activation of STAT3 pathway after muscle damage in human SC. This increment was also observed in the expression of downstream target genes driving specific-cell proliferation and muscle repair after damage[138]. These studies may suggest the existence of a non-autonomous effect after a stressful event such as injury or even aging processes, leading to regeneration and repair of the tissues.

More recently, Zhu et al. 2016 ablated STAT3 in *Pax7* positive cells and observed an impairment in muscle stem cell renewal after damage. Muscular stem cells shown early differentiation rather than proliferation upon STAT3 depletion which may be a result of downregulating this pathway's target genes such as *Pax7*. This team deleted STAT3 through a *Pax7* Cre-mediated manner resulting in the depletion of STAT3 in muscle stem cells and myofibers. Hence, it does not rule out a possible role of STAT3 signaling in myofibers during muscle regeneration since they integrate the muscle stem cell niche[133].

1.5 Genome editing tools

Currently, the generation of new models of disease and methods for gene function assessment, important in biological and biomedical research, depends on genome editing tools[139]–[141]. The terms "genome editing" refers to the nucleotide manipulation of the genome using nucleases[139, 142]. Engineered zinc finger nucleases (ZFNs), transcription activator-like effector nucleases (TALENs) and clustered regularly-interspaced short palindromic repeat (CRISPR)-Cas9, enable the generation of efficient and specific gene manipulation[143, 144].

These genome editing techniques rely on the induction of DNA double stranded breaks (DSB) at specific sites (Figure 1.4). Since DSB are toxic[145], cells rapidly respond through the non-homologous end joining (NHEJ) repair pathway. This is an error-prone process that leads to random insertions or deletions (indels) in the DSB locus, which can result in frameshift or non-sense mutations in coding genes, with the potential of silencing genes[140], [142], [144]–[149].

ZFNs were discovered in 1996 and firstly used in Drosophila[150], [151] and mammalian cells[152]. These endonucleases were the first to be applied in zebrafish[143], being first described in 2008 for targeted gene knockout[149]. ZFNs recognize DNA through a zinc finger mediated DNA binding domain and cleave the genome with a FokI domain with nuclease activity[142]. These endonucleases are designed in pairs, only allowing cleavage through FokI nuclease dimerization, when both pairs identify DNA strands adjacently[143].

TALEN was first discovered in plant pathogens[143], [149] and first described in zebrafish in 2012[153]. This endonuclease is formed by fusing the nuclease domain of FokI to a DNA binding domain with multiple identical repeats from the TALE protein. Each TALE repeat binds to a specific nucleotide through repeat variable di-residues (RVD) allowing DNA recognition[140], [143]. In a similar process to the ZFNs, FokI dimerization only occur when TALENs are paired[143], [149].

CRISPR associated with the Cas9 endonuclease is a genome editing tool used by bacterial immune systems as a defense mechanism against virus[154]–[156]. In this protection strategy, bacteria integrate foreign DNA (spacer) between 5'-NGG-3' PAM (protospacer adjacent motif) sequences specific from infecting virus. Therefore, when the virus attacks the same bacteria, the latter will produce crRNA (complementary sequence to the spacer) and tracrRNA (transactivated CRISPR RNA) and create a complex with Cas9 protein, generating what is normally designated as Cas9 holoendonuclease[145], [155]. This complex has a domain that binds to the genomic PAM, it recognizes the spacer and matches to the genomic virus DNA sequence. Lastly, the Cas9 makes a DSB in the genomic virus DNA sequence near the PAM and deactivates the aggressor DNA[145]. This natural mechanism has been used and optimized for genome editing in the last few years. There are several types of structurally and mechanically different CRISPR/Cas systems[154]. The type II system, using a Cas9 and a guide RNA (sgRNA) which results from the merge of crRNA and tracrRNA, is the most used for genome editing[144], [154], [155], [157], [158]. In this system, a previously designed sgRNA for a target region in the genome is co-injected with Cas9 mRNA or protein into the cell[145], [147], [157], [158]. In the cellular nucleus, the sgRNA anchored to the Cas9 protein allows the recognition of the target region in the genome (complementary to sgRNA) next to a PAM sequence. This complex unwinds the two strands of DNA and cleaves them[145], [155]. As referred before, this error-prone process leads to random mutations with the potential of silencing genes[144]–[147].

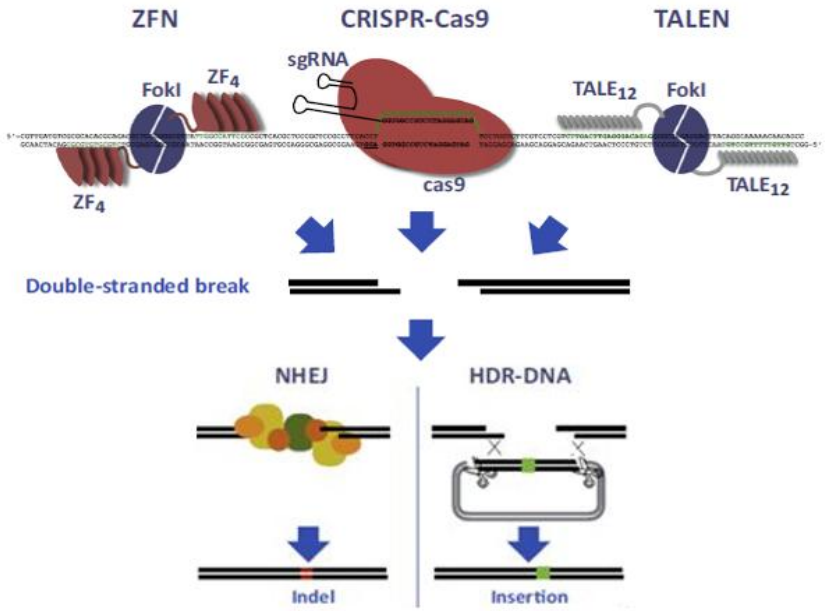

Figure 1.4 Schematic view of genome editing techniques and DNA repair mechanisms. On the upper left there is a ZFN mechanism of DNA editing through FokI coupled to two zinc finger guides, one on each strand of genomic DNA. On the upper centre there is a Cas9 protein coupled to a small sgRNA, recognizing and binding to the genomic target sequence. On the other hand, on the upper right there is FokI coupled to two TALE recognizing the region on DNA. All genome editing techniques allow DNA DSB, imprecisely repaired through Non-Homologous End Joining leading to indel formation. If a DNA template is available, it can also be inserted in the broken DNA region by Homology Directed Repair. (Adapted from Li et al. 2016)

ZFN is an expensive technique, difficult to design[141], it has a high failure rate generating assembly of both endonucleases[143] and there is no guarantee that the protein will be mutagenic *in vivo* since specificity of each protein is variable[145]. TALEN genome editing is more reliable and efficient than ZFN, with less off-targets[143]. However, FokI has been reported to be sensible to DNA methylation[145] and although design is easier than ZFNs, cloning is laborious[141]. Both genome editing techniques require a complex design of two new proteins for each target site[143], [156] and are not fit for high throughput mutagenesis[148]. CRISPR/Cas9 emerged as an easy to design and implement system, only requiring the design of a 20 nucleotide sgRNA[141], [144], [148], [156], simple, economical, scalable[144], [148], [159] with comparable or greater efficiency and more effective on methylated DNA[141], [156]. This mutagenesis technique allows targeting multiple genes at once[148] with higher transmission rates comparing with the abovementioned systems[144], [156] and low potential off-target effects[141], [144], [160].

Although morpholino (MO) is still considered by some as the traditional toolset for complementary functional validation of gene function[144], [149], in zebrafish its use is limited to processes at early developmental stages (0-120hours post fertilization [hpf]) [144], [161]. Several studies have shown that even though morpholinos allow a rapid and effective study of gene function[161], phenotypes often result from off-targets[143], [148], [162] and ≈80% of gene knockouts did not mimic MO phenotypes for the same gene[143], [144], [148], [162]. Rossi and colleagues in 2015 propose that, in a complete gene knockout, a genetic mechanism of compensation by other related genes may occur ablating the phenotypes observed in morphants for the same gene[143], [144], [163]. Thus, morphants cannot precisely recapitulate *in vivo* knockout phenotypes.

1.5.1 CRISPR/Cas9 in zebrafish for gene knockout

To generate a gene knockout in zebrafish in a cheap and high throughput manner, CRISPR/Cas9 technology and consequent NHEJ repair pathway is the easier and more effective technique. The CRISPR-Cas9 was originally adapted and used in zebrafish by Hwang and colleagues in 2013[158]. In this study, they targeted zebrafish *fh* gene by designing a sgRNA complementary to the gene's sequence and microinjected this sgRNA with synthetized Cas9 mRNA in one-cell stage embryos. They observed indel formation at all concentrations tested in almost all embryos. The authors found high frequencies of indels in most of the targeted sites tested and a significant efficiency mutagenesis[158]. Several tools were created for CRISPR/Cas9 implementation in zebrafish[144], [145] making this system a simpler, more efficient and inexpensive alternative for genome editing in this model organism.

1.5.1.1 Tissue-specific gene targeting

Ablain et al. 2015 generated the first tissue-specific (TS) somatic gene knockout (KO) in zebrafish. In their study, the zebrafish *urod* gene was disrupted under the control of several TS promoters driving Cas9 to simulate the predicted porphyria phenotype[146]. Ablain and colleagues, in 2015, designed a system containing a zebrafish codon optimized Cas9 [159] under the control of the promoter of a specific gene (*cmlc2*), an ubiquitously expressed sgRNA and an E-GFP expressed transgenesis marker. The Gateway recombination strategy (described in [164]) was used to generate the vector, and the Tol2 technology allowed the vector integration in the embryos' genome in a transposase mediated way[146], [165]. This transgenesis system allied with the constructed vector is an easy and efficient way to express both Cas9 and the sgRNA in a TS manner using a single transposon[145], [146].

Another method, by Yin et al. 2015, used two different Tol2 transposons, one with a TS expression of Cas9 and another with the sgRNA under the control of an ubiquitous promoter. In this strategy, only animals carrying both transposable elements were mutants for the target gene in the targeted tissue[166]. Although this last approach generates Tol2 elements phenotypically silent when isolated, allowing stock maintenance and flexibility for usage in other studies, it implies the generation of two different transposons, making it a laborious technique[145]. Yin et al. 2015 technique also requires mating two stable lines, expressing each of the transposons created, to generate TS mutants[145], [166]. In this project we will adapt the method carried out by Ablain and colleagues 2015 (see Chapter 2, section 2.3), since it admits more immediate results than Yin et al. 2015.

1.5.1.2 Mosaic loss-of-function assay

Zebrafish mosaic analysis is an efficient way to study gene function in zebrafish[167]. A mosaic is an organism containing cells with different genotypes[167], [168]. Creating mosaic embryos is especially important when the mutated target gene may lead to early embryonic lethality[167]. Thus, mutating only a few specific cells might allow wild type cells to partially rescue the loss of the target's function. The mosaic analysis in zebrafish can help determine if a gene acts cell autonomously or cell non-autonomously and identify late functions for genes essential in early development. Mosaicism is also important to test cell commitment to its fate, characterize the properties of signaling molecules, identify maternal functions of essential genes and evaluate cell behaviors[167], [169]. In zebrafish, mosaics can be created through direct genetic manipulation in groups of cells or by transplantation of genetic modified cells into a host. In the first approach, simply by injecting a DNA construct containing gene targeting system under the control of a TS promoter in a one-cell staged embryo. This way, the gene targeting system is stochastically inherited after injection, generating targeted cells and non-targeted cell. To visualize the effect through time the altered cells may be labeled using fluorescence proteins. The second technique, transplantation, results from transferring cells from a

donor embryo to a host producing a chimera[167]. A chimera is an organism containing cells derived from different individuals (donors) resulting in distinct cellular genotypes[168]. To create chimeras, labelled cells from a donor embryo are co-transplanted into a single host embryo[167].

1.6 Project goals

FoxM1 is a well-studied gene, known as the master regulator of the cell cycle and implicated in several cellular processes and pathologies, including diabetes and cancer. However, the role of this gene in senescence and aging *in vivo* has not been completely understood. Thus, the main objective of this project is to ascertain the role of zebrafish *foxm1* in cellular senescence and aging *in vivo*. To accomplish that, we used zebrafish as an *in vivo* model organism and the CRISPR-Cas9 system to target *foxm1* functional domains. CRISPR-Cas9 technology required designing and testing sgRNAs, which were injected into one-cell stage embryos raised and outcrossed to identify founders, i.e. animals carrying mutations. Resulting offspring were raised to generate stable mutant lines. Since zebrafish is a model organism that reaches sexual maturity three months after fertilization, obtaining homozygous mutants was not viable in this project time span.

Because the loss of function of *foxm1* may have a deleterious effect at early developmental stages, we aimed to further explore this gene function in a TS matter. To do so, we created a CRISPR-Cas9 vector adapted from Ablain *et al.* 2015 targeting *foxm1* in differentiated muscle cells. First, we wanted to understand if *foxm1* was functionally active in differentiated muscle cells. Then, and considering that senescent cells normally produce non cell-autonomous signals, we performed mosaic loss-of-function assays aiming to understand wildtype and *foxm1* mutant cells interactions.

In order to understand zebrafish *foxm1* role in senescence, several markers were also tested through immunohistochemistry and real time-quantitative polymerase chain reaction (RT-qPCR) in mosaic larvae for *foxm1* TS targeting.

Chapter 2. Materials and Methods

2.1 Zebrafish maintenance

Wild-type Tugbingen (TU) zebrafish were used in the experiments, as well as a Tg(elavl:E-GFP) transgenic strain created in the, as a positive mutagenesis control. All fishes were maintained in a recirculating system under controlled conditions in the zebrafish facility of Instituto de Investigação e Inovação em Saúde da Universidade do Porto (i3S), and fed with commercial Zebrafeed 400-600µm (Zebrafeed, Sparos). The conditions were approved by the i3S Animal Welfare and Ethics Review Body and Direção Geral de Alimentação e Veterinária (DGAV).

Fish were kept under a 14:10h light:dark cycle in controlled filtered water (27ºC, 700µS, pH 7.0). For reproduction, a ratio of 3 females per 2 males was used. Fish were mated in the first hours of the light period. After spawning, embryos were incubated in embryonic medium (E3) (diluted 100x from stock solution; see appendix) with or without PTU supplementation (1-phenyl-2-thiourea) to delay pigmentation formation (diluted 100x from stock solution; see appendix)[170][171]. Embryonic staging was performed accordingly to Kimmel *et al.* 1995[172]. At 24 hours post-fertilization (hpf) all animals were disinfected with 0.036% sodium hypochlorite (Sigma-Aldrich) diluted in tap water, to be placed in the facility's nursery system after the fifth day post-fertilization. Up until 5 days post-fertilization (dpf), embryos were kept at 28ºC in petri dishes.

Zebrafish euthanasia was performed by gradually overdosing the embryos older than 5dpf with tricaine solution (MS-222; 300mg/L)[173], [174]. Prior to 5dpf the embryos were sacrificed in a bleach solution.

2.2. CRISPR/Cas9 system

2.2.1 Design of sgRNAs

Target sequences in the *foxm1* gene (ENSDARG00000003200) were selected through the CRISPRscan software (crisprscan.org[175]). The search was limited to the second (ENSDARE00000148522) and eighth (ENSDARE00000243528) exons of the zebrafish *foxm1* gene. Target sites were ranked according to their predicted efficacy and follow the structure5'-GG-N18 NGG-3' [158]. From the obtained list of sgRNAs, six sequences were chosen to target the first coding exon of *foxm1* and three to target the eighth exon of *foxm1*. sgRNAS were chosen by high scores and absence of off-targets. The eighth exon encodes the initial part of the FoxM1 transactive domain (TAD). A mutation in the orthologue region of the human gene leads to loss of FoxM1 activity[46].

For each target site a TAGG- was added at the 5´ of the oligonucleotides, as well as an AAAC- in the initial part of the reverse complement sequence in a 5'-3' orientation to form the required overhanging sequences (underlined) for cloning in the pDR274 vector (sequences ordered from Sigma-Aldrich) (Table 6.1 appendix). The sgRNAs used as a system positive control (sgRNAs against E-GFP) were previously designed and kindly sent by Atsuo Kawahara & Shin-ichi Higashijima[176].

2.2.2 Annealing and cloning into pDR274

Partially complementary oligonucleotides, designed for the sgRNAs, were annealed by mixing at a final concentration of 10µM, diluted into annealing buffer (see appendix). The solution was heated at 95ºC for 5 min and cooled at room temperature (RT). Simultaneously, pDR274 vector (Addgene #42250) was linearized using 5U of BsaI (10U/µL Anza^{TM}36 Eco31I, Thermo Fisher Scientific) in a 20 µL solution overnight (ON) at 37ºC. BsaI digestion creates non-compatible overhanging ends preventing self-ligation of the plasmid and promoting a correct insertion of the annealed

oligonucleotides in the ligation step by matching the overhanging ends of the oligonucleotides. A Tris Acetate EDTA (TAE)-agarose gel (1% agarose; TAE diluted 50x from stock; see appendix) was run with both non-digested circular plasmid and digested sample to check linearization state. The gel was visualized using a UV-transillumination (TFX – 35 M, VILBER LOURMAT) Image Lab software (Image Lab™ BioRad Version 6.0.0). The linearized vector was ligated with annealed oligonucleotides in a 1:10 proportion, in an ON incubation at 16ºC with 2.5weiss units of T4 ligase (5weiss U/µL Thermo Fisher Scientific) in a 10 µL solution.

2.2.3 *E. coli* transformation and positive colonies

The ligation product was used to transform chemically competent *Escherichia coli* (One Shot™ Mach1™, ThermoFisher). All the transformation procedures were performed under a sterile environment. The ligation product was added to bacteria in a 1:25 proportion and the mixture was incubated 30 minutes (min) on ice followed by a heat shock at 42ºC for 30 seconds(s) and incubated 2 min on ice. LB medium was added and the suspension was incubated at 37ºC for 60 min at 220rpm. Then, the culture was centrifuged at 500xg for 5 min RT and bacterial pellet was plated in LB agar with kanamycin (50 µg/µL) and incubated ON at 37ºC. The colonies were picked into liquid LB medium with kanamycin (50µg/µL) and incubated ON at 37ºC and 220rpm. Plasmid DNA was extracted from cultures using NZYMiniprep (NZYTech) commercial kit, according to manufacture instructions. Final DNA samples were quantified using NanoDrop™ 1000 and sequenced by Sanger Sequencing using the M13fw primer (5'-TGTAAAACGACGGCCAGT-3') to confirm oligonucleotide cloning in the plasmid backbone.

2.2.4 *In vitro* transcription of sgRNA using T7 promoter

After sequencing confirmation, the plasmid was linearized downstream the sgRNA. Briefly, plasmids were incubated ON at 37ºC with 6U of HindIII enzyme (20U/µL Anza™ 16 HindIII Thermo Fisher Scientific) and 3µg of DNA in a 20µL solution. Digested DNA was then purified using phenol:chloroform to exclude RNAses. In this purification procedure, to a 100µL DNA solution, phenol-chloroform (UltraPure™ Phenol:Chloroform:Isoamyl Alcohol [25:24:1, v/v],Thermo Fisher Scientific) was added and mixed. The solution was centrifuged for 5 min RT and 13000rpm and the upper aqueous phase was transferred to a new tube where 100µL of chloroform (Thermo Fisher Scientific) was added, mixed and then centrifuged at RT and 13000rpm for 5 min. Per 100µL of aqueous phase collected, DNA was precipitated by adding 10µL of sodium acetate (NaAc 3M, pH 5.2), two volumes of cold 100% ethanol (Merck Millipore). Solution was incubated for 2h at -80ºC or ON at -20ºC. The mix was centrifuged for 15 min at 13000rpm (4ºC) and supernatant discarded. Pellet was dried, resuspended in 15 µL of RNAse free water and quantified using NanoDrop™ 1000.

For *in vitro* transcription reaction of the sgRNAs, A T7 promoter present upstream of the sgRNA in the pDR274 was used. A reaction mix with a final volume of 50 µL was performed, mixing 5µL of dithiothreitol (DTT 50mM, Thermo Fisher Scientific), 5µL NTP mix (10mM; Thermo Fisher Scientific) and water up to 30µL were mixed and incubated at 37ºC for 5min. Purified DNA was added to the mixture (1.5µg) with 100U of Ribonuclease inhibitor (40U/µL NZYTech) and 60U of T7 RNA polymerase (20U/µL Thermo Fisher Scientific) which was incubated for 2 hours (h) at 37ºC. Afterwards, to avoid DNA presence, 2µL of DNAse I (50-375 U/µL Thermo Fisher Scientific) was added and incubated for 1h at 37ºC. Resulting RNA was stored at -80ºC to avoid quality decline and degradation.

2.2.5 *In vitro* transcription of Cas9 mRNA using SP6 promoter

The plasmid used for the Cas9 mRNA synthesis was the pCS2-nCas9n (Addgene #47929), which contained a SP6 promoter upstream of Cas9. The plasmid was digested ON at 37ºC with 6U of NotI enzyme (20 U/µL Anza™ 1 NotI, Thermo Fisher Scientific) in a 20 µL solution. The resulting DNA was purified with phenol:chloroform as described in section 2.2.4. The *in vitro* transcription steps were similar to the described on section 2.2.4. However, since Cas9 mRNA will be translated into protein it needs 5 µL of 5' CAP which is G(5')ppp(5')G RNA Cap Structure Analog (25mM; NewEngBio). For transcription 60 µL of SP6 RNA polymerase (20 U/µL Thermo Fisher Scientific) was used.

2.2.6 RNA purification

The transcribed RNAs were purified using a Sephadex column. Sephadex is a common matrix for gel filtration since it has a high binding capacity allowing the removal of unincorporated nucleotides during RNA synthesis with low molecular weight[177]. A 1mL syringe was sealed using autoclaved aquarium filter and filled with Sephadex suspension (66,6mg/mL, appendix). The syringe was centrifuged for 5 min at 4000rpm (4ºC) and refiled until the compact sephadex column reached the 0.6mL mark. Then a 0.5mL tube was inserted to the tip of the syringe, water was added to the top of the column and the water content in the tube was measured after centrifugation (5 min at 4000rpm at 4ºC). Once the recovery volume was similar to the introduced volume, a new 0.5mL tube was coupled to the tip of the syringe, *in vitro* synthesized RNA (sgRNAs or Cas9 mRNA) was transferred to the Sephadex column and the centrifugation was repeated (5 min at 4000rpm at 4ºC). RNAs collected were pipetted into a new tube and a new centrifugation was performed to the 0.5mL tube after adding an additional amount of water to aggregate the remaining purified RNA in the column in a similar process. After this, a phenol:chloroform purification was performed as described (section 2.2.4). Reagents used were RNAse free. Samples were quantified using NanoDrop™ 1000. A TAE 2% agarose gel was used to check for RNA degradation and presence of genomic DNA.

2.2.7 Micro co-injection of sgRNA and Cas9 mRNA

A mixture containing 150ng/µL of sgRNA and 200ng/µL of Cas9 mRNA and 10% of phenol red was prepared. Microinjections were performed using a 0.58x1.00x100mm glass needle (GB100F-10, SCIENCE PRODUCTS GmbH) prepared in a needle puller (PN-31, NARISHIGE). The tip of the needle was cut using a disinfected small high precision forceps under a binocular scope. The needle was attached to the microinjector (IM 300 Microinjector, NARISHIGE) and calibrated to inject 5nL in each pulse. One cell stage embryos were injected in the cell. Around 300 embryos per condition. GFP sgRNA+Cas9 mRNA co-injected embryos, were developed in PTU supplemented medium to allow visualization the E-GFP pattern. At 24hpf mortality rate was calculated in each batch of 50 embryos raised. Batches with more than 50% mortality in non-injected embryos had their samples excluded due to reproductive problems.

2.2.8 Genomic DNA extraction

At 24hpf embryos were dechorionated and transferred into tubes forming three groups of eight per condition. Embryos were washed with deionized water and dried as much as possible. The samples were incubated at 56ºC for 3h vortexing at 800rpm with genomic extraction buffer (appendix). DNA was precipitated by adding 100µL of 100% ethanol and incubating at -80ºC for 2h or ON a -20ºC. Afterwards, the mixtures were centrifuged for 10 min at 13000rpm (4ºC), the supernatant was removed and 70% ethanol was added. Samples were centrifuged for 2 min at 13000rpm, and the pellet

dried. DNA was resuspended in 20 µL of Tris EDTA+RNAse and incubated at 37ºC for 1h. Genomic DNA was stored at -20ºC.

2.2.9 Primers design and PCR

To detect the imprecise repair alterations in the genome resulted from the CRISPR/Cas9 system, the target site was amplified by a Polymerase Chain Reaction (PCR). The primers (Table 6.2 appendix) were designed using NCBI Primer Blast online tool (www.ncbi.nlm.nih.gov/tools/primer-blast) restricting the regions with Ensembl sequences (www.ensembl.org). The parameter used included primer size between 22-24 bases, primer melting temperatures between 59 and 64ºC and at least one GC clamp. The melting temperatures and self-complementarity was checked using the Oligo Calc online tool (biotools.nubic.northwestern.edu/OligoCalc.html). The PCR reaction was performed in a total volume of 20µL using 2.5U of a proof-reading *i*Max^{-TM} II DNA polymerase (5U/µL INtRON Biotechnology), 2 µL of dNTPs (10mM), 1X *i*Max^{-TM} II PCR buffer and 3µL of template DNA, according to manufacturer's instructions. A thermocycler (Veriti, Applied Biosystems) with the following conditions: initial denaturation at 94°C for 3 min, 30 cycles with denaturing at 94°C for 30s, annealing adjusted to the primers' melting temperature for 45s, elongation at 72°C for 1 min and a final cycle of elongation step at 72°C for 7 min was used. The samples were kept at 8°C until stored at -20ºC.

2.2.10 Polyacrylamide gel electrophoresis (PAGE) confirmation and sequencing validation

Samples were submitted to an additional denaturation and re-annealing process, to allow formation of homo and heteroduplexes[178]. When double stranded DNA (dsDNA) molecules suffer denaturation followed by a gradual re-annealing, each strand of DNA assembles with some other random single-strand of DNA. If the annealed strands are entirely complementary, homoduplexes are formed. However, when the sequence of the strands is different, heteroduplexes are formed. Mismatches in the re-annealed DNA strands alters the DNA conformation and migration rate leading the formation of new visible bands in the gel. The newly shaped dsDNA migrates slower than matched DNA (homoduplex) since there is formation of an angle between matched and un-matched DNA, allowing its identification[179] (Figure 2.1). Consequently, presence of *crispant* embryos is easily identified by the presence of heteroduplexes.

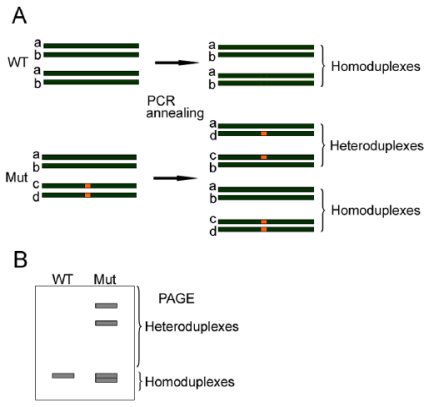

Figure 2.1 Overview of the PAGE analysis regarding the formation of ho homo and heteroduplexes.
(A) Darker bars represent DNA strands (a–d) have monoallelic mutations (orange) in the Mutant. After denaturation and re-annealing, homoduplexes and heteroduplexes will be formed from the Mutant DNA
(B) Homo and heteroduplex DNA fragments in PAGE. (source: Zhu et al. 2014)

An 8% PAGE was suitable for the desired fragment sizes according to several manufactures. Each PAGE gel was made of deionized water, Tris Borate EDTA (TBE) 100x diluted from stock (appendix), acrylamide/bis-acrylamid (29:1 NZYTech), 0.8 mg/mL ammonium persulphate (APS) 10% (BioRad)and tetramethylethylenediamine (TEMED; BioRad) (BioRad). Gel was polymerized into two glass plates with a 1.5Mm spacer and a 10, 12 or 15 comb for 45 min at RT. When polymerized, the gel inside glass plates was inserted into the PAGE tank filled with TBE 1x and the

comb was taken to load DNA samples with loading dye. Electrophoresis run for 1h30 at 150V (BioRad power supply). The gel was carefully removed from the glass plates and stained with Syber safe (SYBR™ Safe, Thermo Fisher Scientific) in a rotating bath of TBE 1x at RT. The gel was washed and visualized in a UV-transillumination (TFX – 35 M, VILBER LOURMAT) with Image Lab software. Bands were carefully cut at the UV-transiluminator and smashed with a pipette tip and 20 µL Tris-EDTA (pH8) and incubated for 2h at 800rpm. This mixture was amplified using primers for the CRISPR-Cas9 target site using the same PCR mixture and conditions previously described (section 2.2.9). The PCR product was sent for Sanger sequencing with the target site reverse primer. Confirmation of mutation in the heteroduplex samples was observed through overlapping sequences in the chromatogram downstream the PAM after sequence alignment with the MAFFT algorithm using Benchling online tool (benchling.com).

2.2.11 Search for *foxm1* crispant founders

When injected animals reached 3month age, search for founders was done by outcrossing fishes in a 1:1 females:male ratio. At 24hpf DNA from the embryos was extracted as described (section 2.2.8). The samples were amplified by PCR with the respective primers for that mutation (section 2.2.9). PCR product was run in a PAGE and DNA from the heteroduplex bands was extracted, amplified and sent for sequencing (section 2.2.10). Results were analysed using Benchling (benchling.com) (section 2.2.10) and TIDE (tide.deskgen.com) online tools. The amino acid content of zebrafish FoxM1 protein (available at uniprot.org/uniprot/F1QRF9) was aligned with the human FOXM1 protein (also online at uniprot.org/uniprot/Q08050) using NCBI COBALT alignment tool (available online at ncbi.nlm.nih.gov/tools/cobalt/cobalt.cgi) to further search for described specific protein alterations.

2.3 CRISPR/Cas9 *mylfpa*-specific knockdown and mosaic loss of function assay

2.3.1 Design constructs

In order to perform mosaic loss of function assays, tissue-specific mutagenesis vectors were created. In 2015, Ablain and colleagues described a tissue-specific construct consisting in three different modules[146]. We have adapted it and built a system with a strong promoter of differentiated muscle cells[169], [180], myosin light chain (*mylfpa*) (kindly given by David Langanau) driving the expression of Cas9 and E-GFP (Addgene #63155) and an ubiquitous promoter (U6) driving the tested sgRNA in a pDestTol2pA2-U6:gRNA backbone created by Leonoard Zon's group (Addgene #63157). The same vector without sgRNA was used (*mylfpa*:Cas9GFP) as a control condition. An additional internal transgenesis control (*mylfpa*:mCherry), with *mylfpa* driving the expression of mCherry (Tol2kit #386) was used in a pDestTol2pA2 backbone (Tol2kit #394) (Figure 2.2).

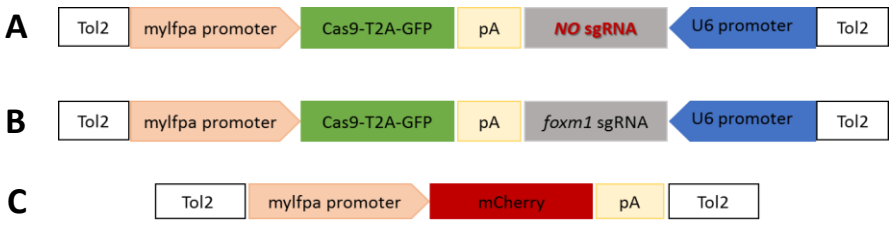

Figure 2.2 Schematic view of the three designed cloning vectors
(A) Representation of the empty vector
(B) Representation of the mutation vector
(C) Representation of the control vector (mCherry)

2.3.2 Gateway Recombination

To build constructs, three different entry vectors were recombined using the Gateway multisite recombination technique[164]. The Multisite Gateway® system for Three-Fragment Vector is a simple method that allows simultaneous cloning of three DNA fragments in a specific order and orientation to create an expression clone. In the recombination process, the enzyme catalyses *in vitro* recombination between entry clones with correspondent attL and attR sites. In the same reaction, the full recombined entry clone flanked with attL sites will recombine with the destination vector flanked with the correspondent attR sites to generate the expression clone[164].

For the construction of the mutation vector, *mylfpa* promoter was previously inserted in the 5' entry vector (prior to this project). The 5' mylfpa, 3' polyA (pA; Tol2kit #302) and middle (Cas9-T2A-GFP) entry vectors were recombined to incorporate the destination vector according the manufacter's instructions (Figure 2.3). Femtomole (fmol) amount of each vector was calculated in NEBioCalculator online software (nebiocalculator.neb.com) to obtain the recommended proportions of entry (10 fmol) and destination (20 fmol) vectors in a 10 µL of total volume of reaction. Vectors were mixed with 2µL of LR Clonase™ II Plus enzyme (Thermo Fisher Scientific) and incubated for a minimum of 16h at 25ºC using the thermocycler (Veriti, Applied Biosystems). The reaction was stopped through a 10 min incubation with addition of 1µL Proteinase K from the same kit. The construction of the mCherry vector followed the same protocol as the mutation vector, however the middle vector was pME-mCherry instead of Cas9-T2A-GFP and the plasmid backbone was pDestTol2pA2.

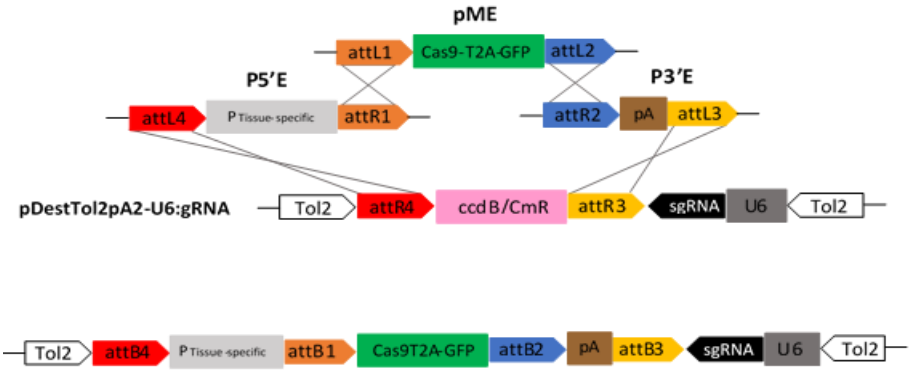

Figure 2.3 Schematic view of the recombination technique for the Mut vector and final expression vector (adapted from Kwan *et al*. 2007)

2.3.3 E. coli transformation and positive colonies

Recombination products were transformed using commercial *E. coli* Mach-1 competent bacteria similarly to the description on section 2.2.3, using ampicillin plates (100µg/µL).

2.3.4 Restriction confirmation, insertion of sgRNA and DNA purification

The sequence of the recombination product was confirmed in a 10µL using the restriction enzymes BamHI (5units from 10U/µL stock, Thermo Fisher Scientific) and EcoRI (6units from 20U/µL stock, Anza™ 11 EcoRI, Thermo Fisher Scientific) cutting multiple times each final vector. This allows visualization of diverse specific size bands in an agarose gel. The sgRNA previously tested was re-designed to have compatible ends with the backbone plasmid in which it would be inserted (Table 6.3 appendix). Compatible sequences were annealed for 5 min at 95ºC using a mix of each oligonucleotide sequence (100 µM) and annealing buffer. The sgRNA sequence was inserted in the recombination vector. Part of the expression vector (5µL) was digested using 6U of BseRI enzyme

(20U/µL, New England Biolabs) in a restriction reaction of 10µL for 1h at 37^{o}C as described by Ablain *et al.* 2015. The digested vector was purified using a commercial Gel Pure Extraction kit (NZYTech) to eliminate enzyme residues from the mixture as well as the region taken out of the vector. NEBioCalculator tool was used to obtain correct ratios of insert and vector. Purified digested vector was ligated overnight at 16^{o}C using of T4 ligase with the annealed sgRNA oligonucleotide insert in a 1:20 ratio following the protocol on section 2.2.2. Ligation product was transformed using Mach-1 competent bacteria and DNA was extracted as described (see section 2.2.3). To confirm the sgRNA cloning in the mutation vector DNA was sent for sequencing using the primer 5'-CCTCACACAAACTCTGGATT-3'[146] and then purified using phenol:chloroform (see section 2.2.4). The empty vector was sequenced after recombination, purified with phenol:chloroform and stored until use.

2.3.5 Tol2 transposase synthesis

The plasmid used for the Tol2 transposase mRNA synthesis was pCS2FA-transposase (Tol2kit #396). 8 µg of the plasmid was linearized ON at 37ºC with 6U of NotI enzyme (20U/µL, Anza™ 1 NotI, Thermo Fisher Scientific), 1x restriction buffer (Thermo Fisher Scientific) in a total volume of 20 µL. Resulting DNA was purified with phenol:chloroform (see section 2.2.4). The *in vitro* transcription steps were similar to the description in section 2.2.5.

2.3.6 Assessment of *foxm1* transcriptional levels in *mylfpa* positive muscle cells

In order to assess the expression of *foxm1* in differentiated muscle cells (*mylfpa*) used for the tissue-specific approach, several steps had to be performed.

2.3.6.1 *mylfpa* vector injection and ZED integrated fishes (F1) crossing

The *mylfpa*:mCherry construct was co-injected with Tol2 transposase mRNA, in a final concentration of 50ng/µL and 25ng/µL respectively, into one-cell stage WT TU embryos as described in section 2.2.7.

F1 fishes expressing dsRed2 in muscle cells derived from the activity of a ZED vector integration[181] were also crossed to generate F2 embryos. All embryos were maintained in E3 medium supplemented with PTU until selection of positive embryos at 24hpf in the injected larvae and at 72hpf in ZED F2 embryos.

2.3.6.2 Cell dissociation of zebrafish embryos

After selection of positive embryos under fluorescent light in a stereoscope (M205, Leica Microsystems), groups of 400 injected embryos were dechorionated in a 1mL solution with pronase at 0.3mg/mL at 28ºC for 15 min with gentle shake. Embryos were then washed with E3 medium to remove the remaining pronase. At this point, Ginzburg Fish Ringer was added to disrupt the embryos' yolks by pipetting up and down and shaking tubes at 1100rpm for 5 min. Samples of both injected and ZED embryos were placed on ice for 5 min and disrupted embryos were centrifuged at 300g for 30s. Pellet was resuspended in 300µL of dissection buffer (appendix) (filtered with a 0.22µm cellulose acetate membrane) and the mixture was centrifuged at 300g for 30s. Pellet was resuspended with a 32ºC pre-warmed digestion buffer (dissection buffer supplemented with collagenase II 0.125mg/mL and TrypLE Select 1x). The mixture was incubated at 32ºC with 800rpm shaking for 30 min and mechanical dissociation was performed by pipetting up and down every 5 min using low adhesion tips. The cell mixture was centrifuged for 4 min at 1800rpm (4ºC) and the pellet washed with PBS 1x. Washed mixture of cells was centrifuged at 1800rpm for 4min (4ºC) and the pellet was resuspended in

FACS buffer (PBS 1x, 0.5% BSA)). Cells in FACS buffer were filtered with a 40µm mesh cell strainer for a 5mL PP flow cytometry tube (FALCON) kept on ice.

2.3.6.3 Fluorescence-activated cell sorting (FACS)

The cell sorting was performed in the BD Aria II FACS cytometer. Cells were selected based on the RFP expression in the "purity" mode and collected into a tube with FACS buffer. After FACS, suspension was centrifuged at 300g for 10 min and the pellet was resuspended in TRIzol (Invitrogen, Thermo Fisher Scientific) vortexed and stored at -20ºC.

2.3.6.4 RNA extraction

Chloroform (100 µL) was added to 500µL of cells in TRIzol and centrifuged at 13300rpm for 20 min (4ºC). Then the upper phase was transferred to a new tube, isopropanol (300 µL) and 2 µL glycogen (4mg/mL, Sigma-Aldrich-Merck, Roche) were added, mixed and the samples precipitated for 2h at -80ºC or ON at -20ºC. Nucleic acids were centrifuged for 20 min at 13000rpm (4ºC). Pellet was dried. In a following DNAse treatment for 1µg of estimated RNA, 1 µL of DNAse I (Thermo Fisher Scientific) was used in a total 10 µL mix with 20U of Ribonuclease Inhibitor (40U/µL NZYtech), 0.1 µL of 50mM DTT and the resuspended nuclei acids. The solution was incubated at 37ºC for 30 min. To stop the reaction, 1 µL of EDTA 50mM was added per each 1µg of estimated RNA. Sample was purified with phenol:chloroform RNAse free and samples were centrifuged at 13300rpm for 5 min. The upper phase was carefully collected (without touching the interface) into a new tube and its volume quantified. RNA was precipitated with a mixture of ethanol and sodium acetate at -80ºC for 2h. The solution was centrifuged for 15 min at 13300rpm (4ºC). The pellet was washed with 70% ethanol and centrifuged at RT, 13300rpm for 10 min, dried and dissolved in water. Samples were quantified in NanoDrop™ 1000 and stored at -80ºC.

2.3.6.5 Reverse transcription (cDNA synthesis)

Samples were added to a PCR tube to be retrotranscribed with 400µL of SuperScript™ II Reverse (200U/µL Thermo Fisher Scientific) Transcriptase according to manufacturer's instructions. The amount of RNA used for RT-qPCR was 1.5µg in final solution of 20µL. RNA for semiquantitative PCR was 50ng in a solution of 10µL.

2.3.6.6 Semiquantitative PCR

A PCR reaction was performed using 2U of HOT FIREPol® DNA Polymerase (5 U/µL Solis BioDyne) according to manufacturer's instructions in a thermocycler (Veriti, Applied Biosystems) using the following conditions: initial denaturation at 95°C for 15 min, 35 cycles with denaturing at 95°C for 30s, annealing adjusted to the primers' melting temperature for 30s, elongation at 72°C for 1 min and a final cycle of elongation step at 72°C for 5 min. The primers for *eef1a1* and *foxm1* used were the same described for RT-qPCR (Table 6.4 appendix). The amplicon size was checked in an agarose gel (1%).

2.3.7 Co-microinjection of Tol2 transposase and constructs

To perform a mosaic loss-of-function assay as well as immunohistochemistry, WT TU zebrafish embryos were microinjected with a mix of two vectors and Tol2 transposase at 50ng/µL. The different conditions used were: empty vector (150ng/µL) + negative control vector (50ng/µL), mutation vector (150ng/µL) + negative control vector (50ng/µL) and negative control vector alone (50ng/µL) (vectors described on section 2.3.1). Microinjection procedure described in section 2.2.7.

2.3.7.1 Mosaic loss-of-function assay

The screening of positive embryos (expressing fluorescence) was performed at 24hpf under a fluorescent light stereoscope. This assay comprises observation and quantification of fluorescent cells at different developmental stages (24, 48 and 72hpf and 120hpf). Images at each timepoint were obtained with a Hamamatsu ORCA-Flash4.0 LT camera, and posteriorly analyzed using ImageJ tools to quantify the fluorescent cells. The number of fluorescent cells quantified at 24hpf represented a threshold from which the variation through time was normalized, from the different embryos and conditions.

2.3.7.2 RT-qPCR

To perform a quantitative expression analysis, RNA was extracted and retrotranscribed (sections 2.3.6.4 and 2.3.6.5) from different groups of embryos injected at 100ng/µL with mutation vector, empty vector and negative control vector (described on section 2.3.1) at 72hpf. The RT-qPCR had 3 biological replicates using 3 technical replicates per target gene. In the quantitative analysis, expression of *foxm1, cyclin B (ccnb1), p21, pax7a, stat3* and the housekeeping reference genes *tbp* and *eef1a1* was assessed.

2.3.7.2.1 Primers design

Primers for *foxm1* (from Sadler *et al*. 2007[182]*), cyclin B (ccnb1), p21, tbp* and *eef1a1* had been previously designed. *stat3* primers were described in Schiavone *et al.* 2014[183]. Primers for *pax7a* were designed using NCBI Primer Blast online tool (https://www.ncbi.nlm.nih.gov/tools/primer-blast/) with a forward primer between exons 2 and 3 from the Ensembl sequences (www.ensembl.org), primer size between 20-23 bases, primer melting temperatures between 57 and 63ºC and at least one GC clamp. Melting temperatures and self-complementarity was checked with Oligo Calc online tool (biotools.nubic.northwestern.edu/OligoCalc.html). Primers listed on Table 6.4 (appendix).

2.3.7.2.2 Primer efficiency, RNA verification, qPCR procedure and analysis

cDNA from 24hpf embryos was used to test primer efficiency, through serial dilutions of DNA (1:2; 1:20; 1:200; 1:2000). Primer efficiency was calculated using CFX Maestro 1.0 (BioRad version 4.0.2325.0418). cDNA was plated into a 96 real-time plate. According to manufacturer's instructions, a mix of primers (10mM) and iTaq™ Universal SYBR Green Supermix (BioRad) was prepared and added to the correspondent well. The program in the thermocycler (CFX BioRad 96-well system) was: denaturation at 95ºC for 3 min, 39 cycles of denaturation 95ºC for 30s, annealing 56ºC for 30s, elongation 72ºC for 30s and a melting curve obtention through raising temperature 0.5ºC per 10s between 55ºC to 95ºC. RNA samples were used as template in a RT-qPCR reaction to ensure the absence of genomic DNA, which could compromise the expression level analysis. Each plate contained a blank for each master mix (one per target gene) to ensure the absence of contaminants.

2.3.8 Immunohistochemistry

Immunohistochemistry for both cleaved Caspase-3 and H2AxS139ph were performed. However, the protocols (appendix) should be improved.

2.4 Statistical analysis

The statistical analysis was performed using Microsoft Office Excel and Graph Pad Prism 6 software. In the analysis it was assumed that sample groups presented asymmetrical variance, verified

by D’Agostino-Pearson e o Shapiro normality tests. The significance of differences among samples means was determined by an unpaired Mann-Whitney *t*-test. Statistical significance was determined for *P*-values lower than 0.05 considered significant.

Chapter 3. Results and Discussion

Zebrafish has been widely used a model to study human disease and aging[87], [93], [184]–[189]. In 2015, Houcke and colleagues have extensively reviewed its usefulness as a gerontology model. In this paper, they overview numerous studies demonstrating molecular, cellular and functional phenotypes of senescence in zebrafish characterizing this model's aging process[83].

In this dissertation we used zebrafish to study the role of *foxm1* in senescence. The main aim was to produce mutant cells and zebrafish mutant lines for this gene through CRISPR-Cas9 technology and describe the resulting phenotype. To validate the ability of this mutagenesis system to generate alterations in the fish genome at the laboratory, a transgenic line *Tg(elalv3:*E-GFP*)* previously generated by Fábio Ferreira, expressing E-GFP throughout the central nervous system, was used. These transgenic animals allowed to observe the alterations induced by the mutagenesis technique *in vivo*. In Figure 3.1, a loss of E-GFP expression can be visualized both in the brain and trunk of larvae co-injected with sgRNA against E-GFP and *in vitro* synthetized Cas9 mRNA, comparing to non-injected negative controls.

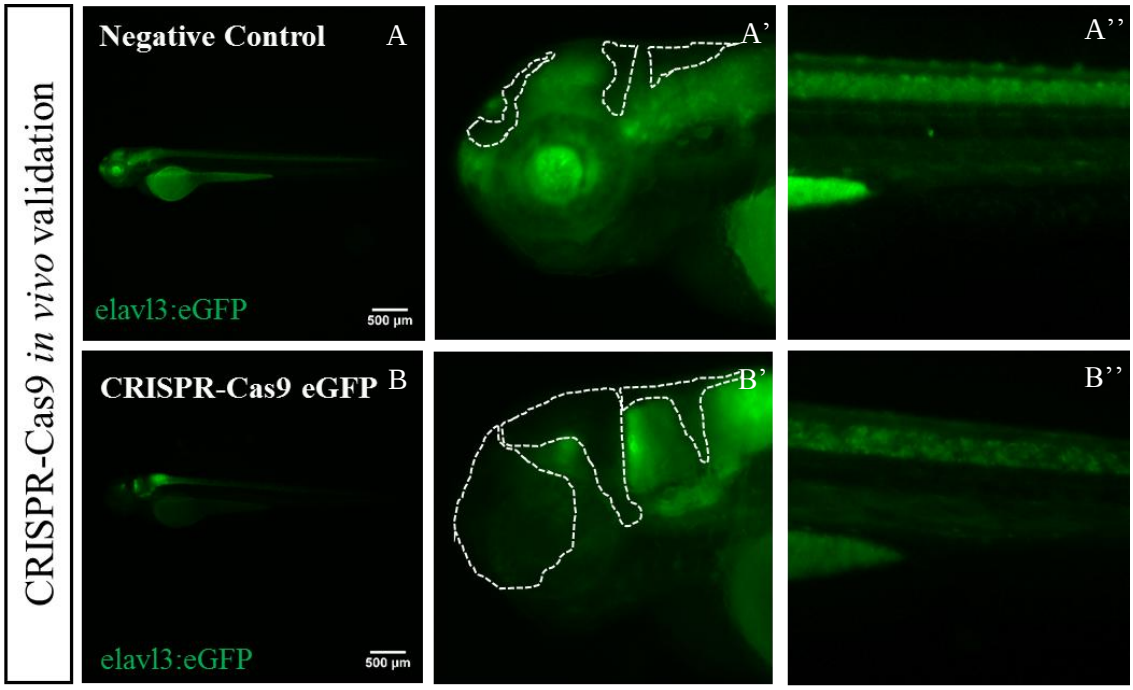

Figure 3.1 Validation of mutagenesis by the CRISPR-Cas9 system. In vivo visualization of E-GFP pattern in a *Tg(elavl3:E-GFP)* larvae at 72hpf. A, A' and A'' imagens correspond to the non-injected negative control - *Tg(elavl3:E-GFP*) fish. B, B' and B'' images correspond to larvae previously injected with a sgRNA against E-GPF and the synthetized Cas9 mRNA. A and B correspond to the whole embryo pattern of expression. A' and B' are a higher magnification of the head with different regions that show loss of *E-GFP* expression (delimited by dashed lines) in B'. A'' and B'' are amplifications of the trunk demonstrating examples of regions with a change in pattern of homogeneity between conditions.

This *in vivo* observation shows that the synthetized Cas9 mRNA as well as the sgRNA against E-GFP seem to be responsible for a E-GFP expression loss in the embryos' nervous system when compared with non-injected animals with the same genetic background. In parallel to the *in vivo* observations, and to validate the functionality of this system, DNA was extracted from batches of injected embryos at 24hpf and amplified with designed and optimized primers for the targeted E-GFP region. The amplified genomic region of both non-injected control embryos and CRISPR-Cas9 injected embryos was then loaded into a polyacrylamide gel (PAGE) to validate E-GPF mutation. Sanger sequencing analysis was performed to evaluate the presence of mutations in the targeted region. In Figure 3.2 A, the presence of additional bands on PAGE in injected transgenic embryos' samples comparing to the negative controls reveals that the CRISPR-Cas9 mutagenesis leads to alterations in the fish genome, as seen by the formation of heteroduplexes. In Figure 3.2 B a chromatogram from Sanger sequencing of both negative control and mutated batches is shown. In this image, the negative control exhibits the reference sequence of the target region. In contrast, the batch of injected embryos reveals the presence of altered nucleotide sequences starting from the PAM, suggesting a successful mutation of the E-GFP targeted region through CRISPR-Cas9. This result mimics and validates the phenotype observed *in vivo*.

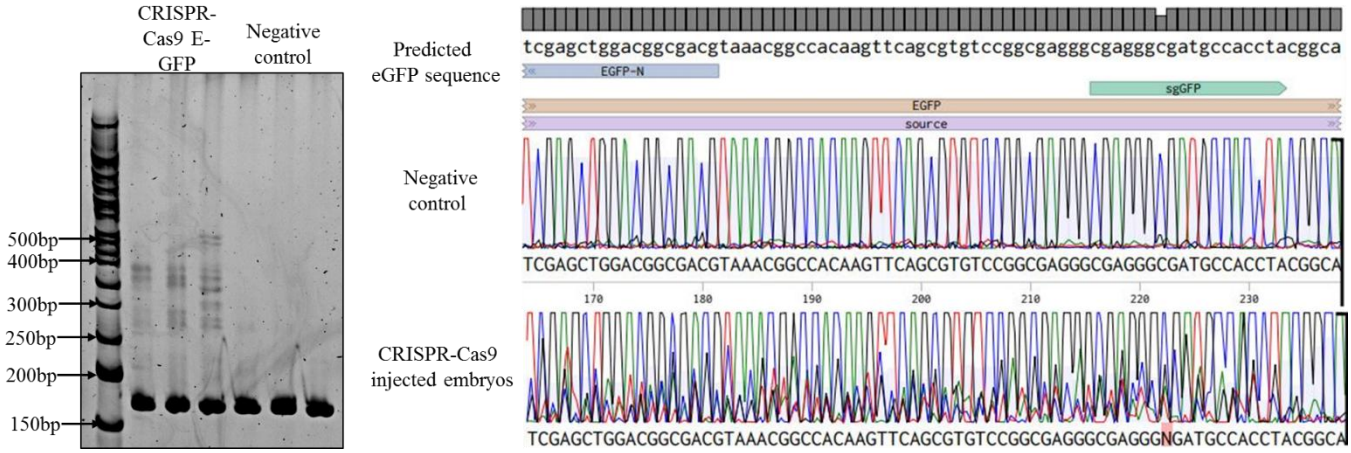

Figure 3.2 PAGE with samples from each condition run in triplicate. First lane corresponds to the ladder, then three batches of sgRNA against *E-GFP*+Cas9 mRNA injected embryos and the last three lanes are the non-injected controls. The amplicon from the target region has 176bp. In the image the bands between 250-500bp correspond to different heteroduplexes (A) On the right is the Sanger sequencing with reference *E-GFP* sequence (B, top), the non-injected embryos' pattern of *E-GFP* expression and on the bottom the results for one of the injected batches.

Since the CRISPR-Cas9 system was functional, we proceeded to design and synthetize sgRNAs targeting different regions of *foxm1:* the first coding region of *foxm1* (exon 2) and the initial part of the TAD domain (exon 8) (Figure 3.3).

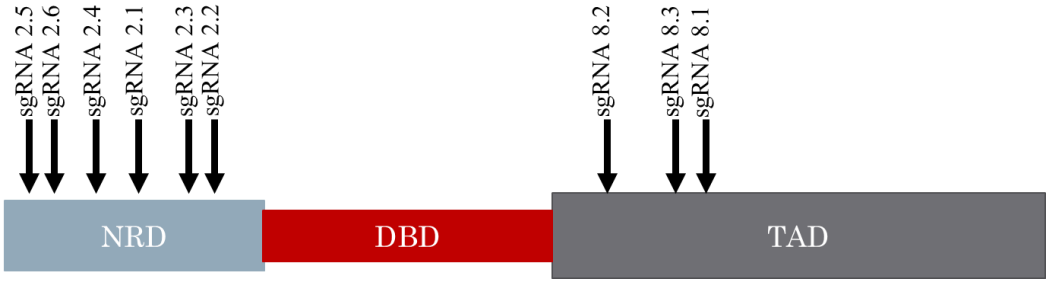

Figure 3.3 All sgRNAs tested predicted targeted regions on FoxM1 protein. FoxM1 protein has 3 different domains that are represented: N-repressor domain (NDR), DNA binding domain (DBD) and transactive domain (TAD).

All sgRNAs were tested as referred above for E-GFP. After PAGE analysis, when a mutation in *foxm1* was suspected, the DNA sample was sequenced. As described in Chapter 2, six sgRNA were tested for the first coding region of *foxm1* (exon 2). None of these sgRNAs induced mutations, as it can be visualized by the absence of heteroduplex formation on the PAGE results, comparing the injected batches of embryos with the respective controls (Figure 3.4).

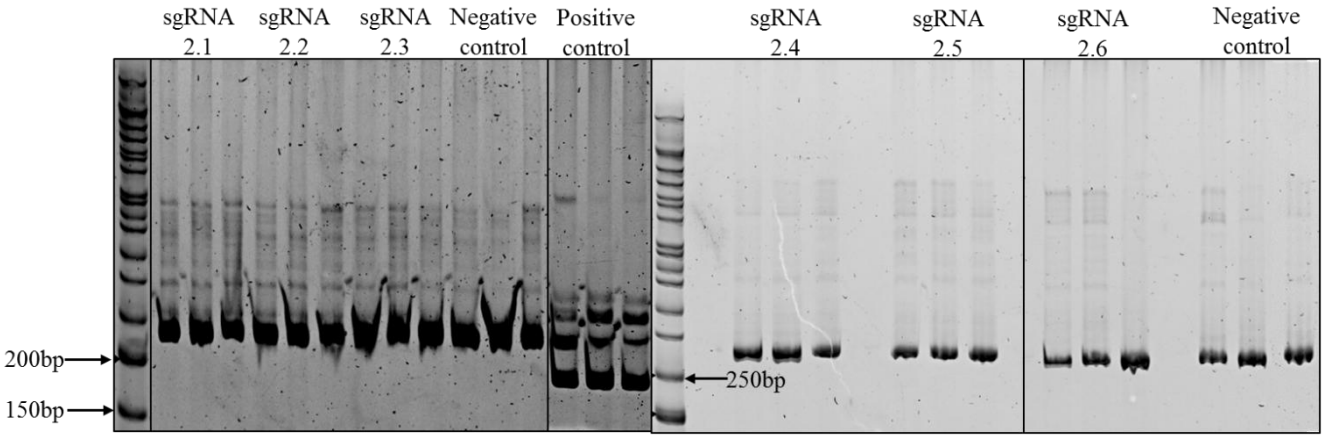

Figure 3.4 PAGE of *foxm1* exon 2 sgRNA tested. All batches of each condition were run in triplicate. The amplicon size of sgRNAs tested on the PAGE on the left was 211bp. The positive control corresponds to DNA from embryos *Tg(elavl:E-GFP)* injected with sgRNA against *E-GFP* (amplicon size 176bp). On the right the amplicon size was 288bp

In 2004, Amesterdam and collaborators described a series of genes vital for zebrafish early embryonic development, however, *foxm1* is not among the described genes[190]. Nevertheless, the initial cell divisions in zebrafish are synchronic and rapid between S phase and mitosis[88], [172]. Since embryos at one-cell stage show this incomplete embryonic cell cycle and *foxm1* carries a great importance as a major regulator of the cell cycle, we hypothesize that the lack of mutations in the initial portion of *foxm1* could indicate that its loss may be lethal, or alternatively, all six sgRNAs tested are indeed ineffective at generating a *foxm1* mutations. Indeed, it has been previously described that some sgRNAs are less efficient or inactive being unsuitable to generate targeted mutations (reviewed on [191]).

We also tested sgRNAs targeting a different region of the gene. Exon eight of *foxm1* encodes for the initial portion of the TAD domain (Figure 3.3). In human cells, a mutation in this domain leads to a dominant negative form of FOXM1[46]. Aligning human and zebrafish sequences, we were able to find the homologue region in the zebrafish *foxm1*, exon eight. The PAGE-based analyses on Figure 3.5 A demonstrates the presence of heteroduplexes in all batches of embryos for one (sgRNA8.2) out of three tested sgRNAs for this region, comparing to the negative controls.

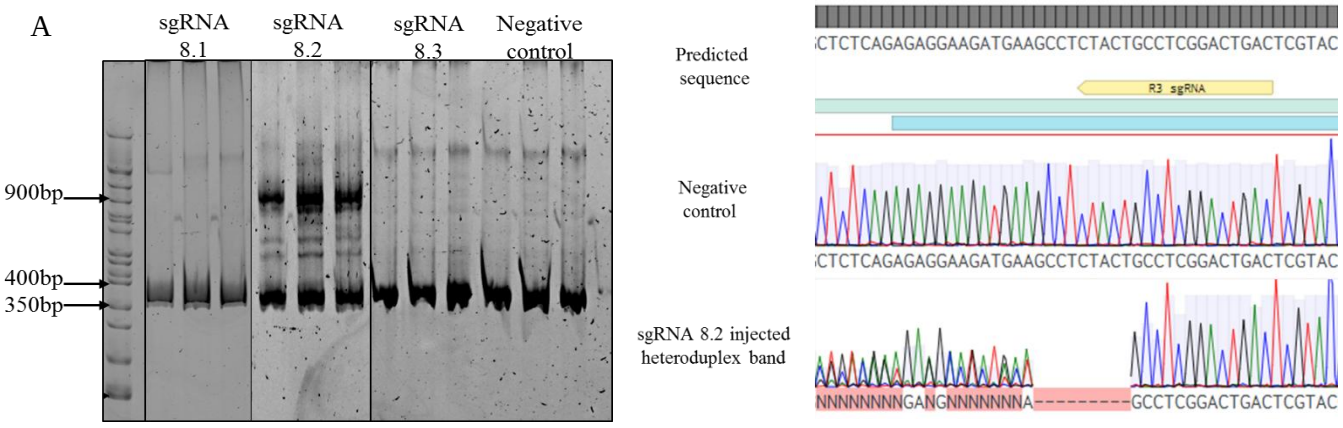

Figure 3.5 (A) corresponds to the PAGE of CRISPR-Cas9 tested sgRNAs for the eighth exon of *foxm1*. All sgRNAs were tested in triplicate batches of embryos. The amplicon size was 370bp. There are heteroduplexes with weights ranging between 500-900 bp. (B) represents predicted WT targeted sequence and the sequencing results from non-injected embryos and from a heteroduplex band

These results suggest that sgRNA 8.2 induces mutations in this *foxm1* targeted region. To further test this possibility, we have sequenced some heteroduplexes bands extracted from the PAGE and we were able to detect mutations in these sequences (Figure 3.5 B). Embryos injected with this sgRNA 8.2 were raised until adulthood and outcrossed to search for carriers of mutations in the germline (founders). All the experiments from this point on were performed using this sgRNA 8.2.

To generate a stable mutant line, the alteration in the targeted gene must be present in the germline to be inherited by the offspring. These germline mutations can be easily identified by progeny screening using standard molecular biology methods. The injected embryos raised until adulthood (F0 animals) were outcrossed and, when possible, the offspring was divided into batches to test for mutation through DNA extraction, amplification, PAGE analysis and sequencing (Figure 6.1 to 6.9 appendix). After the identification of germline mutations, embryos from those F0 animals (F1 embryos) were raised to adulthood, to generate mutant stable lines for *foxm1*. The sequencing results from PAGE-positive samples correspond to batches of eight heterozygous embryos, therefore, different chromatogram sequences appear overlapped making it difficult to determine, at this point, the embryos' exact mutation. However, it is possible to find the most predominant mutations. The precise mutation can be determined later on, when animals reach adulthood, through single-fish analysis.

From the raised animals (F0), 14 fishes were tested and 9 of those (64%) carried a *foxm1* mutation in the germline. After sequencing analysis of the progeny, we verified that the 9 founders were able to generate 3 independent mutations, all of them with no framing shift. The independent detected mutations were short deletions: 1 (11%) had a deletion of three nucleotides and 6 (67%) had a deletion of nine nucleotides and 2 had a deletion of twelve nucleotides (22%; Table 3.1). This is an interesting result since the random probability of mutations resulting in a framing shift is around 67% and we have obtained none out of 9 identified mutations. Framing shifts form through insertions or deletions of 1 or 2 nucleotides or multiples of those numbers. Only mutations of 3 nucleotides and its multiples do not result in a framing shift. This means that, for instance, in 9 *foxm1* mutant founders, about 6 of those should generate a framing shift mutation in the offspring. This outcome suggests that *foxm1* framing shift mutations are not compatible with embryo formation or germline cell survival, which could be explained by the known relevance of *foxm1* in crucial stages of the cell cycle and mitosis[34], [192]. The largest isolated deletions in *foxm1* correspond to a 12-nucleotide deletion. Through protein alignment of human FOXM1 and zebrafish FoxM1 (Figure 6.10 appendix), we confirmed that this deletion in the zebrafish included an amino acid homologue to a human small-ubiquitin-like modification (SUMOylation) site. SUMOylation is relevant in cell cycle regulation[193]. SUMOylation seem to target proteins (e.g. Aurora-B, Cyclin-B1, CENP-F, PLK1, BUB1) responsible for multiple

functions as DNA replication and condensation, chromosome alignment and segregation and cytokinesis. In mice, the loss of these regions has been described to cause genomic instability through chromosome missegregation[194]. We verified that one of the previously studied lysines (K368) of human FOXM1[194] corresponds to deleted lysine (K315) on the crispant F1 offspring of two founders (Figure 6.10 appendix).

Table 3.1 Founders' offspring majority alterations on foxm1 target region in terms of genomic sequence and their predicted protein modification

Founders	***foxm1* targeted sequence**	**Predicted translation**
Wild type	…AAGATGAAGCCTCTACTGCCTCGGACTGAC…	…KMKPLLPRTD…
Founder 1	…AAGATGAAGCCT---CTGCCTCGGACTGAC…	…KMKP-LPRTD…
Founder 2	…AAGATGAA---------GCCTCGGACTGAC…	…KMK---PRTD…
Founder 3	…AAGATGAA---------GCCTCGGACTGAC…	…KMK---PRTD…
Founder 4	…AAGATGAA---------GCCTCGGACTGAC…	…KMK---PRTD…
Founder 5	…AAGATGAA---------GCCTCGGACTGAC…	…KMK---PRTD…
Founder 6	…AAGATGAA---------GCCTCGGACTGAC…	…KMK---PRTD…
Founder 7	…AAGATGAA---------GCCTCGGACTGAC…	…KMK---PRTD…
Founder 8	…AAGA----------TGCCTCGGACTGAC…	…KM----PRTD…
Founder 9	…AAGA----------TGCCTCGGACTGAC…	…KM----PRTD…

The studies concluded that K315 SUMOylation is needed for FoxM1 activation, since it inhibits binding of NRD to TAD domains, allowing the binding of FoxM1 to its DNA target sequences[192], [194]. These data lead us to the hypothesize that zebrafish carrying the deletion on K315 may have a severe impairment of *foxm1* function. SUMOylation have also been linked to numerous genes known to modulate cellular senescence (carefully reviewed in [195]). As described on Chapter 1, p53/p21 is an important network in cellular senescence. For instance, p53, an important cellular senescence marker, can be modified by SUMO proteins that stabilize the protein and consequently induce senescence[196]. Nevertheless, to our knowledge, no study has linked FoxM1 SUMOylation to cellular senescence. Unfortunately, we were not able to raise progeny from animals carrying the mutation on *foxm1* K315, further suggesting its deleterious effect, but F1 carriers of the other deletions are being raised to adulthood.

Since we wanted to achieve a muscle-specific mutation of *foxm1* and assess the consequent phenotypes in differentiated cells, we first tested for the expression of this gene in muscle cells. For that we have sorted by fluorescence-activated cell sorting (FACS) terminally differentiated muscle cells. We have used two *in vivo* reporters for the FACS experiment. We have injected in one cell stage embryos a construct that drives mCherry expression under the control of the *mylfpa* muscle specific promoter (*mylfpa*:mCherry[197], [198]), and we have used a ZED line that is a muscle specific reporter line (cardiac actin-dsRed2[181]). A positive control corresponding to whole embryos was used. To validate RNA extraction and retrotranscription procedures on cells, we also tested the expression of a housekeeping reference gene (elongation factor 1 alpha 1, *eef1a1*). As shown in Figure 3.6 the *eef1a1* 358bp fragment was amplified from the cDNA, as well as the *foxm1* 139bp, both from the *mylfpa* reporter construct (*mylfpa* cells) and from the muscle specific reporter line (ZED cells). These results suggest that there is expression of *foxm1* in differentiated muscle cells. It is important to notice that the experiments lack the result from the PCR reaction using purified RNA before retrotranscription, with which it would be possible to completely rule out the presence of DNA contamination.

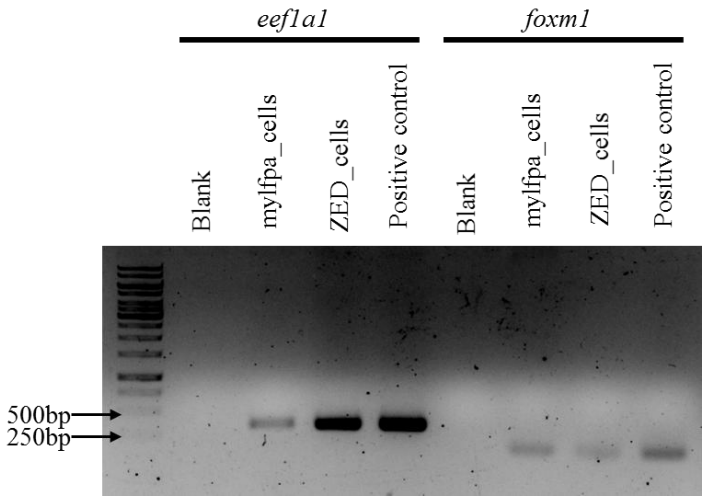

Figure 3.6 Agarose gel of semiquantitative evaluation of both *eef1a1*(358bp) and *foxm1*(139bp) expression in muscle FACS sorted cells (*mylfpa*:mCherry and ZED cells) and whole embryos (positive control). The first and fifth lanes correspond to the blanks for each set of primers without cDNA to check for possible genomic contaminations.

FoxM1 has a key role in cell cycle and proliferation[31], thus it is expected for this gene to be highly expressed in proliferating tissues, rather than in differentiated cells. Recently, Chen and collaborators have shown through immunofluorescence analysis of mice myofibers, that *FoxM1* was not (or minutely) expressed in *Pax7* negative, fully differentiated muscle cells. The authors concluded that this gene's expression decreases rapidly upon satellite cell differentiation in mice[199]. However, we are able to detect *foxm1* expression in the sorted muscle cells by RT-PCR, indicating that this gene is indeed expressed in zebrafish differentiated muscle cells.

To generate mosaics of muscle mutant cells for *foxm1*, we have used the CRISPR-Cas9 mediated system developed by the Zon's group, extensively described in the introduction[146]. In summary, we have used a transposon that encodes Cas9 fused to GFP under the control of the muscle specific promoter *mylfpa* and the sgRNA 8.2 under the ubiquitous promoter U6 (*mylfpa*:Cas9GFP;sgRNA8.2). Upon injection, this construct will generate mosaics of muscle cells mutant for *foxm1* labeled with GFP, allowing to trace these cells *in vivo*. A similar construct but lacking a sgRNA was also generated to be used as a negative control for the experiment (*mylfpa*:Cas9GFP). In addition, we have used another reporter transposon containing the promoter of *mylfpa* driving the expression of mCherry to label WT terminally differentiated cells *in vivo* (*mylfpa*:mCherry). After cloning and confirming that the vectors were correctly assembled, they were purified to be suitable for zebrafish microinjection. These vectors were used to perform a mosaic loss-of-function of *foxm1* in muscle cells. After injection of the transposons in embryos at one-cell stage, we have documented and quantified the GFP and mCherry positive cells at 24, 48, 72 and 120 hpf. We were able to observe that the number of WT mCherry positive cells increase in each timepoint, while the number of GFP positive cells is mostly kept during the experiment, both for *mylfpa*:Cas9GFP;sgRNA8.2 and *mylfpa*:Cas9GFP (Figure 3.7 and Figure 3.8)

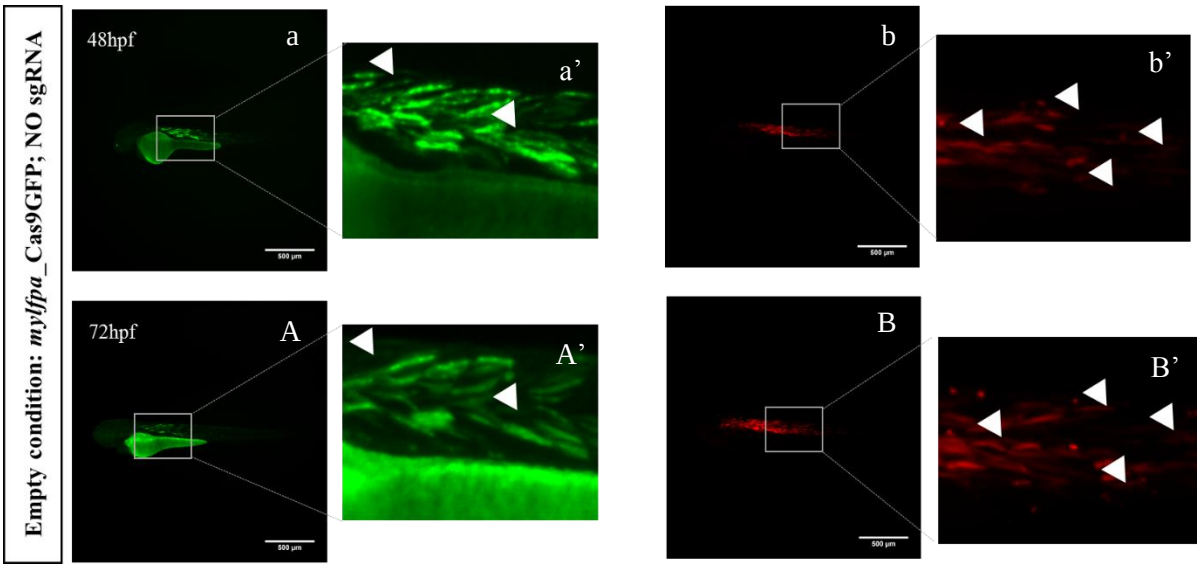

Figure 3.7 Embryo injected with *mylfpa*_Cas9GFP and *mylfpa*_mCherry. A', B', a' and b' are amplification of the regions delimited by squares in A, B, a and b respectively. The white arrows correspond to a few examples of cells which appear between timepoints in the red channel and disappear in the green channel between timepoints

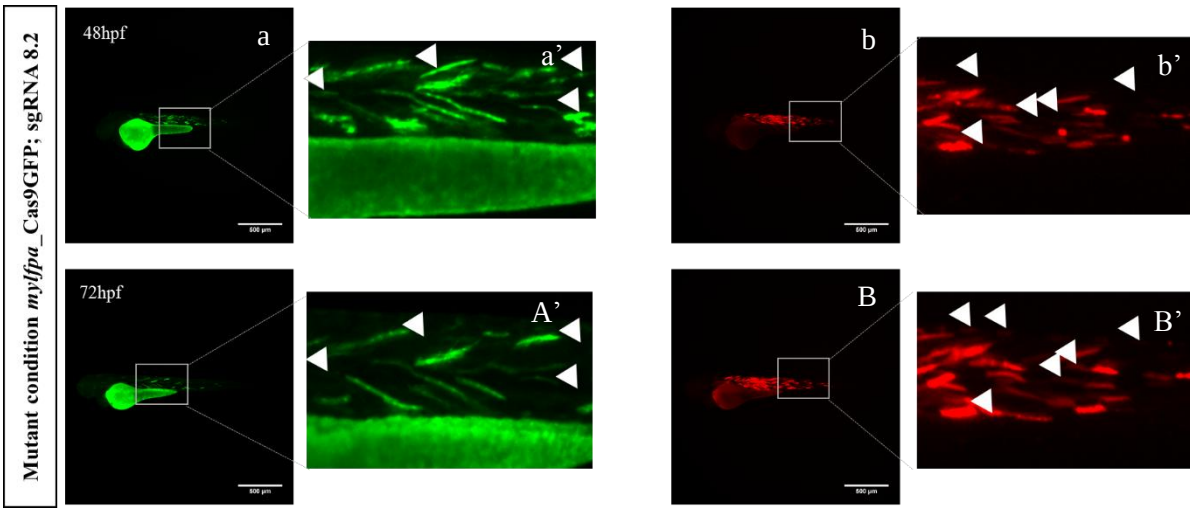

Figure 3.8 Embryo injected with mylfpa_Cas9GFP; sgRNA 8.2 and *mylfpa*_mCherry. A', B', a' and b' are amplification of the regions delimited by squares in A, B, a and b respectively. The white arrows correspond to a few examples of cells which appear between timepoints in the red chanel and disappear in the green channel between timepoints.

These results show that there are two different growth dynamics for cells incorporating the Cas9_GFP expressing vectors, regardless of having the potential to mutate *foxm1*, when comparing with the WT cells labeled with mCherry.

The quantification of Cas9_GFP positive cells revealed that the number of these cells tend to be stable or even decrease in the last timepoint assessed, in both experimental conditions (*mylfpa*:Cas9GFP;sgRNA8.2 and *mylfpa*:Cas9GFP) (Figure 3.9). This reduction leads us to hypothesize that the common reagent, Cas9, may show a toxicity relevance when highly and continuously expressed in cells, independently of having a sgRNA. This toxicity was not reported in Ablain *et al.* 2015 experiments[146], however, toxicity linked to Cas9 has been already reported[200], [201].

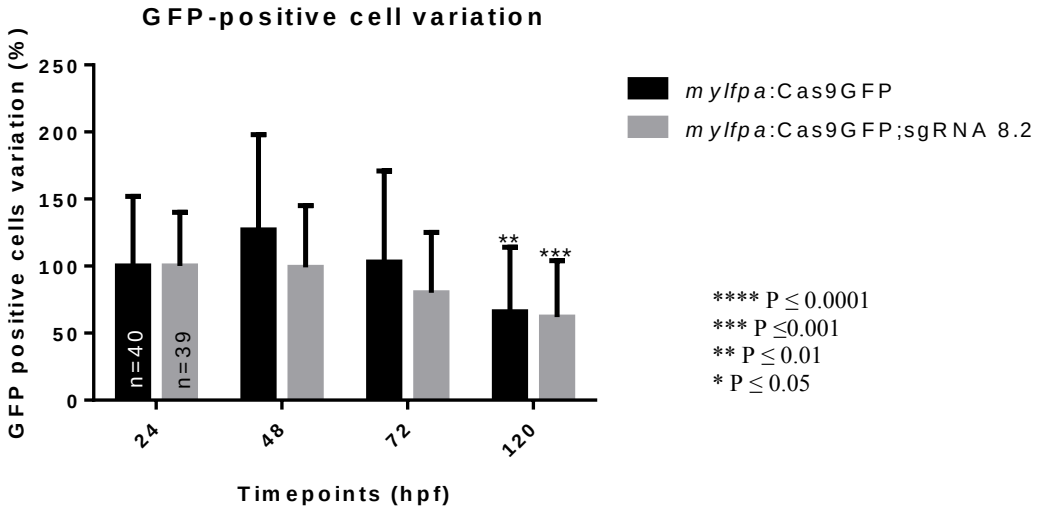

Figure 3.9 Graphical representation of GFP-positive cell variation between timepoints and conditions (empty vector injected (n=40) and *foxm1* mutation vector (n=39) -with sgRNA 8.2- injected embryos). The values were normalized based on the number of GFP positive cells counted in the first timepoint (24hpf) and converted into percentages to facilitate the comparison between timepoints and conditions

To further investigate the mechanism of elimination of cells we performed immunohistochemistry for a DNA damage marker (H2axS139ph) and an apoptosis marker (cleaved Caspase-3). Unfortunately, the results were inconclusive suggesting that a supplementary optimization of the protocol is needed. Therefore, our observation constitutes an important insight for researchers using CRISPR-Cas9 in transgenesis systems. Nevertheless, regardless of the toxic effect, most likely associated to the expression of Cas9, WT mCherry labeled cells, when co-injected with the *mylfpa*:Cas9GFP;sgRNA8.2 vector increase more their number than when co-injected with *mylfpa*:Cas9GFP vector (Figure 3.10).

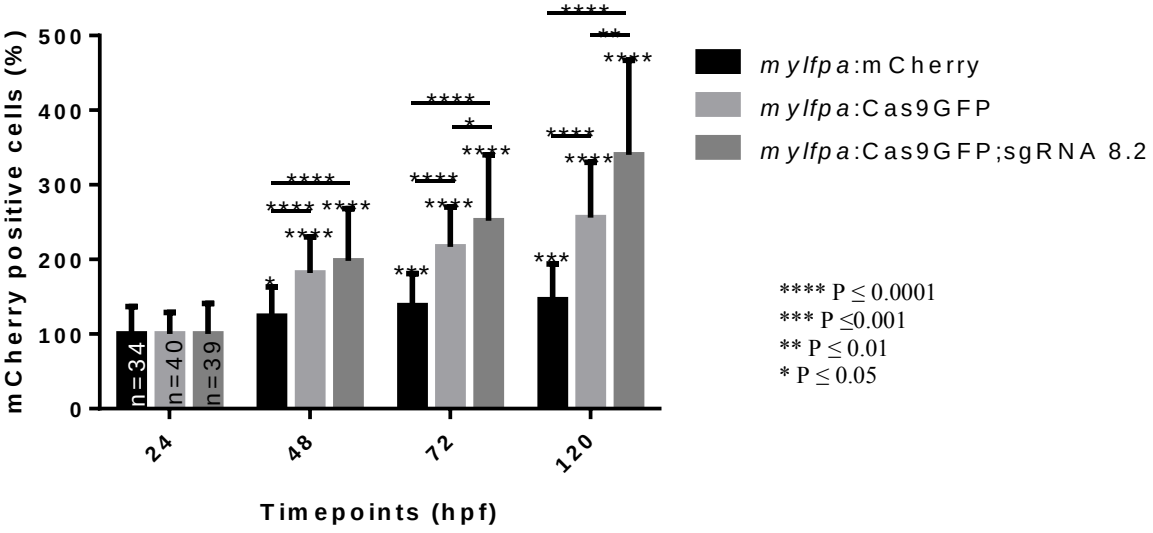

Figure 3.10 Graphical representation of mCherry-positive cell variation between timepoint and condition. On the right there is the mCherry cell variation through time between conditions, negative control consisting on *mylfpa*_mCherry cells (n=34 embryos), empty vector injected (n=40 embryos) consisting on mylfpa_Cas9GFP and foxm1 mutant vector with sgRNA 8.2

affecting *mylfpa*_Cas9GFP cells (n=39 embryos). The values were normalized based on the value of the first timepoint (24hpf) and converted into percentages to facilitate the comparison between timepoints and conditions.

This indicates that mutations in *foxm1* in muscle cells may induce a non-cell autonomous response in the surrounding progenitor cells (SC), or other differentiated cells, stimulating even more the increment of WT mCherry expressing cells. Actually, the *foxm1* mutagenesis condition images' (Figure 3.10) illustrate the increase of the mCherry positive cells surrounding the region where GFP cells disappear, which may be indicative of a signaling mechanism favoring the proliferation and differentiation of mCherry WT cells over the *foxm1* mutated population.

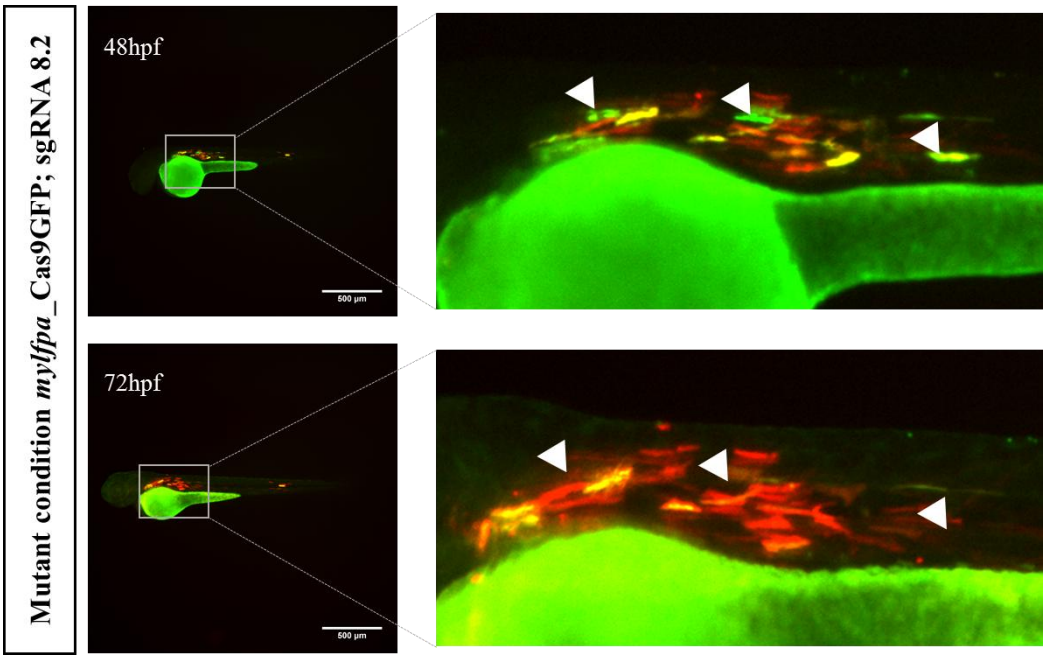

Figure 3.11 Representative images of the same embryo injected with the mutant condition at two different timepoints: 48hpf (upper images) and 72hpf (lower images). The images on the right are amplifications of the regions delimited by squares in the left images. The white arrows indicate cells expressing GFP that disappear with time with a noticeable increase in the mCherry positive population in the surroundings of the lost cells.

To better understand the dynamics of the increase in cell number of WT cells, we have repeated the same experiment injecting the *mylfpa*:mCherry vector alone (Figure 3.10; Figure 3.12). Surprisingly, the increase in the number of mCherry cells was much milder comparing with the co-injections of *mylfpa*:Cas9GFP;sgRNA8.2 or *mylfpa*:Cas9GFP vector. These results suggest that Cas9 expressing cells, *mylfpa*:Cas9GFP;sgRNA8.2 or *mylfpa*:Cas9GFP, induce non-autonomously the increase in the number of WT mCherry cells. This might be explained by a compensatory mechanism, most likely related with tissue regeneration, as a response to the toxicity of Cas9, forcing progenitor cells to compensate for the limited and low numbers of Cas9 expressing cells. This effect is even stronger when embryos are co-injected with *mylfpa*:Cas9GFP;sgRNA8.2 vector, targeting *foxm1*, suggesting that the loss of *foxm1* might enhance this compensatory effect non-autonomously.

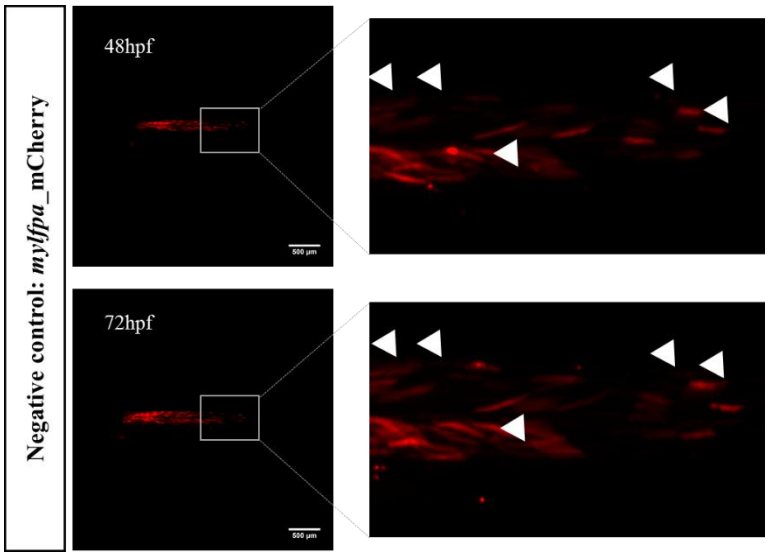

Figure 3.12 Animal injected with mylfpa_mCherry vector to visualize the fluorescence variation between 48 (upper images) and 72hpf (lower images). The images on the right are amplifications of the regions delimited by squares in the left images. The white arrow triangles correspond to a few examples of cells which appear between timepoints

In 2015, Fridlyanskaya *et al.* proposed that cellular responses are determined by the tissue environment. Authors exemplify this statement with studies of lymphoid, hematopoietic and embryonic stem cells which respond to an induced stress by activating apoptosis when either adult stem cells or fibroblast-like cells induce senescence. Authors also mention that tissue repair is guaranteed when mesenchymal stem cells are exposed to a stress factor[202]. The senescent state may induce remodeling and proliferation of cells in the vicinity as described in Storer et al 2013 and Munoz-Espín et al 2014[102], [203]. As previously described in Chapter 1, cells exposed to stressful events can promote "de-differentiation" of cells to improve proliferation and tissue remodeling[120]–[124]. As previously shown, skeletal muscle repair was also linked with a progenitor independent process[120], [121]. Interpreting our results under this light, we theorize that the increased number of WT mCherry cells nearby cells incorporating the *mylfpa*:Cas9GFP;sgRNA8.2 construct, might be due to a signaling secretome (possibly SASP) from *foxm1* mutant cells, that could be acquiring a senescent state. Indeed, it has been demonstrated that senescent cells change dramatically their secretome[54], [204]. This secretome may induce SC and progenitor cells in the vicinity to proliferate or induce "de-differentiation" of mature healthy myofiber cells boosting tissue remodeling and repair.

To understand the signaling processes that may be occurring in the *foxm1* mutant cells, we measured the expression levels of several genes associated with the senescence process and cell signaling. Quantitative analysis was obtained through a RT-qPCR of whole embryos injected with one of three conditions: *mylfpa*:Cas9GFP;sgRNA8.2 to induce *foxm1* mutant cells, *mylfpa*:Cas9GFP as a non-mutagenic control and *mylfpa*:mCherry labeling WT cells. The results are displayed in two sets of data, the cell cycle markers (Figure 3.13 A) and muscle specific genes (Figure 3.13 B). Although the outcome of this analysis was not statistically significant, we can observe a tendency to increase both *foxm1* and *cyclin B* expression levels in the *mylfpa*:Cas9GFP;sgRNA8.2 condition comparing to the other conditions (*mylfpa*:Cas9GFP and *mylfpa*:mCherry; Figure 3.13 A). Knowing that the mutagenesis system should induce a *foxm1* knockdown in the target cells, this result may seem contrary to the expected. However, because gene expression was assayed on whole embryos, SC cells may be increasing their proliferation rate, or differentiated cells might dedifferentiate and enter cell cycle, as a signaling response from the *foxm1* mutant cells. Taken together, both assays lead us to hypothesize that *foxm1* may have an important role in fully differentiated cells, modulating their

ability to signal other differentiated or progenitor cells. The p21 expression values were not substantially altered, suggesting that either *foxm1* mutant cells are not truly senescent or the limited amount of these cells is so underrepresented in the whole embryo that does not allow to detect a significative increase in this senescence marker. To bypass this problem, immunohistochemistry, *in situ* hybridization or RT-PCR after cell sorting should be used.

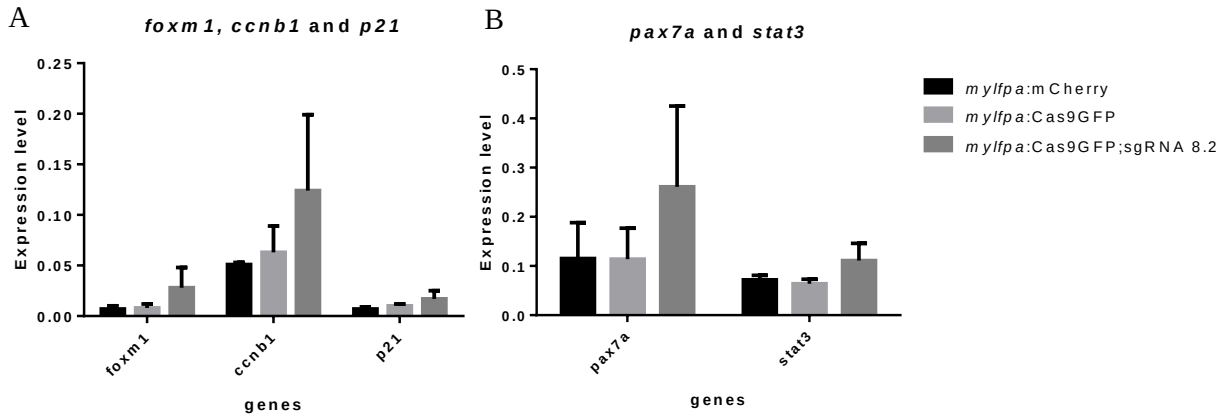

Figure 3.13 Expression levels of cell cycle markers (left) and muscle cell proliferation and signaling (right) on the three conditions studied negative control (mCherry only), empty vector and foxm1 mutation vector. Analysis after RT-qPCR of whole embryos injected with the respective condition.

pax7a and *stat3* transcriptional levels were also evaluated to assess whether the putative senescent cells were communicating with the surrounding cells potentially through the release of cytokines and chemokines, such as IL-6. This molecule could then act on muscle cells by activating the JAK-STAT response signaling pathway, of which Stat3 is part. Figure 3.13 B shows that *stat3* is most expressed in the embryos with *foxm1* mutation, supporting the role of the JAK-STAT pathway in the response to *foxm1* mutation and downregulation. The data also shows an increment on *pax7a* expression levels in this condition, reflecting the activity of some regeneration or repair mechanism occurring in this tissue in response to the *foxm1* mutation, potentially via IL-6 and Stat3. In concordance to our results and as seen in Chapter 1, JAK-STAT signaling seems to be activated in aging processes and related to regeneration processes[133], [135], [138]. Although future work is required to describe the cell-to-cell communication and regenerative mechanisms involved in the response to *foxm1* mutant cells, this study associates a *foxm1* mutation with autonomous loss of proliferative capacity or cell death, resulting into a decreased number of *foxm1* mutant cells. Non-autonomously, *foxm1* mutant cells might be promoting the organism's response through signaling pathways, likely JAK-STAT, stimulating repair and regeneration of the muscle.

Further analysis would be necessary to disclose the processes occurring in the *foxm1* mutant cells. In the future, it would be vital to perform RT-qPCR in mutated cells and their neighbors to strength the hypothesis of IL6 and Stat3 signaling between the *foxm1* mutant and WT cell populations. This quantitative study would provide useful information not only regarding *foxm1* mutation, but also its consequences. As described in the Chapter 1, there is a lack of adequate senescence markers to study this process *in vivo*. However, an additional analysis including a SA-β gal staining in the mutated embryos would clarify the state of senescence in *foxm1* mutant cells. A complementary investigation through RNA-seq would also provide a database of altered genes in each of the cell populations.

Chapter 4. Conclusion remarks and Future perspectives

In this project, the CRISPR-Cas9 system was applied to mutate the zebrafish *foxm1*. A sgRNA (8.2) was shown to induce mutations in the gene of interest, in injected zebrafish embryos. Moreover, animals carrying a stable mutation were generated from multiple founders and different small deletions were observed. Interestingly, none of the isolated deletions corresponded to a frameshift in *foxm1*, suggesting that a mutant allele for this gene might be deleterious during embryogenesis or gametogenesis. An alternative explanation could be that the used sgRNA (8.2) might act with a strong bias to generate the uncovered mutations[205, 206], although taking into account that the uncovered mutations always corresponded to deletions of codons, maintaining the frame of the coding protein, this last scenario is highly unlikely. Although the uncovered mutations have a low potential to generate a strong loss of function of *foxm1*, this must be addressed in future experiments. In addition, senescence-associated phenotypes must be also assessed to better understand the implications of *foxm1* in aging *in vivo*.

In this study CRISPR-Cas9 mediated muscle-specific mutant fish was successfully created. It was verified that integration of large vectors containing a continuous expression of Cas9 gene, induces toxicity in differentiated muscle cells. This observation, previously unreported, points to new a limitation in the use of expression vectors combined with the CRISPR-Cas9 system in zebrafish. Nevertheless, further technological developments should be able to bypass this limitation, as for instance the development of transiently active promoters. In addition, future studies might take these experiments as a cautionary tale to the use of tissue specific CRISPR-Cas9 induced mutations using expression vectors. Although the limitations of the used technique, we were able to show that: 1) *foxm1* is expressed in differentiated muscle cells, 2) the loss of function of *foxm1* in muscle somatic cells results in a mild and slow decrease of cell numbers, 3) the loss of function of *foxm1* has a non-autonomous effect in the surrounding WT cells. Altogether, we present evidence that suggest that *foxm1*, a well-known cell cycle gene, might have an important role in differentiated muscle cells. Interestingly, the non-autonomous effect observed in the loss of function of *foxm1* results in a significant increase of the number of surrounding WT. This might suggest that *foxm1* mutant cells might be signaling to differentiated muscle cells and SCs. Supporting this, we have observed a tendency, although not statistically significant, for the transcriptional increase of *pax7a* and *stat3* a component of the JAK-STAT signaling pathway. These results could be compatible with a model where *foxm1* mutant cells acquire a senescent state, starting to signal to surrounding cells, maybe through IL-6, inducing a boost in the regenerative response of neighboring *foxm1* positive cells. Further investigation is needed to determine if this hypothesis is correct. Some assays, such as immunohistochemistry for apoptotic and senescence markers, would be useful to understand the events associated with the state and loss of cells expressing Cas9 and sgRNA. Additionally, it would be useful to perform a quantitative analysis of expression on *foxm1* mutant FACS sorted cells to fully comprehend the processes occurring in the zebrafish *foxm1* mosaic loss-of-function assay. Complementary studies using SA-β gal staining would also be a valuable approach to confirm senescence in mutated cells. Another interesting technique to use in future studies is RNA-seq. This technique would allow us to understand the genes involved in the processes taking place on the cells of embryos from the mutation condition, in an unbiased way.

Overall, this work enabled the generation of *foxm1* mutant fishes through CRISPR-Cas9 technology. The results endorse the conclusion of a possible senescent state in *foxm1* mutated muscle cells and a recognition of a non-autonomous response to *foxm1* mutation *in vivo*, likely to include IL-6 and JAK-STAT signaling.

5. Bibliography

[1] B. Giotti, A. Joshi, and T. C. Freeman, "Meta-analysis reveals conserved cell cycle transcriptional network across multiple human cell types," *BMC Genomics*, vol. 18, no. 1, pp. 1–12, 2017.

[2] S. van den Heuvel, "Cell-cycle regulation," *WormBook*, pp. 1–16, 2005.

[3] K. T. Duffy *et al.*, "Coordinate control of cell cycle regulatory genes in zebrafish development tested by cyclin D1 knockdown with morpholino phosphorodiamidates and hydroxyprolyl-phosphono peptide nucleic acids," *Nucleic Acids Res.*, vol. 33, no. 15, pp. 4914–4921, 2005.

[4] T. Sandal, "Molecular Aspects of the Mammalian Cell Cycle and Cancer," *Oncologist*, vol. 7, no. 1, pp. 73–81, 2002.

[5] B. Zhivotovsky and S. Orrenius, "Cell cycle and cell death in disease: Past, present and future," *J. Intern. Med.*, vol. 268, no. 5, pp. 395–409, 2010.

[6] D. Faust, F. Al-Butmeh, B. Linz, and C. Dietrich, "Involvement of the transcription factor FoxM1 in contact inhibition," *Biochem. Biophys. Res. Commun.*, vol. 426, no. 4, pp. 659–663, 2012.

[7] M. L. Casem, *Case Studies in Cell Biology*, 1st ed. Academic Press, 2016.

[8] J. M. Fu, Zheng; Malureanu, Liviu; Huang, Jun; Wang, Wei; Li, Hao; van Deursen and J. Tindall, Donald J. and Chen, "Plk1-dependent phosphorylation of FoxM1 regulates a transcriptional programme required for mitotic progression," *Nat. Cell Biol.*, pp. 1212–1217, 2008.

[9] Y. Budirahardja and P. Gonczy, "Coupling the cell cycle to development," *Development*, vol. 136, no. 17, pp. 2861–2872, 2009.

[10] B. Strauss, A. Harrison, P. A. Coelho, K. Yata, M. Zernicka-Goetz, and J. Pines, "Cyclin B1 is essential for mitosis in mouse embryos, and its nuclear export sets the time for mitosis," *J. Cell Biol.*, vol. 217, no. 1, pp. 179–193, 2018.

[11] J. Yang, E. S. G. Bardes, J. D. Moore, J. Brennan, M. A. Powers, and S. Kornbluth, "Control of Cyclin B1 localization through regulated binding of the nuclear export factor CRM1," *Genes Dev.*, vol. 12, no. 14, pp. 2131–2143, 1998.

[12] M. Brandeis *et al.*, "Cyclin B2-null mice develop normally and are fertile whereas cyclin B1-null mice die in utero," *Proc. Natl. Acad. Sci.*, vol. 95, no. 8, pp. 4344–4349, 1998.

[13] K. H. Jeong, J. Y. Jeong, H. O. Lee, E. Choi, and H. Lee, "Inhibition of Plk1 induces mitotic infidelity and embryonic growth defects in developing zebrafish embryos," *Dev. Biol.*, vol. 345, no. 1, pp. 34–48, 2010.

[14] K. Kishi, M. A. T. M. van Vugt, K. -i. Okamoto, Y. Hayashi, and M. B. Yaffe, "Functional Dynamics of Polo-Like Kinase 1 at the Centrosome," *Mol. Cell. Biol.*, vol. 29, no. 11, pp. 3134–3150, 2009.

[15] S.-Y. Lee, C. Jang, and K.-A. Lee, "Polo-like kinases (plks), a key regulator of cell cycle and new potential target for cancer therapy.," *Balsaeng'gwa saengsig*, vol. 18, no. 1, pp. 65–71, 2014.

[16] R. H. Costa, "FoxM1 dances with mitosis," *Nat. Cell Biol.*, vol. 7, no. 2, pp. 108–110, 2005.

[17] J. Laoukili *et al.*, "FoxM1 is required for execution of the mitotic programme and chromosome stability," *Nat. Cell Biol.*, vol. 7, no. 2, pp. 126–136, 2005.

[18] G. D. Grant *et al.*, "Identification of cell cycle-regulated genes periodically expressed in U2OS cells and their regulation by FOXM1 and E2F transcription factors," *Mol. Biol. Cell*, vol. 24, no. 23, pp. 3634–3650, 2013.

[19] I. Wierstra and J. Alves, “FOXM1, a typical proliferation-associated transcription factor,” *Biol. Chem.*, vol. 388, no. 12, pp. 1257–1274, 2007.

[20] I. C. Wang *et al.*, “FoxM1 regulates transcription of JNK1 to promote the G1/S transition and tumor cell invasiveness,” *J. Biol. Chem.*, vol. 283, no. 30, pp. 20770–20778, 2008.

[21] X. Chen *et al.*, “The Forkhead Transcription Factor FOXM1 Controls Cell Cycle-Dependent Gene Expression through an Atypical Chromatin Binding Mechanism,” *Mol. Cell. Biol.*, vol. 33, no. 2, pp. 227–236, 2013.

[22] F. C. Kelleher and H. O’Sullivan, “FOXM1 in sarcoma: role in cell cycle, pluripotency genes and stem cell pathways.,” *Oncotarget*, vol. 7, no. 27, pp. 42792–42804, 2016.

[23] L. Xue, L. Chiang, B. He, Y. Y. Zhao, and A. Winoto, “FoxM1, a forkhead transcription factor is a master cell cycle regulator for mouse mature T cells but not double positive thymocytes,” *PLoS One*, vol. 5, no. 2, pp. 1–9, 2010.

[24] L. Anders *et al.*, “A Systematic Screen for CDK4/6 Substrates Links FOXM1 Phosphorylation to Senescence Suppression in Cancer Cells,” *Cancer Cell*, vol. 20, no. 5, pp. 620–634, 2011.

[25] K. Krupczak-Hollis *et al.*, “The mouse Forkhead Box m1 transcription factor is essential for hepatoblast mitosis and development of intrahepatic bile ducts and vessels during liver morphogenesis,” *Dev. Biol.*, vol. 276, no. 1, pp. 74–88, 2004.

[26] C. Bolte, Y. Zhang, I. C. Wang, T. V. Kalin, J. D. Molkentin, and V. V. Kalinichenko, “Expression of Foxm1 transcription factor in cardiomyocytes is required for myocardial development,” *PLoS One*, vol. 6, no. 7, 2011.

[27] I. Wierstra, *The transcription factor FOXM1 (Forkhead box M1): Proliferation-specific expression, transcription factor function, target genes, mouse models, and normal biological roles*, 1st ed., vol. 118. Copyright © 2013 Elsevier Inc. All rights reserved., 2013.

[28] I. Wang *et al.*, “Forkhead Box M1 Regulates the Transcriptional Network of Genes Essential for Mitotic Progression and Genes Encoding the SCF (Skp2-Cks1) Ubiquitin Ligase Forkhead Box M1 Regulates the Transcriptional Network of Genes Essential for Mitotic Progression and,” *Mol. Cell. Biol.*, vol. 25, no. 24, pp. 10875–10894, 2005.

[29] K. Qu *et al.*, “Negative regulation of transcription factor FoxM1 by p53 enhances oxaliplatin-induced senescence in hepatocellular carcinoma,” *Cancer Lett.*, vol. 331, no. 1, pp. 105–114, 2013.

[30] S. Uddin *et al.*, “Overexpression of FoxM1 offers a promising therapeutic target in diffuse large B-cell lymphoma,” *Haematologica*, vol. 97, no. 7, pp. 1092–1100, 2012.

[31] J. Laoukili, M. Stahl, and R. H. Medema, “FoxM1: At the crossroads of ageing and cancer,” *Biochim. Biophys. Acta - Rev. Cancer*, vol. 1775, no. 1, pp. 92–102, 2007.

[32] S. Ramakrishna *et al.*, “Myocardium defects and ventricular hypoplasia in mice homozygous null for the Forkhead Box M1 transcription factor,” *Dev. Dyn.*, vol. 236, no. 4, pp. 1000–1013, 2007.

[33] C. Yang *et al.*, “Inhibition of FOXM1 transcription factor suppresses cell proliferation and tumor growth of breast cancer,” *Cancer Gene Ther.*, vol. 20, no. 2, pp. 117–124, 2013.

[34] T. V. Kalin, V. Ustiyan, and V. V. Kalinichenko, “Multiple faces of FoxM1 transcription factor: Lessons from transgenic mouse models,” *Cell Cycle*, vol. 10, no. 3, pp. 396–405, 2011.

[35] H. Zhu, “Forkhead box transcription factors in embryonic heart development and congenital heart disease,” *Life Sci.*, vol. 144, pp. 194–201, 2016.

[36] D. R. Littler *et al.*, “Structure of the FoxM1 DNA-recognition domain bound to a promoter sequence,” *Nucleic Acids Res.*, vol. 38, no. 13, pp. 4527–4538, 2010.

[37] S. Zona, L. Bella, M. J. Burton, G. Nestal de Moraes, and E. W. F. Lam, “FOXM1: An emerging master regulator of DNA damage response and genotoxic agent resistance,” *Biochim. Biophys. Acta - Gene Regul. Mech.*, vol. 1839, no. 11, pp. 1316–1322, 2014.

[38] L. Bella, S. Zona, G. Nestal de Moraes, and E. W. F. Lam, "FOXM1: A key oncofoetal transcription factor in health and disease," *Semin. Cancer Biol.*, vol. 29, no. C, pp. 32–39, 2014.

[39] C. Y. Koo, K. W. Muir, and E. W. F. Lam, "FOXM1: From cancer initiation to progression and treatment," *Biochim. Biophys. Acta - Gene Regul. Mech.*, vol. 1819, no. 1, pp. 28–37, 2012.

[40] M. Halasi and A. L. Gartel, "Targeting FOXM1 in cancer," *Biochem. Pharmacol.*, vol. 85, no. 5, pp. 644–652, 2013.

[41] J. Tao *et al.*, "Down-regulation of FoxM1 inhibits viability and invasion of gallbladder carcinoma cells, partially dependent on inducement of cellular senescence," *World J. Gastroenterol.*, vol. 20, no. 28, pp. 9497–9505, 2014.

[42] Z. Wang, A. Ahmad, Y. Li, S. Banerjee, D. Kong, and F. H. Sarkar, "Forkhead box M1 transcription factor: A novel target for cancer therapy," *Cancer Treat. Rev.*, vol. 36, no. 2, pp. 151–156, 2010.

[43] C. Huang, J. Du, and K. Xie, "FOXM1 and its oncogenic signaling in pancreatic cancer pathogenesis," *Biochim. Biophys. Acta - Rev. Cancer*, vol. 1845, no. 2, pp. 104–116, 2014.

[44] A. Smirnov *et al.*, "FOXM1 regulates proliferation, senescence and oxidative stress in keratinocytes and cancer cells," *Aging (Albany. NY).*, vol. 8, no. 7, pp. 1384–1397, 2016.

[45] B. A. Benayoun, S. Caburet, and R. A. Veitia, "Forkhead transcription factors: Key players in health and disease," *Trends Genet.*, vol. 27, no. 6, pp. 224–232, 2011.

[46] Y. H. Kim, M. H. Choi, J. H. Kim, I. K. Lim, and T. J. Park, "C-terminus-deleted FoxM1 is expressed in cancer cell lines and induces chromosome instability," *Carcinogenesis*, vol. 34, no. 8, pp. 1907–1917, 2013.

[47] V. Ustiyan *et al.*, "Foxm1 transcription factor is critical for proliferation and differentiation of Clara cells during development of conducting airways," *Dev. Biol.*, vol. 370, no. 2, pp. 198–212, 2012.

[48] V. Ustiyan *et al.*, "Forkhead Box M1 Transcriptional Factor is Required for Smooth Muscle Cells during Embryonic Development of Blood Vessels and Esophagus," vol. 336, no. 2, pp. 266–279, 2010.

[49] W. Korver *et al.*, "Uncoupling of S phase and mitosis in cardiomyocytes and hepatocytes lacking the winged-helix transcription factor Trident," *Curr. Biol.*, vol. 8, no. 24, pp. 1327-S1, 1998.

[50] D. H. Ly, D. J. Lockhart, R. A. Lerner, and P. G. Schultz, "Mitotic misregulattion and human aging," *Science (80-.).*, vol. 287, no. March, pp. 2486–2492, 2000.

[51] I.-M. Kim, S. Ramakrishna, G. A. Gusarova, H. M. Yoder, R. H. Costa, and V. V. Kalinichenko, "The Forkhead Box M1 Transcription Factor Is Essential for Embryonic Development of Pulmonary Vasculature," *J. Biol. Chem.*, vol. 280, no. 23, pp. 22278–22286, 2005.

[52] H. Zhang *et al.*, "The FoxM1 Transcription Factor Is Required to Maintain Pancreatic β-Cell Mass," *Mol. Endocrinol.*, vol. 20, no. 8, pp. 1853–1866, 2006.

[53] F. Triana-Martínez, G. Pedraza-Vázquez, L. A. Maciel-Barón, and M. Königsberg, "Reflections on the role of senescence during development and aging," *Arch. Biochem. Biophys.*, vol. 598, pp. 40–49, 2016.

[54] N. K. Lebrasseur, T. Tchkonia, and J. L. Kirkland, "Cellular Senescence and the Biology of Aging, Disease, and Frailty," *Nestle Nutr. Inst. Workshop Ser.*, vol. 83, pp. 11–18, 2015.

[55] J. Campisi, "Aging, Cellular Senescence, and Canc," *Annu Rev Physiol*, pp. 685–705, 2014.

[56] C. López-Otín, M. A. Blasco, L. Partridge, M. Serrano, and G. Kroemer, "The hallmarks of aging," *Cell*, vol. 153, no. 6, 2013.

[57] B. G. Childs, M. Durik, D. J. Baker, and J. M. Van Deursen, "Cellular senescence in aging and

age-related disease: From mechanisms to therapy," *Nat. Med.*, vol. 21, no. 12, pp. 1424–1435, 2015.

[58] D. McHugh and J. Gil, "Senescence and aging: Causes, consequences, and therapeutic avenues," *J. Cell Biol.*, vol. 217, no. 1, pp. 65–77, 2017.

[59] F. Lanigan, J. G. Geraghty, and A. P. Bracken, "Transcriptional regulation of cellular senescence," *Oncogene*, vol. 30, no. 26, pp. 2901–2911, 2011.

[60] L. Hayflick and P. S. Moorhead, "The serial cultivation of human diploid cell strains," *Exp. Cell Res.*, vol. 25, no. 3, pp. 585–621, 1961.

[61] D. J. Baker *et al.*, "Clearance of p16Ink4a -positive senescent cells delays ageing-associated disorders," vol. 479, no. 7372, pp. 232–236, 2012.

[62] P. Khongkow *et al.*, "FOXM1 targets NBS1 to regulate DNA damage-induced senescence and epirubicin resistance," *Oncogene*, vol. 33, no. 32, pp. 4144–4155, 2014.

[63] J. C. Acosta *et al.*, "A complex secretory program orchestrated by the inflammasome controls paracrine senescence," *Nat. Cell Biol.*, vol. 15, no. 8, pp. 978–990, 2013.

[64] F. Rodier and J. Campisi, "Four faces of cellular senescence," *J. Cell Biol.*, vol. 192, no. 4, pp. 547–556, 2011.

[65] J. M. Van Deursen and J. M. van Deursen, "The role of senescent cells in aging," *Nature*, vol. 509, no. 7501, pp. 439–446, 2014.

[66] D. M. Cooper, "The Balance between Life and Death: Defining a Role for Apoptosis in Aging," *J. Clin. Exp. Pathol.*, vol. s4, no. 01, pp. 1–10, 2012.

[67] M. P. Baar *et al.*, "Targeted Apoptosis of Senescent Cells Restores Tissue Homeostasis in Response to Chemotoxicity and Aging," vol. 169, no. 1, pp. 132–147, 2017.

[68] S. Mursalimov, N. Permyakova, E. Deineko, A. Houben, and D. Demidov, "Cytomixis doesn't induce obvious changes in chromatin modifications and programmed cell death in tobacco male meiocytes," *Front. Plant Sci.*, vol. 6, no. October, pp. 1–13, 2015.

[69] F. D'Adda Di Fagagna, "Living on a break: Cellular senescence as a DNA-damage response," *Nat. Rev. Cancer*, vol. 8, no. 7, pp. 512–522, 2008.

[70] D. J. Baker, B. G. Childs, M. Durik, and E. Al., "Naturally occurring p16Ink4a -positive cells shorten healthy lifespan," *Nature*, vol. 530, no. 7589, pp. 184–189, 2016.

[71] D. Kamimura, K. Ishihara, and T. Hirano, *IL-6 signal transduction and its physiological roles: the signal orchestration model*. 2003.

[72] A. L. Serrano, B. Baeza-Raja, E. Perdiguero, M. Jardí, and P. Muñoz-Cánoves, "Interleukin-6 Is an Essential Regulator of Satellite Cell-Mediated Skeletal Muscle Hypertrophy," *Cell Metab.*, vol. 7, no. 1, pp. 33–44, 2008.

[73] A. Bonetto *et al.*, "JAK/STAT3 pathway inhibition blocks skeletal muscle wasting downstream of IL-6 and in experimental cancer cachexia," *AJP Endocrinol. Metab.*, vol. 303, no. 3, pp. E410–E421, 2012.

[74] D. Jurk *et al.*, "Postmitotic neurons develop a p21-dependent senescence-like phenotype driven by a DNA damage response," *Aging Cell*, vol. 11, no. 6, pp. 996–1004, 2012.

[75] X. Wang, E. Quail, N. J. Hung, Y. Tan, H. Ye, and R. H. Costa, "Increased levels of forkhead box M1B transcription factor in transgenic mouse hepatocytes prevent age-related proliferation defects in regenerating liver.," *Proc. Natl. Acad. Sci. U. S. A.*, vol. 98, no. 20, pp. 11468–73, 2001.

[76] X. Wang, H. Kiyokawa, M. B. Dennewitz, and R. H. Costa, "The Forkhead Box m1b transcription factor is essential for hepatocyte DNA replication and mitosis during mouse liver regeneration.," *Proc. Natl. Acad. Sci. U. S. A.*, vol. 99, no. 26, pp. 16881–6, 2002.

[77] X. Wang, K. Krupczak-Hollis, Y. Tan, M. B. Dennewitz, G. R. Adami, and R. H. Costa, "Increased hepatic Forkhead Box M1B (FoxM1B) levels in old-aged mice stimulated liver

regeneration through diminished p27Kip1protein levels and increased Cdc25B expression," *J. Biol. Chem.*, vol. 277, no. 46, pp. 44310–44316, 2002.

[78] V. V. Kalinichenko *et al.*, "Ubiquitous expression of the Forkhead Box M1B transgene accelerates proliferation of distinct pulmonary cell types following lung injury," *J. Biol. Chem.*, vol. 278, no. 39, pp. 37888–37894, 2003.

[79] S. K. M. Li *et al.*, "FoxM1c counteracts oxidative stress-induced senescence and stimulates Bmi-1 expression," *J. Biol. Chem.*, vol. 283, no. 24, pp. 16545–16553, 2008.

[80] D. J. Baker *et al.*, "BubR1 insufficiency causes early onset of aging-associated phenotypes and infertility in mice," *Nat. Genet.*, vol. 36, no. 7, pp. 744–749, 2004.

[81] R. E. Karess, K. Wassmann, and Z. Rahmani, *New insights into the role of BubR1 in mitosis and beyond*, 1st ed., vol. 306. Elsevier Inc., 2013.

[82] J. C. Macedo *et al.*, "FoxM1 repression during human aging leads to mitotic decline and aneuploidy-driven full senescence," *Nat. Commun.*, vol. 9, no. 1, pp. 1–17, 2018.

[83] J. Van houcke, L. De Groef, E. Dekeyster, and L. Moons, "The zebrafish as a gerontology model in nervous system aging, disease, and repair," *Ageing Res. Rev.*, vol. 24, pp. 358–368, 2015.

[84] T. Sasaki *et al.*, "Aberrant Autolysosomal Regulation Is Linked to The Induction of Embryonic Senescence: Differential Roles of Beclin 1 and p53 in Vertebrate Spns1 Deficiency," *PLoS Genet.*, vol. 10, no. 6, 2014.

[85] M. J. H. Gilbert, T. C. Zerulla, and K. B. Tierney, "Zebrafish (Danio rerio) as a model for the study of aging and exercise: Physical ability and trainability decrease with age," *Exp. Gerontol.*, vol. 50, no. 1, pp. 106–113, 2013.

[86] T. Sasaki and S. Kishi, "Molecular and chemical genetic approaches to developmental origins of aging and disease in zebrafish," *Biochim. Biophys. Acta - Mol. Basis Dis.*, vol. 1832, no. 9, pp. 1362–1370, 2013.

[87] S. Kishi *et al.*, "The identification of zebrafish mutants showing alterations in senescence-associated biomarkers," *PLoS Genet.*, vol. 4, no. 8, 2008.

[88] D. Verduzco and J. Amatruda, "Analysis of Cell Proliferation, Senescence and Cell Death in Zebrafish Embryos," *Methods Cell Biol.*, vol. 101, no. 214, pp. 19–38, 2011.

[89] S. Ota and A. Kawahara, "Zebrafish: A model vertebrate suitable for the analysis of human genetic disorders," *Congenit. Anom. (Kyoto).*, vol. 54, no. 1, pp. 8–11, 2014.

[90] S. Kishi, B. E. Slack, J. Uchiyama, and I. V. Zhdanova, "Zebrafish as a genetic model in biological and behavioral gerontology: Where development meets aging in vertebrates - A mini-review," *Gerontology*, vol. 55, no. 4, pp. 430–441, 2009.

[91] N. G. Holtzman, M. Kathryn Iovine, J. O. Liang, and J. Morris, "Learning to fish with genetics: A primer on the vertebrate model Danio rerio," *Genetics*, vol. 203, no. 3, pp. 1069–1089, 2016.

[92] K. Howe *et al.*, "The zebrafish reference genome sequence and its relationship to the human genome," *Nature*, vol. 496, no. 7446, pp. 498–503, 2013.

[93] M. C. Carneiro, C. M. Henriques, J. Nabais, T. Ferreira, T. Carvalho, and M. G. Ferreira, "Short Telomeres in Key Tissues Initiate Local and Systemic Aging in Zebrafish," *PLoS Genet.*, vol. 12, no. 1, pp. 1–31, 2016.

[94] S. Kishi, J. Uchiyama, A. M. Baughman, T. Goto, M. C. Lin, and S. B. Tsai, "The zebrafish as a vertebrate model of functional aging and very gradual senescence," *Exp. Gerontol.*, vol. 38, no. 7, pp. 777–786, 2003.

[95] M. C. Carneiro, I. P. de Castro, and M. G. Ferreira, "Telomeres in aging and disease: lessons from zebrafish," *Dis. Model. Mech.*, vol. 9, no. 7, pp. 737–748, 2016.

[96] H. E. Jackson and P. W. Ingham, "Control of muscle fibre-type diversity during embryonic development: The zebrafish paradigm," *Mech. Dev.*, vol. 130, no. 9–10, pp. 447–457, 2013.

[97] J. D. Doles and B. B. Olwin, “The impact of JAK-STAT signaling on muscle regeneration,” *Nat. Med.*, vol. 20, no. 10, pp. 1094–1095, 2014.
[98] B. R. McKay, D. I. Ogborn, J. M. Baker, K. G. Toth, M. A. Tarnopolsky, and G. Parise, “Elevated SOCS3 and altered IL-6 signaling is associated with age-related human muscle stem cell dysfunction,” *AJP Cell Physiol.*, vol. 304, no. 8, pp. C717–C728, 2013.
[99] H. Augustin and L. Partridge, “Invertebrate models of age-related muscle degeneration,” *Biochim. Biophys. Acta - Gen. Subj.*, vol. 1790, no. 10, pp. 1084–1094, 2009.
[100] F. D. Price *et al.*, “Inhibition of JAK/STAT signaling stimulates adult satellite cell function,” *Nat. Med.*, vol. 20, no. 10, pp. 1174–1181, 2014.
[101] P. N. Siparsky, D. T. Kirkendall, and W. E. Garrett, “Muscle Changes in Aging: Understanding Sarcopenia,” *Sports Health*, vol. 6, no. 1, pp. 36–40, 2014.
[102] P. Muñoz-Cánoves, C. Scheele, B. K. Pedersen, and A. L. Serrano, “Interleukin-6 myokine signaling in skeletal muscle: A double-edged sword?,” *FEBS J.*, vol. 280, no. 17, pp. 4131–4148, 2013.
[103] H. Yin, F. Price, and M. A. Rudnicki, “Satellite Cells and the Muscle Stem Cell Niche,” *Physiol. Rev.*, vol. 93, no. 1, pp. 23–67, 2013.
[104] D. Ratnayake and P. D. Currie, “Stem cell dynamics in muscle regeneration: Insights from live imaging in different animal models,” *BioEssays*, vol. 39, no. 6, pp. 1–9, 2017.
[105] C. Lepper, T. A. Partridge, and C.-M. Fan, “An absolute requirement for Pax7-positive satellite cells in acute injury-induced skeletal muscle regeneration,” *Development*, vol. 138, no. 17, pp. 3639–3646, 2011.
[106] M. M. Murphy, J. A. Lawson, S. J. Mathew, D. A. Hutcheson, and G. Kardon, “Satellite cells, connective tissue fibroblasts and their interactions are crucial for muscle regeneration,” *Development*, vol. 138, no. 17, pp. 3625–3637, 2011.
[107] R. Sambasivan *et al.*, “Pax7-expressing satellite cells are indispensable for adult skeletal muscle regeneration,” *Development*, vol. 138, no. 19, pp. 4333–4333, 2011.
[108] D. B. Gurevich *et al.*, “Asymmetric division of clonal muscle stem cells coordinates muscle regeneration in vivo,” *Science (80-.).*, vol. 353, no. 6295, 2016.
[109] G. E. Hollway, R. J. Bryson-Richardson, S. Berger, N. J. Cole, T. E. Hall, and P. D. Currie, “Whole-Somite Rotation Generates Muscle Progenitor Cell Compartments in the Developing Zebrafish Embryo,” *Dev. Cell*, vol. 12, no. 2, pp. 207–219, 2007.
[110] C. Seger, M. Hargrave, X. Wang, R. J. Chai, S. Elworthy, and P. W. Ingham, “Analysis of Pax7 expressing myogenic cells in zebrafish muscle development, injury, and models of disease,” *Dev. Dyn.*, vol. 240, no. 11, pp. 2440–2451, 2011.
[111] H. Zhang and J. E. Anderson, “Satellite cell activation and populations on single muscle-fiber cultures from adult zebrafish (Danio rerio),” *J. Exp. Biol.*, vol. 217, no. 11, pp. 1910–1917, 2014.
[112] J.-M. Tee *et al.*, “*asb11* Is a Regulator of Embryonic and Adult Regenerative Myogenesis,” *Stem Cells Dev.*, vol. 21, no. 17, pp. 3091–3103, 2012.
[113] H. C. Seo, B. O. Sætre, B. Håvik, S. Ellingsen, and A. Fjose, “The zebrafish Pax3 and Pax7 homologues are highly conserved, encode multiple isoforms and show dynamic segment-like expression in the developing brain,” *Mech. Dev.*, vol. 70, no. 1–2, pp. 49–63, 1998.
[114] J. E. N. Minchin and S. M. Hughes, “Sequential actions of Pax3 and Pax7 drive xanthophore development in zebrafish neural crest,” *Dev. Biol.*, vol. 317, no. 2, pp. 508–522, 2008.
[115] T. G. Pipalia, J. Koth, S. D. Roy, C. L. Hammond, K. Kawakami, and S. M. Hughes, “Cellular dynamics of regeneration reveals role of two distinct Pax7 stem cell populations in larval zebrafish muscle repair,” *Dis. Model. Mech.*, vol. 9, no. 6, pp. 671–684, 2016.
[116] M. A. Berberoglu *et al.*, “Satellite-like cells contribute to pax7-dependent skeletal muscle

repair in adult zebrafish," vol. 162, no. 3, pp. 561–567, 2017.
[117] S. Knappe, P. S. Zammit, and R. D. Knight, "A population of Pax7-expressing muscle progenitor cells show differential responses to muscle injury dependent on developmental stage and injury extent," *Front. Aging Neurosci.*, vol. 7, no. AUG, pp. 1–17, 2015.
[118] M. E. Carlson and I. M. Conboy, "Loss of stem cell regenerative capacity within aged niches," *Aging Cell*, vol. 6, no. 3, pp. 371–382, 2007.
[119] B. Chazaud and G. Mouchiroud, "Inflamm-aging: STAT3 signaling pushes muscle stem cells off balance," *Cell Stem Cell*, vol. 15, no. 4, pp. 401–402, 2014.
[120] A. Saera-Vila, P. E. Kish, and A. Kahana, "Fgf regulates dedifferentiation during skeletal muscle regeneration in adult zebrafish," vol. 91, no. 2, pp. 165–171, 2016.
[121] A. Saera-Vila *et al.*, "Myocyte Dedifferentiation Drives Extraocular Muscle Regeneration in Adult Zebrafish," *Investig. Opthalmology Vis. Sci.*, vol. 56, no. 8, p. 4977, 2015.
[122] K. Geurtzen, F. Knopf, D. Wehner, L. F. A. Huitema, S. Schulte-Merker, and G. Weidinger, "Mature osteoblasts dedifferentiate in response to traumatic bone injury in the zebrafish fin and skull," *Development*, vol. 141, no. 11, pp. 2225–2234, 2014.
[123] S. Stewart and K. Stankunas, "Limited dedifferentiation provides replacement tissue during zebrafish fin regeneration," *Dev. Biol.*, vol. 365, no. 2, pp. 339–349, 2012.
[124] J. Wan, R. Ramachandran, and D. Goldman, "HB-EGF Is Necessary and Sufficient for Müller Glia Dedifferentiation and Retina Regeneration," *Dev. Cell*, vol. 22, no. 2, pp. 334–347, 2012.
[125] I. M. Conboy, M. J. Conboy, A. J. Wagers, E. R. Girma, I. L. Weismann, and T. A. Rando, "Rejuvenation of aged progenitor cells by exposure to a young systemic environment," *Nature*, vol. 433, no. 7027, pp. 760–764, 2005.
[126] M. T. Tierney *et al.*, "STAT3 signaling controls satellite cell expansion and skeletal muscle repair," *Nat. Med.*, vol. 6, no. 9, pp. 2166–2171, 2014.
[127] Y. C. Jang, M. S. Sinha, M. Cerletti, C. D. Osso, and A. J. Wagers, "Skeletal Muscle Stem Cells : Effects of Aging and Metabolism on Muscle Regenerative Function," vol. LXXVI, 2011.
[128] J. F. Ma, B. J. Sanchez, D. T. Hall, A. K. Tremblay, S. Di Marco, and I. Gallouzi, "STAT3 promotes IFNγ/TNFα-induced muscle wasting in an NF-κB-dependent and IL-6-independent manner," *EMBO Mol. Med.*, vol. 9, no. 5, pp. 622–637, 2017.
[129] J. S. Rawlings, kristin M. Rosler, and D. A. Harrison, "The JAK/STAT signaling pathway," *J. Cell Sci.*, vol. 117, no. 8, pp. 1281–1283, 2004.
[130] D. A. Harrison, "The JAK / STAT Pathway," *Cold Spring Harb. Perspect. Biol.*, vol. 4, no. 3, pp. 1–4, 2012.
[131] Y. Yang *et al.*, "STAT3 induces muscle stem cell differentiation by interaction with myoD," *Cytokine*, vol. 46, no. 1, pp. 137–141, 2009.
[132] P. Sousa-Victor *et al.*, "Geriatric muscle stem cells switch reversible quiescence into senescence," *Nature*, vol. 506, no. 7488, pp. 316–321, 2014.
[133] H. Zhu *et al.*, "STAT3 Regulates Self-Renewal of Adult Muscle Satellite Cells during Injury-Induced Muscle Regeneration," *Cell Rep.*, vol. 16, no. 8, pp. 2102–2115, 2016.
[134] Y. Chung, B. Park, Y. Kang, T. Kim, C. J. Eaves, and I. Oh, "Unique effects of," *Blood*, vol. 108, no. 4, pp. 1208–1215, 2006.
[135] T. Tadokoro, Y. Wang, L. S. Barak, Y. Bai, S. H. Randell, and B. L. M. Hogan, "IL-6/STAT3 promotes regeneration of airway ciliated cells from basal stem cells," *Proc. Natl. Acad. Sci.*, vol. 111, no. 35, pp. E3641–E3649, 2014.
[136] J. V Chakkalakal, K. M. Jones, M. A. Basson, and A. S. Brack, "Europe PMC Funders Group The aged niche disrupts muscle stem cell quiescence," vol. 490, no. 7420, pp. 355–360, 2013.
[137] D. Palacios *et al.*, "TNF/p38 alpha/Polycomb signalling to Pax7 locus in satellite cells links

inflammation to the epigenetic control of muscle regeneration," *Cell Stem Cell.*, vol. 7, no. 4, pp. 455–469, 2010.
[138] K. G. Toth, B. R. McKay, M. de Lisio, J. P. Little, M. A. Tarnopolsky, and G. Parise, "IL-6 induced STAT3 signalling is associated with the proliferation of human muscle satellite cells following acute muscle damage," *PLoS One*, vol. 6, no. 3, 2011.
[139] M. H. Porteus, "Towards a new era in medicine: therapeutic genome editing," *Genome Biol.*, vol. 13, no. 5, pp. 625–639, 2015.
[140] T. K. Guha, A. Wai, and G. Hausner, "Programmable Genome Editing Tools and their Regulation for Efficient Genome Engineering," *Comput. Struct. Biotechnol. J.*, vol. 15, pp. 146–160, 2017.
[141] A. Hruscha *et al.*, "Efficient CRISPR/Cas9 genome editing with low off-target effects in zebrafish," *Development*, vol. 140, no. 24, pp. 4982–4987, 2013.
[142] D. Ma and F. Liu, "Genome Editing and Its Applications in Model Organisms," *Genomics, Proteomics Bioinforma.*, vol. 13, no. 6, pp. 336–344, 2015.
[143] R. Sertori, M. Trengove, F. Basheer, A. C. Ward, and C. Liongue, "Genome editing in zebrafish: A practical overview," *Brief. Funct. Genomics*, vol. 15, no. 4, pp. 322–330, 2016.
[144] J. Liu *et al.*, "CRISPR/Cas9 in zebrafish: an efficient combination for human genetic diseases modeling," *Hum. Genet.*, vol. 136, no. 1, pp. 1–12, 2017.
[145] M. Li, L. Zhao, P. S. Page-McCaw, and W. Chen, "Zebrafish Genome Engineering Using the CRISPR–Cas9 System," *Trends Genet.*, vol. 32, no. 12, pp. 815–827, 2016.
[146] J. Ablain, E. M. Durand, S. Yang, Y. Zhou, and L. I. Zon, "A CRISPR/Cas9 vector system for tissue-specific gene disruption in zebrafish," *Dev. Cell*, vol. 32, no. 6, pp. 756–764, 2015.
[147] U. Irion, J. Krauss, and C. Nusslein-Volhard, "Precise and efficient genome editing in zebrafish using the CRISPR/Cas9 system," *Development*, vol. 141, no. 24, pp. 4827–4830, 2014.
[148] G. K. Varshney *et al.*, "A high-throughput functional genomics workflow based on CRISPR/Cas9-mediated targeted mutagenesis in zebrafish," *Nat. Protoc.*, vol. 11, no. 12, pp. 2357–2375, 2016.
[149] H. Ata, K. J. Clark, and S. C. Ekker, *The zebrafish genome editing toolkit*, vol. 135. Elsevier Ltd, 2016.
[150] M. Bibikova, M. Golic, K. G. Golic, and D. Carroll, "Targeted chromosomal cleavage and mutagenesis in Drosophila using zinc-finger nucleases," *Genetics*, vol. 161, no. 3, pp. 1169–1175, 2002.
[151] M. Bibikova, K. Beumer, J. K. Trautman, and D. Carroll, "Enhancing gene targeting with designed zinc finger nucleases," *Science (80-.).*, vol. 300, no. 5620, p. 764, 2003.
[152] M. H. Porteus and D. Baltimore, "Chimeric nucleases stimulate gene targeting in human cells," *Science (80-.).*, vol. 300, no. 5620, p. 763, 2003.
[153] T. J. Dahlem *et al.*, "Simple Methods for Generating and Detecting Locus-Specific Mutations Induced with TALENs in the Zebrafish Genome," *PLoS Genet.*, vol. 8, no. 8, 2012.
[154] H. K. Ratner, T. R. Sampson, and D. S. Weiss, "Overview of CRISPR-Cas9 biology," *Cold Spring Harb. Protoc.*, vol. 2016, no. 12, pp. 1023–1038, 2016.
[155] E. Kouranova *et al.*, "CRISPRs for Optimal Targeting: Delivery of CRISPR Components as DNA, RNA, and Protein into Cultured Cells and Single-Cell Embryos," *Hum. Gene Ther.*, vol. 27, no. 6, pp. 464–475, 2016.
[156] A. P. W. Gonzales and J. R. Joanna Yeh, *Cas9-based genome editing in Zebrafish*, 1st ed., vol. 546, no. C. Elsevier Inc., 2014.
[157] F. A. Ran, P. D. Hsu, J. Wright, V. Agarwala, D. A. Scott, and F. Zhang, "Genome engineering using the CRISPR-Cas9 system," *Nat. Protoc.*, vol. 8, no. 11, pp. 2281–2308, 2013.
[158] W. Y. Hwang *et al.*, "Efficient genome editing in zebrafish using a CRISPR-Cas system," *Nat.*

Biotechnol., vol. 31, no. 3, pp. 227–229, 2013.
[159] L.-E. Jao, S. R. Wente, and W. Chen, "Efficient multiplex biallelic zebrafish genome editing using a CRISPR nuclease system," *Proc. Natl. Acad. Sci.*, vol. 110, no. 34, pp. 13904–13909, 2013.
[160] A. Veres *et al.*, "Low incidence of off-target mutations in individual CRISPR-Cas9 and TALEN targeted human stem cell clones detected by whole genome sequencing," *Cell Stem Cell*, vol. 31, no. 3, pp. 477–479, 2014.
[161] A. Seth, D. L. Stemple, and I. Barroso, "The emerging use of zebrafish to model metabolic disease," *Dis. Model. Mech.*, vol. 6, no. 5, pp. 1080–1088, 2013.
[162] F. O. Kok *et al.*, "Reverse genetic screening reveals poor correlation between Morpholino-induced and mutant phenotypes in zebrafish," *Dev. Cell*, pp. 97–108, 2015.
[163] A. Rossi *et al.*, "Genetic compensation induced by deleterious mutations but not gene knockdowns," *Nature*, vol. 524, no. 7564, pp. 230–233, 2015.
[164] K. M. Kwan *et al.*, "The Tol2kit: A multisite gateway-based construction Kit for Tol2 transposon transgenesis constructs," *Dev. Dyn.*, vol. 236, no. 11, pp. 3088–3099, 2007.
[165] K. Kawakami, H. Takeda, N. Kawakami, M. Kobayashi, N. Matsuda, and M. Mishina, "A Transposon-Mediated Gene Trap Approach Identifies Developmentally Regulated Genes in Zebrafish," vol. 7, pp. 133–144, 2004.
[166] L. Yin *et al.*, "Multiplex conditional mutagenesis using transgenic expression of Cas9 and sgRNAs," *Genetics*, vol. 200, no. 2, pp. 431–441, 2015.
[167] A. Carmany-Rampey and C. B. Moens, "Modern mosaic analysis in the zebrafish," *Methods*, vol. 39, no. 3, pp. 228–238, 2006.
[168] J. Rossant and A. Spence, "Chimeras and mosaics in mouse mutant analysis," *Trends Genet.*, vol. 14, no. 9, pp. 358–363, 1998.
[169] X. Li, F. Nie, Z. Yin, and J. Y. He, "Enhanced hyperplasia in muscles of transgenic zebrafish expressing Follistatin1," *Sci. China Life Sci.*, vol. 54, no. 2, pp. 159–165, 2011.
[170] J. Karlsson, J. von Hofsten, and P.-E. Olsson, "Generating Transparent Zebrafish: A Refined Method to Improve Detection of Gene Expression During Embryonic Development," *Mar. Biotechnol.*, vol. 3, no. 6, pp. 0522–0527, 2001.
[171] M. Ishibashi, A. S. Mechaly, T. S. Becker, and S. Rinkwitz, "Using zebrafish transgenesis to test human genomic sequences for specific enhancer activity," *Methods*, vol. 62, no. 3, pp. 216–225, 2013.
[172] C. B. Kimmel, W. W. Ballard, S. R. Kimmel, B. Ullmann, and T. F. Schilling, "Stages of embryonic development of the zebrafish.," *Dev. Dyn. an Off. public*, vol. 203, no. 3, pp. 253–310, 1995.
[173] N. Topic Popovic *et al.*, "Tricaine methane-sulfonate (MS-222) application in fish anaesthesia," *J. Appl. Ichthyol.*, vol. 28, no. 4, pp. 553–564, 2012.
[174] A. M. Valentim *et al.*, "Euthanizing zebrafish legally in Europe: Are the approved methods of euthanizing zebrafish appropriate to research reality and animal welfare?," *EMBO Rep.*, vol. 37, no. 2, pp. 264–278, 2016.
[175] M. A. Moreno-Mateos *et al.*, "CRISPRscan: Designing highly efficient sgRNAs for CRISPR-Cas9 targeting in vivo," *Nat. Methods*, vol. 12, no. 10, pp. 982–988, 2015.
[176] Y. Kimura, Y. Hisano, A. Kawahara, and S. I. Higashijima, "Efficient generation of knock-in transgenic zebrafish carrying reporter/driver genes by CRISPR/Cas9-mediated genome engineering," *Sci. Rep.*, vol. 4, pp. 1–7, 2014.
[177] C. Srisawat, I. J. Goldstein, and D. R. Engelke, "Sephadex-binding RNA ligands: rapid affinity purification of RNA from complex RNA mixtures.," *Nucleic Acids Res.*, vol. 29, no. 2, p. E4, 2001.

[178] P. D. Hsu *et al.*, "DNA targeting specificity of RNA-guided Cas9 nucleases," *Nat. Biotechnol.*, vol. 31, no. 9, pp. 827–832, 2013.
[179] X. Zhu *et al.*, "An efficient genotyping method for genome-modified animals and human cells generated with CRISPR/Cas9 system," *Sci. Rep.*, vol. 4, pp. 1–8, 2014.
[180] B. Ju *et al.*, "Recapitulation of fast skeletal muscle development in zebrafish by transgenic expression of GFP under the mylz2 promoter," *Dev. Dyn.*, vol. 227, no. 1, pp. 14–26, 2003.
[181] J. Bessa *et al.*, "Zebrafish Enhancer Detection (ZED) vector: A new tool to facilitate transgenesis and the functional analysis of cis-regulatory regions in zebrafish," *Dev. Dyn.*, vol. 238, no. 9, pp. 2409–2417, 2009.
[182] K. C. Sadler, K. N. Krahn, N. a Gaur, and C. Ukomadu, "Liver growth in the embryo and during liver regeneration in zebrafish requires the cell cycle regulator, uhrf1.," *Proc. Natl. Acad. Sci. U. S. A.*, vol. 104, no. 5, pp. 1570–1575, 2007.
[183] M. Schiavone *et al.*, "Zebrafish reporter lines reveal in vivo signaling pathway activities involved in pancreatic cancer," *Dis. Model. Mech.*, vol. 7, no. 7, pp. 883–894, 2014.
[184] G. S. Gerhard, "Comparative aspects of zebrafish (Danio rerio) as a model for aging research," *Exp. Gerontol.*, vol. 38, no. 11–12, pp. 1333–1341, 2003.
[185] S. Kishi, "Functional aging and gradual senescence in zebrafish," *Ann. N. Y. Acad. Sci.*, vol. 1019, pp. 521–526, 2004.
[186] L. Yu, V. Tucci, S. Kishi, and I. V. Zhdanova, "Cognitive aging in zebrafish," *PLoS One*, vol. 1, no. 1, 2006.
[187] S. B. Tsai *et al.*, "Differential effects of genotoxic stress on both concurrent body growth and gradual senescence in the adult zebrafish," *Aging Cell*, vol. 6, no. 2, pp. 209–224, 2007.
[188] I. V. Zhdanova, L. Yu, M. Lopez-Patino, E. Shang, S. Kishi, and E. Guelin, "Aging of the circadian system in zebrafish and the effects of melatonin on sleep and cognitive performance," *Brain Res.*, pp. 433–441, 2008.
[189] S. Kishi, "The search for evolutionary developmental origins of aging in zebrafish: A novel intersection of developmental and senescence biology in the zebrafish model system," *Birth Defects Res. Part C - Embryo Today Rev.*, vol. 93, no. 3, pp. 229–248, 2011.
[190] A. Amsterdam, R. M. Nissen, Z. Sun, E. C. Swindell, S. Farrington, and N. Hopkins, "Identification of 315 genes essential for early zebrafish development," *Proc. Natl. Acad. Sci.*, vol. 101, no. 35, pp. 12792–12797, 2004.
[191] R. Peng, G. Lin, and J. Li, "Potential pitfalls of CRISPR/Cas9-mediated genome editing," *FEBS J.*, vol. 283, no. 7, pp. 1218–1231, 2016.
[192] S. S. Myatt *et al.*, "SUMOylation inhibits FOXM1 activity and delays mitotic transition," *Oncogene*, vol. 33, no. 34, pp. 4316–4329, 2014.
[193] J. Wan, D. Subramonian, and X.-D. Zhang, "SUMOylation in Control of Accurate Chromosome Segregation during Mitosis," *Curr. Protein Pept. Sci.*, vol. 13, no. 5, pp. 467–481, 2012.
[194] J. Schimmel *et al.*, "Uncovering SUMOylation dynamics during cell-cycle progression reveals foxM1 as a key mitotic SUMO target protein," *Mol. Cell*, vol. 53, no. 6, pp. 1053–1066, 2014.
[195] A. Princz and N. Tavernarakis, "The role of SUMOylation in ageing and senescent decline," *Mech. Ageing Dev.*, vol. 162, pp. 85–90, 2017.
[196] L. Ivanschitz, Y. Takahashi, F. Jollivet, O. Ayrault, M. Le Bras, and H. de Thé, "PML IV/ARF interaction enhances p53 SUMO-1 conjugation, activation, and senescence," *Proc. Natl. Acad. Sci.*, vol. 112, no. 46, pp. 14278–14283, 2015.
[197] M. S. Ignatius *et al.*, "In Vivo Imaging of Tumor-Propagating Cells, Regional Tumor Heterogeneity, and Dynamic Cell Movements in Embryonal Rhabdomyosarcoma," *Cancer Cell*, vol. 21, no. 5, pp. 680–693, 2012.

[198] Q. Tang *et al.*, “Imaging tumour cell heterogeneity following cell transplantation into optically clear immune-deficient zebrafish,” *Nat. Commun.*, vol. 7, 2016.
[199] Z. Chen *et al.*, “FoxM1 Transcriptionally Regulates the Expression of Long Noncoding RNAs Snhg8 and Gm26917 to Promote Proliferation and Survival of Muscle Satellite Cells,” *Stem Cells*, 2018.
[200] D. W. Morgens *et al.*, “Genome-scale measurement of off-target activity using Cas9 toxicity in high-throughput screens,” *Nat. Commun.*, vol. 8, no. May, pp. 1–8, 2017.
[201] R. J. Ihry *et al.*, “P53 inhibits CRISPR-Cas9 engineering in human pluripotent stem cells,” *Nat. Med.*, vol. 24, no. 7, pp. 939–946, 2018.
[202] I. Fridlyanskaya, L. Alekseenko, and N. Nikolsky, “Senescence as a general cellular response to stress: A mini-review,” *Exp. Gerontol.*, vol. 72, pp. 124–128, 2015.
[203] M. Storer *et al.*, “XSenescence is a developmental mechanism that contributes to embryonic growth and patterning,” *Cell*, vol. 155, no. 5, pp. 1119–1130, 2013.
[204] P. L. J. de Keizer, “The Fountain of Youth by Targeting Senescent Cells?,” *Trends Mol. Med.*, vol. 23, no. 1, pp. p6-17, 2017.
[205] M. F. Sentmanat, S. T. Peters, C. P. Florian, J. P. Connelly, and S. M. Pruett-Miller, “A Survey of Validation Strategies for CRISPR-Cas9 Editing,” *Sci. Rep.*, vol. 8, no. 1, pp. 1–8, 2018.
[206] J. Guo *et al.*, “A simple and cost-effective method for screening of CRISPR/Cas9-induced homozygous/biallelic mutants,” *Plant Methods*, vol. 14, no. 1, pp. 1–10, 2018.

6. Appendix

Reagents and Medium constitutions

E3 medium (5mM NaCl, 0.17mM KCl, 0.33mM $CaCl_2.2H_2O$, 0.33mM $MgSO_4.7H_2O$, 0.01% methylene blue [Sigma-Aldrich], pH 7.2)

Annealing buffer (10mM Tris, at pH 7.5-8.0, 50mM NaCL,1m EDTA)

NTP mix (10mM of ATP, UTP, CTP, GTP)

Sephadex suspension (3.33g Sephadex G-50 fine DNA grade in 50mL of DEPC treated Tris-EDTA, GE)

Genomic extraction buffer (10mM Tris pH8.2, 10mM EDTA, 200mM NaCl, 0.5% SDS and 200ug/mL proteinase K)

TE+RNAse (10mM Tris, 1mM EDTA pH8, 100µg/mL RNAse)

RNA extraction mixture of ethanol and sodium acetate (0.03ml 3M NaAc, pH 5.6, in 0.997mL EtOH 100%)

Ginzburg Fish Ringer (6.50g KCl, 0.30g $CaCl_2$, 0.20g $NaHCO_3$ and ddH_2O)

Dissection buffer (HBSS 1x, Hepes 10mM, EDTA 2mM)

PDT (PBS 1x; 0.1% Tween-20, 0.3% Triton and 1% DMSO)

ISH blocking buffer (PDT, 2% goat serum, 2mg/mL BSA)

Tables

Table 6.2 List of oligonucleotides designed and ordered for targeting foxm1. gRNA sequences are in a 5'-3' orientation

	Forward	Reverse
Targeting foxm1 exon 2		
sgRNA 2.1	TAGGGGAAGGAGTGTGGGCCTC	AAACGAGGCCCACACTCCTTCC
sgRNA 2.2	TAGGTGTTTTTCTACAGAACTT	AAACAAGTTCTGTAGAAAAACA
sgRNA 2.3	TAGGTTTTGCTCTCCTCCAAAC	AAACGTTTGGAGGAGAGCAAAA
sgRNA 2.4	TAGGGTGTCCGGCATAGTAGGG	AAACCCCTACTATGCCGGACAC
sgRNA 2.5	TAGGGTCGAGGTGGTCTTACAG	AAACCTGTAAGACCACCTCGAC
sgRNA 2.6	TAGGGAGCAGTGGACTGGGTCG	AAACCGACCCAGTCCACTGCTC
Targeting foxm1 exon 8		
sgRNA 8.1	TAGGGAACAGTGACTGACCCAG	AAACCTGGGTCAGTCACTGTTC
sgRNA 8.2	TAGGGTCAGTCCGAGGCAGTAG	AAACCTACTGCCTCGGACTGAC
sgRNA 8.3	TAGGGGAAGCTGAATGGGTACC	AAACGGTACCCATTCAGCTTCC

Table 6.3 Designed primers for groups of sgRNA designed with melting temperatures and resulting fragment sizes

primers	Forward (fw) (5'-3')	Tm	Reverse (rv) (5'-3')	Tm	Fragment

					size (bp)
		***foxm1* exon 2**			
sgRNA 2.1-2.3	CACCCTACTATGCCGGACAC	62.5ºC	GAGCTTGGGAAAGGTGAGTTA	59.5ºC	211
sgRNA 2.4-2.6	GGGAGAGCCCAAGGAGACC	63.6ºC	GGCGAAACAAGTTCATCCTGC	61.2ºC	288
		***foxm1* exon 8**			
sgRNA 8.1-8.3	AAAGCCATACCTGCATTGGGTG	62.5ºC	CATTCTGGCAAAGCAAGTGATGA	60.9ºC	371
		GFP			
sgRNA GFP	GGTGGTGCCCATCCTGG	59.8ºC	CCTGACCTACGGCGTGC	59.8ºC	176

Table 6.4 Re-design of sgRNA 8.3 to fit the recombination vector

	sgRNA 8.3	**sgRNA 8.3GW**
Forward (fw)	TAGG**GTCAGTCCGAGGCAGTAG**	**GTCAGTCCGAGGCAGTAG**GT
Reverse (rv)	AAAC**CTACTGCCTCGGACTGAC**	**CTACTGCCTCGGACTGAC**GA

Table 6.5 Primers used for qPCR with melting temperatures and fragment size

primers	**Forward (fw) (5'-3')**	**Tm**	**Reverse (rv) (5'-3')**	**Tm**	**Fragment size (bp)**
foxm1	TCAGCCTGTGACCTCATCTG	60.5ºC	AAGAGAGTGCTGTCGGGGTA	60.5ºC	139
ccnb1	CAGGCTTTGAAGAAGAAGGAGG	62.1ºC	GGCTCAGACACAACCTTAACG	61.2ºC	131
p21	GACCAACATCACAGATTTCTAC	58.4ºC	CTGTCAATAACGCTGCTACG	58.4ºC	166
stat3	GTTGGAGACGCGGTATCTGG	62.5ºC	CCCAGCAGGTTGTGGAAGAC	62.5ºC	159
pax7a	GGGGATAAAGGTAATCGCACG	61.2ºC	ATGTGGTACGACTGCGTCTC	60.5ºC	94
eef1a1	CCGCTAGCATTACCCTCC	58.4ºC	CTTCTCAGGCTGACTGTGC	59.5ºC	358
tbp	GATCACGCGGATTTGATCTT	56.4ºC	GGGGCTATTGGGAGACCTAC	62.5ºC	118

Figures

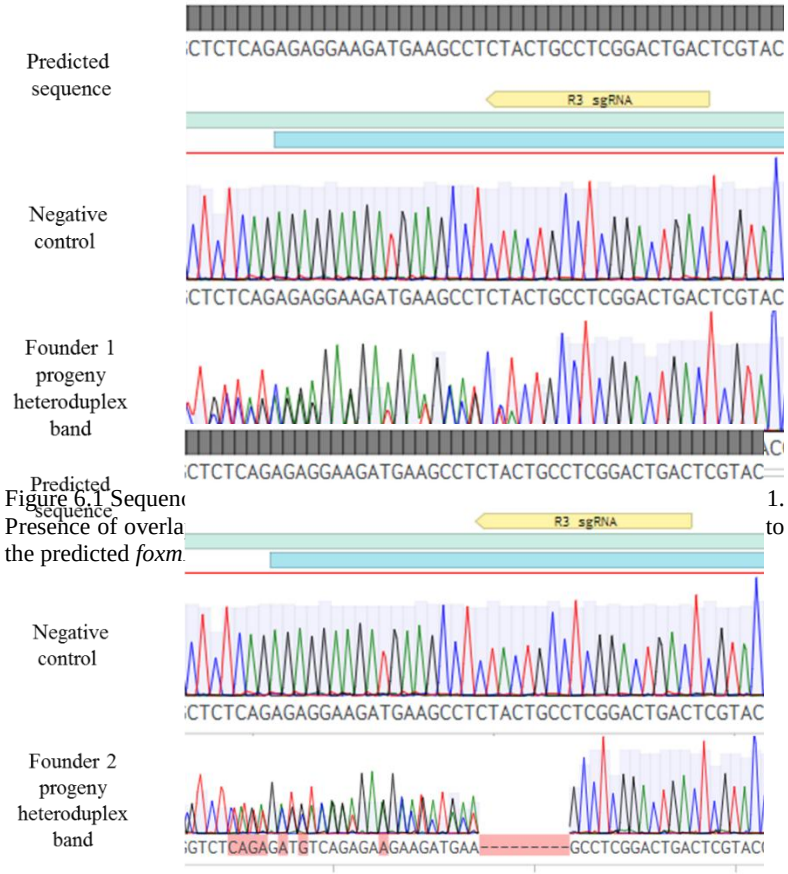

Figure 6.1 Sequen 1. Presence of overla to the predicted *foxm*

Figure 6.2 Sequencing results from the progeny heteroduplex band of Founder 2. Presence of overlapped peaks on the chromatogram near the PAM comparing to the predicted *foxm1* wildtype sequence and negative control.

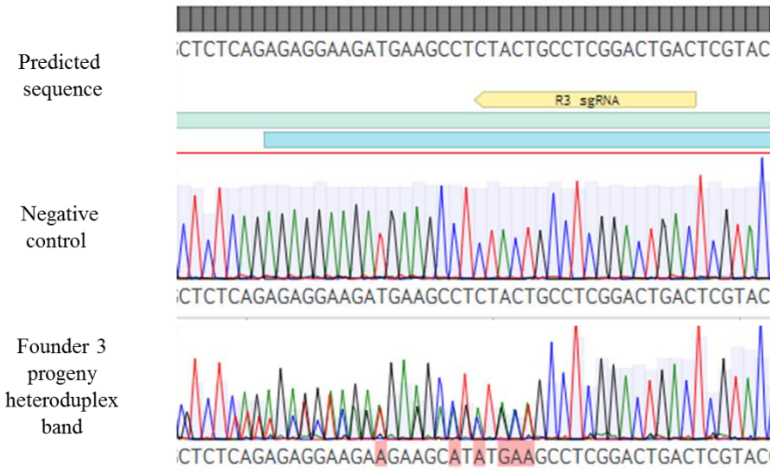

Figure 6.3 Sequencing results from the progeny heteroduplex band of Founder 3. Presence of overlapped peaks on the chromatogram near the PAM comparing to the predicted *foxm1* wildtype sequence and negative control.

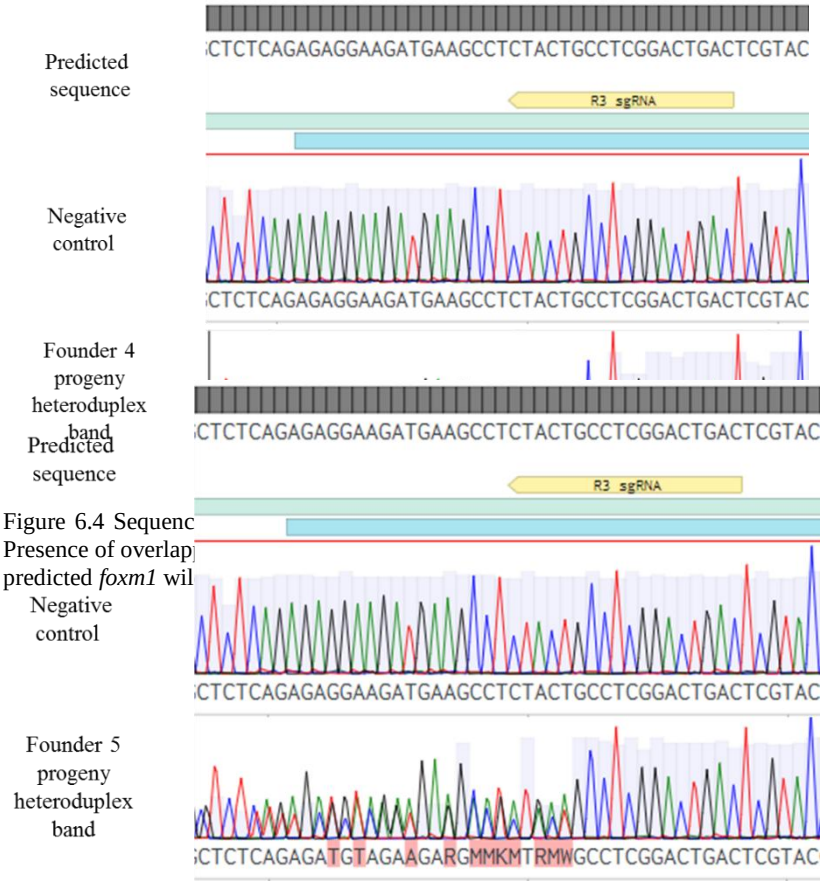

Figure 6.4 Sequenc
Presence of overlap
predicted *foxm1* wil

Figure 6.5 Sequencing results from the progeny heteroduplex band of Founder 5. Presence of overlapped peaks on the chromatogram near the PAM comparing to the predicted *foxm1* wildtype sequence and negative control.

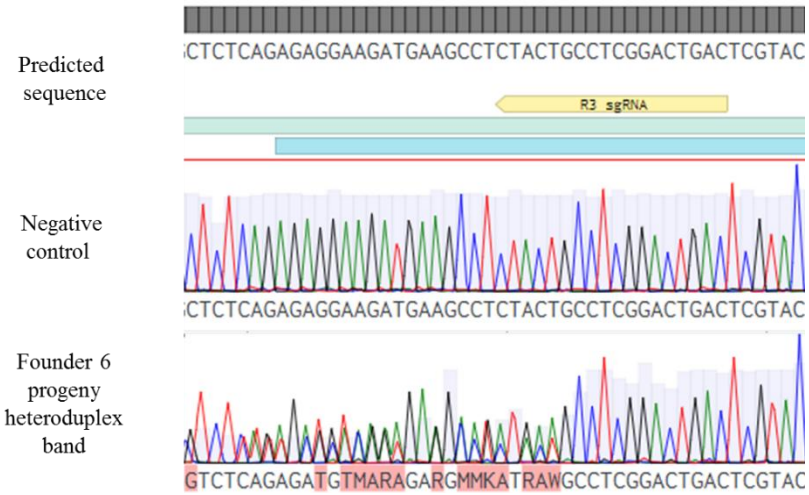

Figure 6.6 Sequencing results from the progeny heteroduplex band of Founder 6. Presence of overlapped peaks on the chromatogram near the PAM comparing to the predicted foxm1 wildtype sequence and negative control.

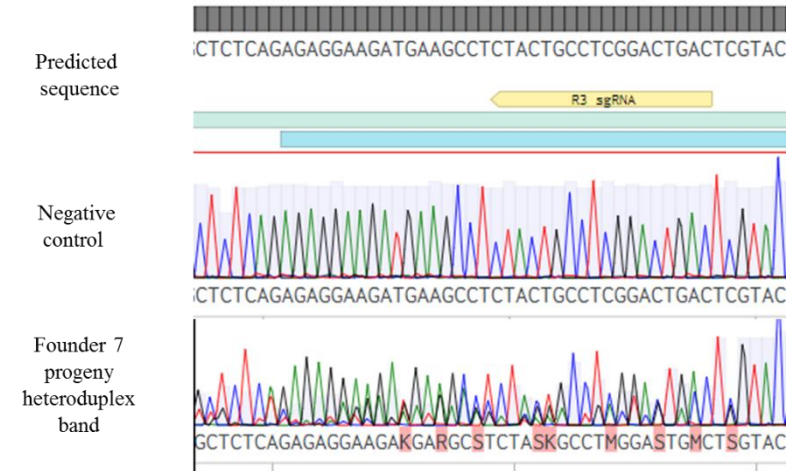

Figure 6.7 Sequencing results from the progeny heteroduplex band of Founder 7. Presence of overlapped peaks on the chromatogram near the PAM comparing to the predicted *foxm1* wildtype sequence and negative control.

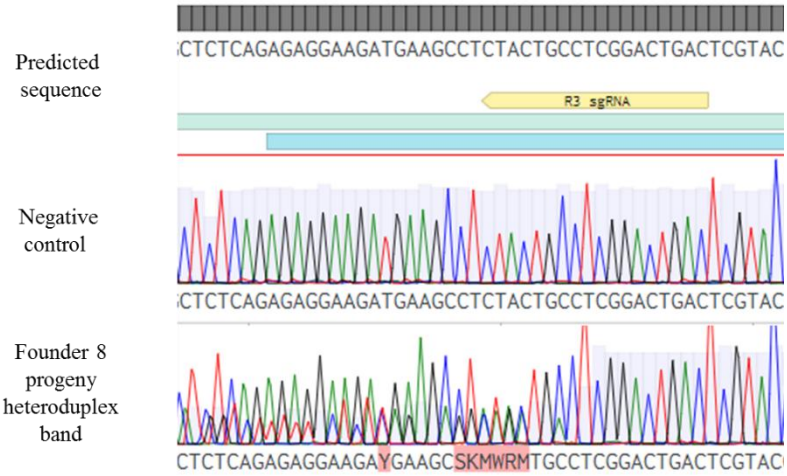

Figure 6.8 Sequencing results from the progeny heteroduplex band of Founder 8. Presence of overlapped peaks on the chromatogram near the PAM comparing to the predicted *foxm1* wildtype sequence and negative control.

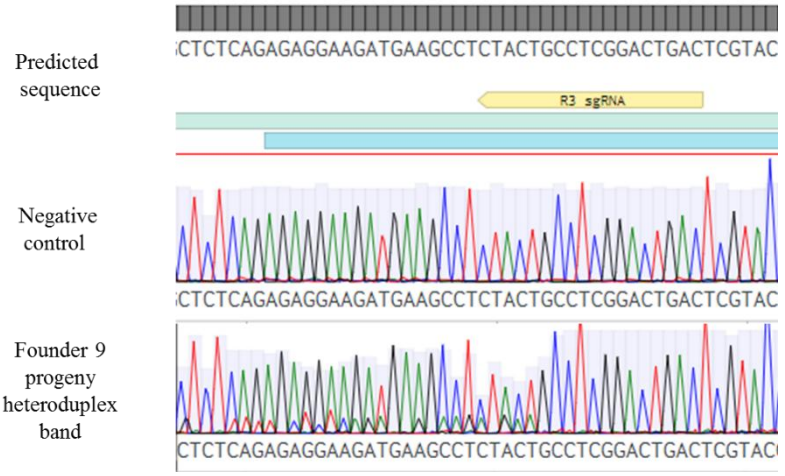

Figure 6.9 Sequencing results from the progeny heteroduplex band of Founder 9. Presence of overlapped peaks on the chromatogram near the PAM comparing to the predicted *foxm1* wildtype sequence and negative control.

```
Human     1  MKTSPRRPLILKRRRLPLPVQNAPSETSEEEPKRSPAQQESNQAEASKEVAESNSCKFPAGIKIINHPTMPNTQVVAIPN  80
Zebrafish 1  MRESPRRPIILKRRKLPF--LKSESDLGCDEADGTRCKTTSTQSTARS---------FPDGIRVMDHPTMPDTQVVVIPK  69

Human    81  NANIHSIITALTAKGKESGSSGPNKFILISCGGAPTQPPGLRPQTQTSYDAKRTEVTLET-LGPKPAARDVNLPRPPGAL  159
Zebrafish 70  SADLQSVISVLTAKGKECGPQGRNKFILLS--------------GDTSLEESKTLGCFSTELGSE--------------L  121

Human   160  CEQKRET-CADGEAAGCTINNSLSNIQWLRKMSSDGLGSRSIKQEMEEKENCHLEQRQVKVEEPSRPSASWQNSVSERPP  238
Zebrafish 122  GKVKKESECFP-------LDDSLTNIQWLGKMSSDGLGS----EKCPNKDNPNDSQQQSKGPEKEN------DPHSERPP  184

Human   239  YSYMAMIQFAINSTERKRMTLKDIYTWIEDHFPYFKHIAKPGWKNSIRHNLSLHDMFVRETSANGKVSFWTIHPSANRYL  318
Zebrafish 185  YSYMAMIQFAINSKNNRHMTLKEIYNWIEDHFPYFRDVAKPGWKNSIRHNLSLHDMFIRETSPDGKISYWTIRPEANRCL  264

Human   319  TLDQVFKPLD----PGSPQLPE-HLESQQKRPNPELRRNMTIKTELPLGARRKNKPLLPRVSSYLVPIQFPVNQSLVLQP  393
Zebrafish 265  TLDQVYKPLGDPLTPTCPQIPQVAIHQQQKRGAPELKKAIPALG----GTERKNPLLPRTDSYLVPIQLPLGQSLFLPT  340

Human   394  SVKVPLPLAASLMSSELARHSKRVRIAPKVLLAEEGIAPLSSAGPGKEEKLLFGEGFSPLLPVQTIKEEEIQPGEEMPHL  473
Zebrafish 341  SSPVSLSTPPQTQNSSTPSSSKRVRIAPKVSQSDLSSVLLCKPAP-----------------QEIKEE-----------  391

Human   474  ARPIKVESPPLEEWPSPAPSFKEESSHSWEDSSQSPTPRPKKSYSGLRSPTRCVSEMLVIQHREERERSRSRRKQHLLPP  553
          392  ------------------PVFQPVTS------SEAPPPKSR----------------------RTDNSSSRRKQRLVLP  424

Human   554  CVDEPELLFSEGPSTSRWAAELPFPADSSDPASQLSYSQEVGGP-----FKTPIKETLPISSTPSKSVLPR-TPESWRLT  627
Zebrafish 425  ATEEPVLLY---PDSTLFDSGVISDISTFQDTREADPKPELDSPNREYSFKTPIKSSHPSSSTPSK--LPTVTLEPWRIT  499

Human   628  PPAKVGGLDFSPVQTSQGAS-DPLPDPLGLMDLSTTPLQSAPPLESPQRLLSSEPLDLISVPFGNSSPSDIDVPKPGSPE  706
Zebrafish 500  PVGKGGVLDFSPIRTPTGPHVTPQRNQHTSLSFTSTPFKELPLFNSPRELLTCS----------RSSPKR---SAPACSR  566

Human   707  PQVSGLAANRSLTEGLVLDTMNDSLSKILLDISFPGLDEDPLGPDNINWSQFIPELQ  763
Zebrafish 567  ELLQVGAANRSLTEGFVLDTMNDSLSKILVDISFSGLEDEDLGMGNISWSQFIPELK  623
```

Figure 6.10 Protein alignment of human FOXM1 and zebrafish FoxM1. Surrounded with a black rectangle is zebrafish lysine K315 (human K368)